

**STABILITY OF DOUBLE PEROVSKITE CATHODES UNDER
HIGH HUMIDTY FOR SOLID OXIDE FUEL CELLS**

A Dissertation
Presented to
The Academic Faculty

by

Yuchen Liu

In Partial Fulfillment
of the Requirements for the Degree
Master of Science in the
Material Science and Engineering

Georgia Institute of Technology
May 2019

COPYRIGHT © 2019 BY YUCHEN LIU

**STABILITY OF DOUBLE PEROVSKITE CATHODES UNDER
HIGH HUMIDTY FOR SOLID OXIDE FUEL CELLS**

Approved by:

Dr. Meilin Liu, Advisor
School of Material Science and Engineering
Georgia Institute of Technology

Dr. Preet Singh
School of Material Science and Engineering
Georgia Institute of Technology

Dr. Faisal Alamgir
School of Material Science and Engineering
Georgia Institute of Technology

Date Approved: April 25, 2019

ACKNOWLEDGEMENTS

I would like to thank all the professors who made this thesis possible. My advisor Dr. Meilin Liu, who without with help, support, and guidance, this work would not have been possible. Thank you to Dr. Preet Singh, and Dr. Faisal Alamgir for serving on my committee.

I would also like to acknowledge and thank my research group for all their help and support. To Ryan Murphy for maintaining the groups equipment and Dr. Yu Chen for scientific discussion over the results of my work. Also, to Dr. Ben deGlee, Dr. Jun Hyuk Kim, and Luke Soule for Raman Spectroscopy and the analysis of its data.

This work would also not be possible without the Materials Characterization Facility of Georgia Tech's Institute for Electronics and Nanotechnology for the use of its characterization equipment and software databases. Special thanks to David Tavakoli and Todd Walters for help with XRD and SEM.

Lastly, I would like to thank my friends and my family for all their support and guidance. To my family who always gives me advice and to my friends who have helped to brighten up my life even during the times I was stressing over finals or this dissertation.

TABLE OF CONTENTS

ACKNOWLEDGEMENTS	iv
LIST OF TABLES	vii
LIST OF FIGURES	viii
LIST OF SYMBOLS AND ABBREVIATIONS	xvi
SUMMARY	xviii
Chapter 1: Introduction	1
1.1 Demand for Clean Energy	1
1.2 Why Fuel Cells?	2
1.3 Basics of SOFCs/SOECs	3
1.4 Research Objective	5
1.5 Thesis Structure	6
Chapter 2: Literature Review	7
2.1 Analyzing Cathode Degradation	7
2.2 Water	8
2.3 Carbon Dioxide	10
2.4 SO_x Compounds	12
2.5 Chromium	13
2.6 Silicon	15
2.7 Material Selection for this work	16
Chapter 3: Methodology	19
3.1 Technical Approach Overview	19
3.2 Powder Synthesis	22
3.3 Fabrication of the Cathodes	23
3.4 Fabrication of Dense Electrolyte	24
3.5 Carbon Co-Precipitated SDC	25
3.6 Symmetric Cell Fabrication	26
3.7 Testing Apparatus	26
Chapter 4: Results and Discussion	31
4.1 Symmetric Cell Characteristics	31
4.2 How to Interpret EIS and Activation Energy	32
4.3 Structural Stability	36
4.4 Cell Fabrication Verification	42

4.5	EIS Long-term Performance	48
4.6	Degradation Mechanism	52
4.7	Applied Voltage	53
4.8	Raman on Applied Voltage Cells	68
chapter 5: Conclusion		69
chapter 6: Recommendations and Future work		70
APPENDIX A. Supplementary Data		72
REFERENCES		87

LIST OF TABLES

Table 1: Humidification System Temperature to get % Moisture.....	29
Table 2. List of cathode activation energies in eV.....	35
Table 3. Degradation Comparison Rate for the cathodes using similar time frames.	51
Table 4. Long-term Impedance data summary	51
Table 5. Overpotential (V) on electrode for applied voltage on PBSCF symmetric cells.	66
Table 6. Overpotential (V) on electrode for applied voltage on NBSCF symmetric cells.	67
Table 7. Overpotential (V) on electrode for applied voltage on PBCC symmetric cells..	67
Table 8. Overpotential (V) on electrode for applied voltage on PBCC symmetric cells under 1.3 Amp/cm ²	85

LIST OF FIGURES

Figure 1. Human development (health, education, and living standards) vs. per capita power consumption for various countries [4].	1
Figure 2. SOFC schematic (a) oxide-ion conducting electrolyte, (b) proton conducting electrolyte. Also shows fuel and oxidant locations [8].	3
Figure 3. SOEC schematic with an oxygen conducting electrolyte [9].	4
Figure 4. Nyquist plot for a simple fuel cell impedance model showing the R_p of the cathode (bigger semicircle) being much bigger than the R_p of the anode (smaller semicircle) [11].	8
Figure 5. Cation segregation/ex-solution. Left side shows strong oxidizing atmosphere promotes A-site cation segregation. Right side shows reducing atmosphere can exsolve B-site metals [17].	9
Figure 6. Performance of various cathodes: BSCF, LSCF, etc. as cathode/YSZ/Ni-YSZ cells operated at 750 °C and 0.8 V. Air as the oxidant was supplied to the cathode side and the fuel $H_2-3\% H_2O$ was supplied to the anode side. [20].	10
Figure 7. Impedance of (a) SSNC and (b) BSCF cathodes at 600°C at varying CO_2 and balance air under OCV. CO_2 removed after 15 minutes. Symmetric cells as cathode/SDC/cathode [Adapted from Zhang Yuan et al. 23].	11
Figure 8. (I) is the adsorption of SO_2 on LSCF and $SrSO_4$ formation at grain boundary. (II) is $SrSO_4$ concentrating itself closer to the cathode/electrolyte interface [25].	13
Figure 9. Cr poisoning schematic for LSM, showing places around the cathode for Cr to react with [13].	15

Figure 10. Schematic of a cubic ABO_3 perovskite with (a) showing a $[BO_6]$ octahedra at the corner of the cube and (b) showing the A ion with a 12-sided polyhedral [33].
..... 17

Figure 11. Schematic of the PBSCF double perovskite crystal structure [32]. 17

Figure 12. Diagram of techniques used to analyze the cathode performance and stability.
..... 19

Figure 13. Schematic of the symmetric cell used for testing. 20

Figure 14. An example how EIS is used to measure durability of cathodes by showing cells with good (green arrow) and bad (red arrow) performance. LSCF and PBCC symmetric cells using SDC under OCV with various CO_2 concentrations at $750^\circ C$. ASR vs time (hr) [37]. 21

Figure 15. An example of a possible degradation mechanism for cathodes. Here, Strontium can segregate to the surface under strong oxidizing conditions to form SrO , which can react with other contaminates in the atmosphere [38]. 22

Figure 16. a). Location where symmetric cell is placed between 2 silver wires. b). testing components: alumina tube, alumina rod, and rubber stopper. 27

Figure 17. Shows how the symmetric cell testing apparatus is assembled into the alumina rod. 27

Figure 18. Fuel Cell Testing Rack. 28

Figure 19. Humidification System from Fuel Cell Technologies, Inc. 29

Figure 20. PTFE wrapped in heat tape that connects the humidification system output into the alumina rods to prevent water from condensing 30

Figure 21. Cross-section of the cathode symmetric cell, black line indicates the SDC pellet thickness of 500 microns.....	31
Figure 22. Porous cathode with the orange line showing the cathode thickness of 50 microns.....	32
Figure 23. Sample impedance plot on how to determine R_{ohmic} and R_p	33
Figure 24. Shows what happens to the measured EIS data if the electrolyte/ohmic resistance increases after testing.	33
Figure 25. Plots for cathode activation energy. Fitted lines for each cathode can be used to get a slope to calculate activation energy based on Equation 3.....	35
Figure 26. XRD showing the chemical stability of the cathodes: a). PBCC, b). PBSCF, c). NBSCF, and d). PNM before and after 500hrs in 40% moisture at 700°C.....	37
Figure 27. XRD on PNM after 500hrs in 40% moisture at 700°C with blue arrows show peak disappearances and red arrows show new peaks.....	38
Figure 28. NBSCF powder initial Raman scan.....	39
Figure 29. a). PBSCF powder and b). NBSCF powder Raman scan after 500hr in 40% moisture at 700°C.....	39
Figure 30. Raman shift for initial PNM powder for 2 samples. The two peaks represent $PrMnO_x$ and PrO_x	40
Figure 31. PNM powder Raman shift after 40% moisture exposure for 766 hours at 700°C.....	40
Figure 32: a). PBCC powder Raman scan after 500hr in 700°C with 40% moisture exposure. Sharp lines due to cosmic rays/artifacts. Orange arrows represent $BaCoO_3$ at around 610 cm^{-1}	41

Figure 33. Initial PBCC/SDC/PBCC symmetric cell ASR EIS data in ambient air at 700°C under OCV conditions. Cells 1-2 made with BL and Cells 3+ with NBL.	42
Figure 34. Initial PBSCF/SDC/PBSCF symmetric cell ASR EIS data in ambient air (~3% H ₂ O) at 700°C under OCV. Cells 1-2 made with BL and Cells 3+ with NBL.	43
Figure 35. Initial NBSCF/SDC/NBSCF symmetric cell ASR EIS data in ambient air (~3% H ₂ O) at 700°C under OCV. Cells 1-2 made with BL and Cells 3+ with NBL.....	44
Figure 36. PBSCF/SDC/PBSCF symmetric cell ASR EIS data after water promoting effect. Shows lowest ASR after moisture exposure. Testing conditions are 40% moisture and balance air at 700°C under OCV. Cells 1-2 made with BL and Cells 3+ with NBL.	45
Figure 37. PBCC/SDC/PBCC symmetric cells short term repeatability in 40% moisture and balance air at 700°C under OCV conditions. NBL error bars average 2 cells.	46
Figure 38. PBSCF/SDC/PBSCF symmetric cell short term repeatability in 40% moisture and balance air at 700°C under OCV. BL error bars average 2 cells and NBL error bars average 3 cells.	47
Figure 39. NBSCF/SDC/NBSCF symmetric cell short term repeatability in 40% moisture and balance air at 700°C under OCV. BL error bars average 2 cells and NBL error bars average 2 cells.	47
Figure 40. PNM/SDC/PNM symmetric cell long-term data in 40% moisture and balance air for 650hrs at 700°C under OCV.....	48

Figure 41. Long-term cathode/SDC/cathode ASR vs time(hr) in 40% moisture and balance air at 700°C for double perovskites under OCV.	49
Figure 42: SEM image of PBCC on the surface before and after symmetric cell testing (40% moisture and balance air) at 700°C under OCV.	50
Figure 43: SEM image of PBCC cross-section before and after symmetric cell testing (40% moisture and balance air) at 700°C under OCV.	50
Figure 44. a). bulk and b). surface of PBCC both after 1150hr symmetric cell testing in 40% moisture and balance air at 700°C under OCV.	52
Figure 45. PBSCF/SDC/PBSCF symmetric cell under constant alternating +/- 1.65 Volts at 18hr. Switch to 20% moisture at 0hr, and 30% moisture at 114hr. Balance air at 700°C. Plots voltage, current, and current density vs time (hr).....	56
Figure 46. Another PBSCF/SDC/PBSCF symmetric cell under constant alternating +/- 1.65 Volts at 18hr. Switch to 20% moisture at 0hr, and 30% moisture at 114hr. Balance air at 700°C. Plots voltage, current, and current density vs time (hr).	57
Figure 47. PBSCF/SDC/PBSCF EIS data under constant +/- 1.65 Volts at 18hr. Switch to 20% moisture at 0hr, and 30% moisture at 114hr. Balance air at 700°C. Shows error bars for 2 cells tested. Plots total resistance, ohmic resistance and ASR vs time (hr).	58
Figure 48. NBSCF/SDC/NBSCF symmetric cell under constant alternating +/- 1.7 Volts at 43hr. Initial 10% moisture at 0hr, switch to 20% moisture at 109hr, 30% moisture at 209hr and 40% moisture at 403hr. Balance air at 700°C. Plots voltage, current, and current density vs time (hr).....	59

Figure 49: Another NBSCF/SDC/NBSCF symmetric cell under constant alternating +/- 1.7 Volts at 43hr. Initial 10% moisture at 0hr, switch to 20% moisture at 109hr, 30% moisture at 209hr and 40% moisture at 403hr. Balance air at 700°C. Plots voltage, current, and current density vs time (hr). 60

Figure 50. NBSCF/SDC/NBSCF EIS data under constant +/- 1.7 Volts at 43hr. Initial 10% moisture at 0hr, switch to 20% moisture at 109hr, 30% moisture at 209hr and 40% moisture at 403hr. Balance air at 700°C. Shows error bars for 2 cells tested. Plots total resistance, ohmic resistance and ASR vs time (hr)..... 61

Figure 51. PBCC/SDC/PBCC long-term stability under constant alternating +/- 1.4 Volts at 18hr. Initial 20% moisture at 0hr, switched to 30% moisture at 114hr. Balance air at 700 °C. Plots voltage, current, and current density vs time. 63

Figure 52. Another PBCC/SDC/PBCC long-term stability under constant alternating +/- 1.4 Volts at 18hr. Initial 20% moisture at 0hr, switched to 30% moisture at 114hr. Balance air at 700 °C. Plots voltage, current, and current density vs time 64

Figure 53. PBCC/SDC/PBCC EIS long-term stability under constant +/- 1.4 Volts at 18hr. Initial 20% moisture at 0hr, switched to 30% moisture at 114hr. Balance air at 700°C. Shows error bars for 2 cells tested. Plots total resistance, ohmic resistance and ASR vs time..... 65

Figure 54. Raman spectra of PBSCF from Figure 47, NBSCF from Figure 50, and PBCC from Figure 70 symmetric cells after alternating voltage tests, and PBCC powder after moisture exposure for 500hrs at 700°C..... 68

Figure 55. Raman scan of initial PBCC powder, 2 samples 72

Figure 56. Raman scan of initial PBSCF powder, 2 samples. 72

Figure 57. Raman scans from PBCC symmetric cell after testing from Figure 53 73

Figure 58. XRD of Carbon Co-precipitated SDC vs. SDC reference (01-080-5538) from PDF-4+ database. 74

Figure 59. a) Midgrade SDC from Fuel Cell Materials b). Carbon Co-Precipitated SDC. CCP SDC has a finer grain size. 75

Figure 60. SEM image of PBSCF a) surface and b) cross-section before testing 75

Figure 61. SEM image of NBSCF a) surface and b) cross-section before testing..... 76

Figure 62. PBSCF symmetric cell a) surface and b) cross-section after testing (40% moisture, balance air) for 500hrs at 700 Celsius under OCV. 76

Figure 63. NBSCF symmetric cell a) surface and b) cross-section after testing (40% moisture, balance air) for 766hrs at 700 Celsius under OCV. 77

Figure 64. Long-term ASR for PBCC and PBSCF (both cells same) symmetric cells with SDC electrolyte in 40% moisture and balance air at 700 Celsius under OCV. 78

Figure 65. Long-term ASR NBSCF (both cells same) and PNM symmetric cells with SDC electrolyte in 40% moisture and balance air at 700 Celsius under OCV. 79

Figure 66: Data of a PBCC/SDC/PBCC with a constant alternating +/-1.8 Volts. It shows the voltage, current, and current density based on the time in hours. The orange line at 93hrs is when the air/moisture feed is switched to 40% moisture. 160hrs it is swapped to 10% moisture and 305hrs it is swapped to 20% moisture. The initial moisture is 0%. 700°C 80

Figure 67: Data of a PBSCF/SDC/PBSCF with a constant alternating +/-1.8 Volts. It shows the voltage, current, and current density based on the time in hours. The orange line at 93hrs is when the air/moisture feed is switched to 40% moisture.

160hrs it is swapped to 10% moisture and 305hrs it is swapped to 20% moisture.

The initial moisture is 0%. 700°C 81

Figure 68: EIS results for PBCC/SDC/PBCC under constant +/-1.8 volts for cells 1 and 2.

Cell 3 was not under voltage. The figure shows the total symmetric cell resistance, the electrolyte/ohmic resistance and R_p *area of one cathode vs time(hr). The orange lines are the same as Figure 67. 700°C 82

Figure 69: EIS results for PBSCF/SDC/PBSCF under constant +/-1.8 volts. The figure

shows the total symmetric cell resistance, the electrolyte/ohmic resistance and R_p *area of one cathode vs time(hr). The orange lines are the same as Figure 67. 700°C 83

Figure 70. PBCC/SDC/PBCC EIS data under constant +/- 1.5 Volts at 43hr. Initial 10%

moisture at 0hr, switch to 20% moisture at 109hr, 30% moisture at 209hr and 40% moisture at 403hr. Balance air at 700 °C. Current Density 1.3Amp/cm². Plots total resistance, ohmic resistance and ASR vs time..... 84

Figure 71. PBSCF symmetric cell after testing from Figure 67 and Figure 69. a). shows

cathode still adhered to the electrolyte while b). some sections of the cathode are delaminating from the electrolyte. 86

Figure 72. NBSCF symmetric cell after testing from Figure 48 to Figure 50 a). shows

cathode still adhered to the electrolyte while b). some sections of the cathode are delaminating from the electrolyte. 86

LIST OF SYMBOLS AND ABBREVIATIONS

PBCC	$\text{Pr}_1\text{Ba}_{0.8}\text{Ca}_{0.2}\text{Co}_2\text{O}_{5+\delta}$
PBSCF	$\text{Pr}_1\text{Ba}_{0.5}\text{Sr}_{0.5}\text{Co}_{1.5}\text{Fe}_{0.5}\text{O}_{5+\delta}$
NBSCF	$\text{Nd}_1\text{Ba}_{0.5}\text{Sr}_{0.5}\text{Co}_{1.5}\text{Fe}_{0.5}\text{O}_{5+\delta}$
PNM	$\text{Pr}_2\text{Ni}_{0.5}\text{Mn}_{0.5}\text{O}_{4+\delta}$
LSCF	$\text{La}_1\text{Sr}_{0.8}\text{Co}_{0.2}\text{Fe}_2\text{O}_{3-\delta}$
SSNC	$\text{SrSc}_{0.175}\text{Nb}_{0.025}\text{Co}_{0.8}\text{O}_{3-\delta}$
BSCF	$\text{Ba}_{0.5}\text{Sr}_{0.5}\text{Co}_{0.8}\text{Fe}_{0.2}\text{O}_{3-\delta}$
LSM	$(\text{La}_{0.85}\text{Sr}_{0.15})_{0.95}\text{MnO}_3$
LSCM	$\text{La}_{0.75}\text{Sr}_{0.25}\text{Cr}_{0.5}\text{Mn}_{0.5}\text{O}_{3\pm\delta}$
SDC	$\text{Sm}_{0.20}\text{Ce}_{0.80}\text{O}_{2-x}$
EIS	Electrochemical Impedance Spectroscopy
XRD	X-ray Diffraction
SEM	Scanning Electron Microscope
XPS	X-ray Photoelectron Spectroscopy
EXAFS	Extended X-ray Absorption Fine Spectroscopy
SOFCs	Solid Oxide Fuel Cells
SOECs	Solid Oxide Electrolyzer/Electrolysis Cells
ORR	Oxygen Reduction Reaction
OER	Oxygen Evolution Reaction
MIEC	Mixed Ionic Electronic Conductors
TPB	Triple Phase Boundary
R_p	Polarization Resistance

R_{ohmic}	Electrolyte Resistance
ASR	Area Specific Resistance
OCV	Open Cell Voltage
BL	Buffer Layer
NBL	New Buffer Layer
CCP	Carbon Co-Precipitated

SUMMARY

Solid Oxide Fuel Cells (SOFCs) can directly convert a wide variety of fuels to electricity efficiently. They can also be run in reverse as Solid Oxide Electrolysis Cells (SOECs) to produce hydrogen (and carbon-containing fuels) from electrolysis of water (and carbon dioxide). However, the kinetics of oxygen reduction reaction (ORR) on the cathode is often hindered by various contaminants, which may react with the cathode to form insulating phases and degrade fuel cell performance. The stability and performance of the cathode in moisture is critical to the cell performance as SOFCs and SOECs. Several state-of-the-art cathode materials are investigated in a high moisture environment to uncover their performance and degradation mechanism.

First, powders of electrode materials were analyzed for any degradation before and after long-term moisture exposure using XRD to probe the bulk and Raman Spectroscopy to probe the surface. SEM was also used to characterize any morphological changes during the exposure. Second, electrochemical impedance spectroscopy (EIS) was used to monitor the long-term performance of symmetric cells under various conditions. Finally, current-voltage relationships of symmetric cells were acquired under typical operating conditions for SOFCs and SOECs to determine the polarization resistance, stability and durability of the cathode materials.

CHAPTER 1: INTRODUCTION

1.1 Demand for Clean Energy

One of the greatest issues that humanity faces in the next coming years is energy [1]. Currently, most of the world uses fossil fuels for electricity in their homes, for transportation, and for industrial applications. However, fossil fuels are a finite resource, so it is unsustainable in the long run and its pollution causes global warming and harms the environment. Even though coal is slowly being phased due to the emergence of fracking, oil and natural gas are still fossil fuels even though they produce less pollution than coal. With the increasing global record high temperatures and increasingly severe natural disasters, the global carbon footprint must be decreased to prevent the worst-case scenario of the global ice caps melting [2, 3]. Another issue is as third world countries develop and as the population rises, the demand for energy will increase as shown in Figure 1 [4].

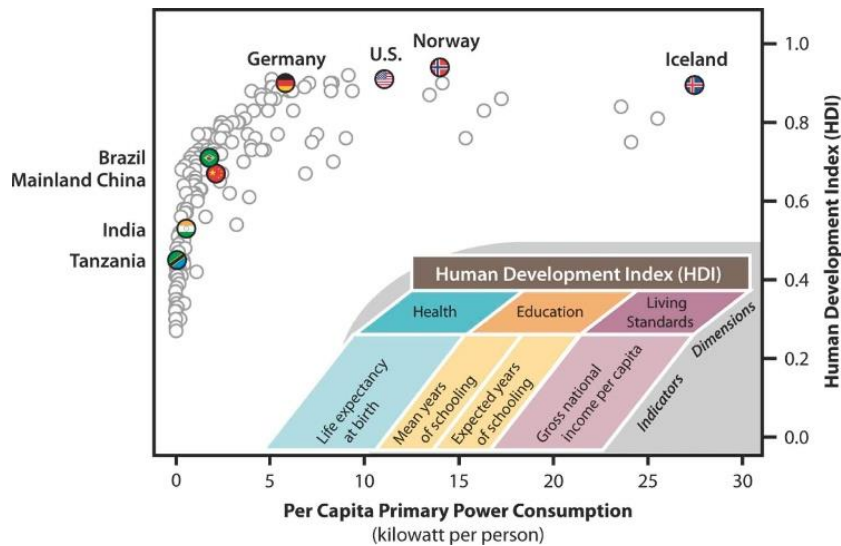


Figure 1. Human development (health, education, and living standards) vs. per capita power consumption for various countries [4].

1.2 Why Fuel Cells?

An alternative and sustainable energy technology must be developed to eventually replace fossil fuels. One promising alternative is fuel cells, which have several advantages: they can directly convert chemical energy to electrical energy, are not limited to the Carnot efficiency, and are typically made of inexpensive materials [5].

Of the fuel cell family, one type of fuel cells is called Solid Oxide Fuel Cells (SOFCs). Current SOFCs are operated at ~600-800°C to produce viable conductivity for an electric current to be produced due to diffusion in the electrolyte [5]. The current infrastructure uses electricity generated from fossil fuels. Power plants produce electricity, which is then sent out across transmission lines and then distributed to the location where it is used. Electricity produced this way is only 33-44% efficient depending on the fuel used and suffers from 5% losses on average from transmission and distribution [6]. If the power plant is replaced by a SOFC plant, the efficiency would not only increase but also the current infrastructure would not have to be replaced. There is also the option for large scale buildings or chemical plants to generate electricity locally and avoid power loss through the transmission lines if SOFCs are used. Other alternative energies such as solar and wind are variable in nature, thus limiting the production location and efficiency. Biofuels also have the issue of needing large areas of land and water to grow the crops needed to produce biofuels [7].

1.3 Basics of SOFCs/SOECs

The schematic of the SOFC is shown in Figure 2. It consists of a solid conducting electrolyte that is sandwiched in between a porous cathode and anode. The cell is run on a redox reaction where reduction occurs at the cathode and oxidation occurs at the anode. The reaction at the cathode is called the oxygen reduction reaction (ORR), because oxygen (air) is taken in to be reduced to form the ion that moves through the electrolyte. Fuel is oxidized at the anode to mainly produce water vapor and electrons that flow to produce electric current under high temperature operation. Fuel cells are classified into two categories: oxygen ion or proton conducting electrolyte [8]. SOFC's have the oxide in the name since typically oxygen is the ion moving across the electrolyte.

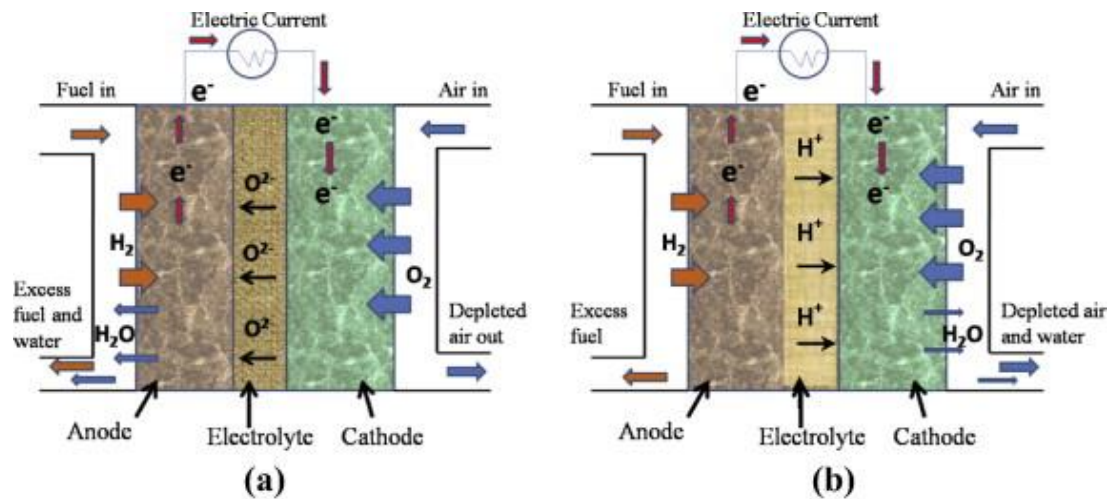


Figure 2. SOFC schematic (a) oxide-ion conducting electrolyte, (b) proton conducting electrolyte. Also shows fuel and oxidant locations [8].

When SOFCs are run in reverse, they are called Solid Oxide Electrolysis Cells (SOECs). SOECs consume electricity for the steam electrolysis of H_2O into H_2 shown in Figure 3 and can also convert carbon dioxide into carbon monoxide or other hydrocarbons. This process would be greatly beneficial because of the current hydrogen source. Currently,

over 90% of the H₂ consumed is produced from hydrocarbons through steam reforming, which is costly and emits a great amount of CO₂ [9]. Steam reforming using methane is about 65-75% efficient and while the efficiency for SOECs to produce hydrogen is unclear; SOECs is more efficient in the splitting of water both thermodynamically and kinetically than the process in steam reforming [9, 10]. The cathode in SOFCs that does ORR, does the oxygen evolution reaction (OER) in SOECs. The OER is the process of generating a molecular oxygen shown in the air electrode in Figure 3. By combing SOFCs and SOECs, the system can generate electricity in SOFC mode and then produce hydrogen in SOEC mode.

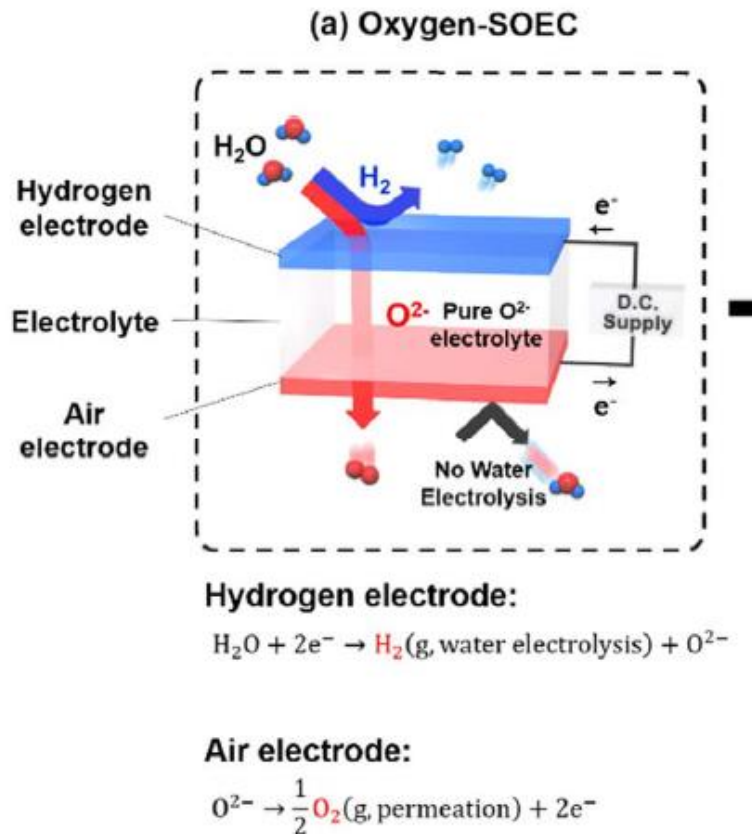


Figure 3. SOEC schematic with an oxygen conducting electrolyte [9].

1.4 Research Objective

The key issue is that SOFCs are still limited by the cathode polarization resistance as the rate limiting step [11]. Therefore, there is intensive research done on improving the cathode to be more resistant to cathode degradation. One type of cathode that have drawn the attention of researchers is perovskite cathodes, due to its high electro-catalytic activity. To further increase performance, more reaction area to transport electrons and oxygen is needed. A new type of perovskite cathode called the mixed ionic electronic conducting (MIEC) ceramic is created like LSCF ($\text{La}_1\text{Sr}_{0.8}\text{Co}_{0.2}\text{Fe}_2\text{O}_{3-\delta}$) [12]. However, these single perovskite structure suffer from degradation due to contaminants such as humidity, carbon dioxide, sulfur, etc. [13]. Improving upon the perovskite structure, new double perovskite cathodes have been recently created, but the lack of information of the structure and degradation mechanism due to the contaminants is still unclear.

This research attempts to improve the understanding of how contaminants, mainly high-water vapor content affects the stability and performance of the double perovskite cathodes for SOFCs/SOECs. These high-performance cathodes for SOFCs may not be stable under high concentrations of water vapor needed for SOECs. Recent studies of SOECs have had steam content anywhere from 10-45% of the total gas feed [9, 14]. The high H_2O content may react with the electrode material and increase the polarization resistance and degradation rate. Therefore, the goal is to explore the electrochemical performance and the structural changes in the new double perovskite cathodes for SOFCs/SOECs at high humidity through impedance, XRD, and Raman Spectroscopy. By testing the double perovskites in high humidity, it can also elucidate if the cathodes have suitable performance for ORR and OER activities under reversible conditions. Knowledge

of the degradation mechanism of the new cathodes could be used to further develop contaminant resistant cathodes for longer SOFC run times.

1.5 Thesis Structure

SOFCs and why they are being researched was introduced here in Chapter 1. Chapter 2 will go over some of the current contaminants that hinder cathode performance shown in literature. State-of-the-art cathodes tested in this work and how they were chosen will also be introduced. Chapter 3 will show the technical approach to accomplish the research objectives. Chapter 4 will examine the results of the state-of-the-art cathodes under high moisture content at 700 Celsius. The final two parts will consist of any conclusions that can be made and recommendations for future work. Appendix A will include some supplementary figures to support the results.

CHAPTER 2: LITERATURE REVIEW

2.1 Analyzing Cathode Degradation

SOFC cathodes have many different structures such as spinel, pyrochlore, Ruddlesden-Popper, etc. [15]. The focus of this literature review will mainly be on the perovskite-type cathodes that contain alkaline earth metal elements. One of the major causes of cathode degradation is when the cathode reacts with contaminants. There are many contaminants such as water, carbon dioxide, chromium compounds, silicon compounds, and sulfur SO_x compounds. When these compounds poison the cathode, the performance degrades as seen by the increased cathode polarization resistance (R_p) [11].

The Oxygen Reduction Reaction (ORR) in the cathode is much slower than the anode reaction when it comes to kinetics, therefore the cathode R_p is usually much bigger [11]. Thus, it is important for the cathode to be corrosion resistant since the ORR is the rate limiting step. An example of the R_p difference shown on the impedance plot is shown in Figure 4.

The book Fuel Cell Fundamentals by O'Hayre et al. goes into electrochemical impedance spectroscopy (EIS) analysis into far more detail. As an example, increasing water content will typically increase the corrosion rate (or increasing cathode R_p) and this is paralleled by greater surface reaction rates on the cathode as humidity rises [13, 16]. This may be attributed to the surface cation segregation, meaning a specific cation in the cathode will rise to the cathode surface. The challenges and degradation mechanisms for cathode degradation will be discussed in later sections.

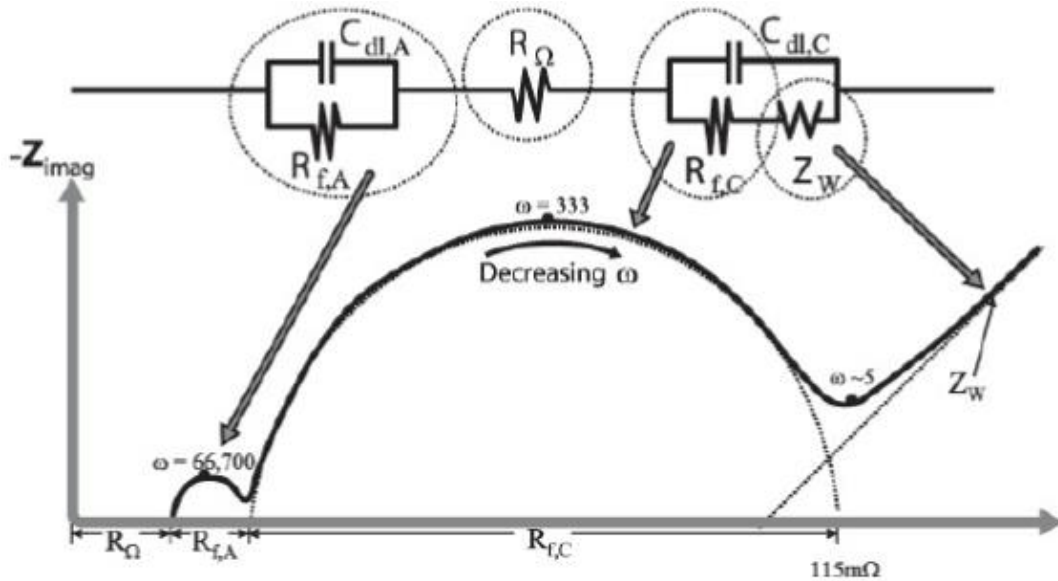


Figure 4. Nyquist plot for a simple fuel cell impedance model showing the R_p of the cathode (bigger semicircle) being much bigger than the R_p of the anode (smaller semicircle) [11].

2.2 Water

One of the major issues with cathode degradation comes from poisoning due to the cathode reacting with gaseous water. Water is always present in ambient air (~3% water), where most SOFCs may operate at, and most SOFCs will also produce water as a byproduct. SOFCs on the cathode side are in a strong oxidizing atmosphere at high temperature and with moisture, cations such as La, Sr, and Ba tend to segregate to the surface as shown in Figure 5 [17]. The cations could then hinder the ORR by forming a blocking layer. It is also known that water corrosion on the cathode is reversible until a certain point [13].

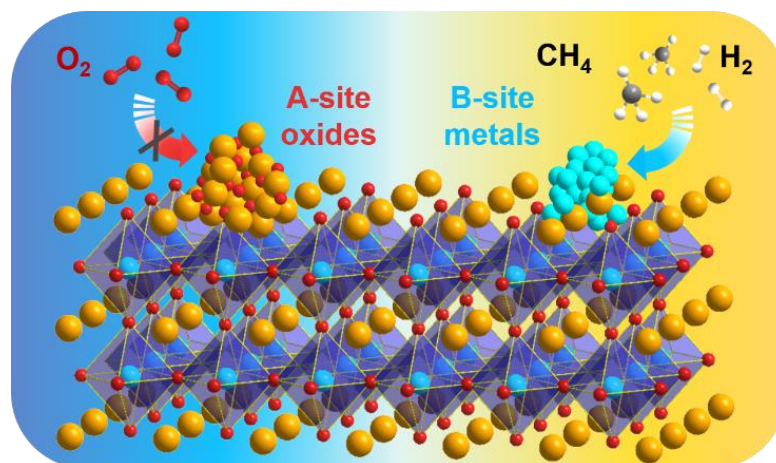


Figure 5. Cation segregation/ex-solution. Left side shows strong oxidizing atmosphere promotes A-site cation segregation. Right side shows reducing atmosphere can exsolute B-site metals [17].

To overcome the contamination issues, the mechanism and how the degradation occurs must be understood. Huang, Yi-Lin et al. discovered that water and oxygen may share the same surface exchange sites, which would slow down the ORR [13, 18]. This would also explain why the cathode performance degradation increases with increasing humidity [16]. It has also been discovered that alkali earth metals, such as strontium (Sr) in LSCF ($\text{La}_{0.6}\text{Sr}_{0.4}\text{Co}_{0.2}\text{Fe}_{0.8}\text{O}_{3-\delta}$)/LSM ($(\text{La}_{0.85}\text{Sr}_{0.15})_{0.95}\text{MnO}_3$), tends to segregate out to the surface under humidity [16, 19]. Other A-site elements have also been a concern, like Lanthanum (La) and Barium (Ba) [13]. It has been hypothesized that the water-soluble metals, like Sr and La, could react with water and the remaining materials from the bulk to form oxides or hydroxides that further increase metal segregation from the cathodes [16, 19]. Different cathodes would have different reaction mechanisms, where only possible reaction processes have been reported so far. Regardless, once enough A-site materials have been removed or enough insulating phases are formed, the cathode performance, transport, etc. will be affected [16]. Metal segregation has also been shown to exist in

cathode materials that do not have alkali earth elements shown in Figure 6 [20]. Segregation of A-site cations that react with other compounds to form a blocking layer, oxides or hydroxides mentioned earlier, may be another cause of long-term performance degradation.

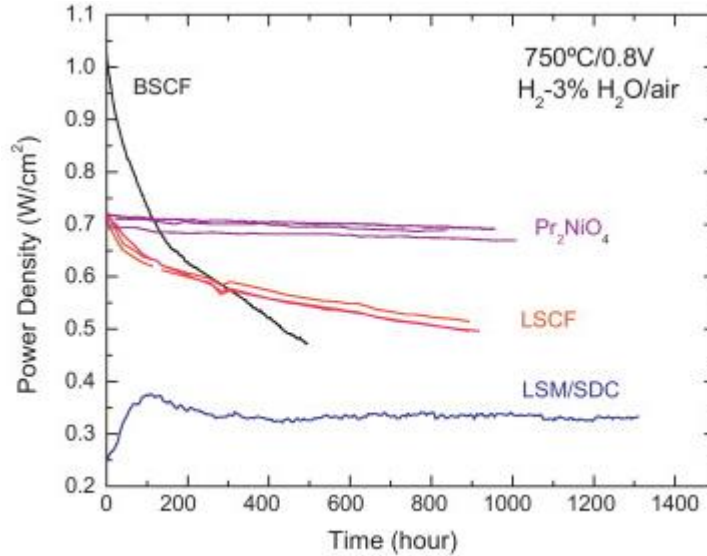


Figure 6. Performance of various cathodes: BSCF, LSCF, etc. as cathode/YSZ/Ni-YSZ cells operated at 750 °C and 0.8 V. Air as the oxidant was supplied to the cathode side and the fuel H₂-3% H₂O was supplied to the anode side. [20].

2.3 Carbon Dioxide

Hydrocarbons can be used as the fuel, thereby forming carbon dioxide instead of water. Therefore, one interesting research area is on using CO₂ as a fuel for fuel cells since the current infrastructure produces an abundance of CO₂ from the burning fossil fuels and this would also help relieve the rising atmospheric CO₂ level [21, 22]. Thus, carbon dioxide resistant cathodes are also important in making reversible fuel cells more viable. SOECs runs fuel cells in reverse for the electrolysis of water or carbon dioxide to produce hydrogen and carbon monoxide, respectively. This would be greatly beneficial to produce hydrogen

and other useful chemicals [22]. CO₂ causes corrosion on most cathodes by hindering the ORR, although iron and niobium in the B site have shown resistance to the corrosion [13]. Most cathode materials have some amounts of alkali earth metals, which carbon dioxide has a high affinity to react with [20].

Carbon dioxide will hinder the ORR by competing against water for the active sites on the cathode surface due to CO₂ having an easy tendency for adsorption [13]. As water and CO₂ compete, the cathode's performance degradation is reversible depending on the temperature and exposure time [13]. The CO₂ will also want to react with A-site cations (especially Sr, Ba, and La) to form carbonates on the cathode surface because it is thermodynamically favorable [13, 23]. The carbonates would form a blocking layer that would also hinder the ORR and lower electrochemical performance [23]. As an example, Figure 7 shows the effect of CO₂ on the performance for 2 different cathodes: SrSc_{0.175}Nb_{0.025}Co_{0.8}O_{3-δ} (SSNC) and Ba_{0.5}Sr_{0.5}Co_{0.8}Fe_{0.2}O_{3-δ} (BSCF).

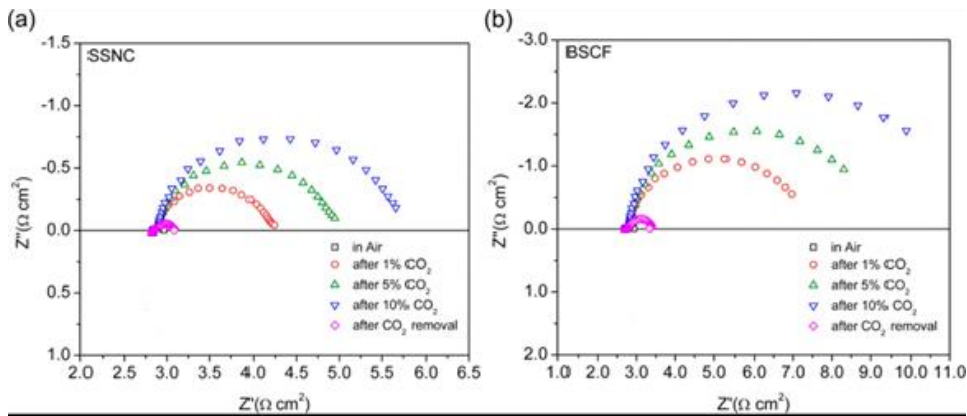


Figure 7. Impedance of (a) SSNC and (b) BSCF cathodes at 600°C at varying CO₂ and balance air under OCV. CO₂ removed after 15 minutes. Symmetric cells as cathode/SDC/cathode [Adapted from Zhang Yuan et al. 23].

2.4 SO_x Compounds

A third contaminant is sulfur SO_x compounds which is in a trace amount in air. The source of sulfur for lab testing is typically feeding in a SO₂-air mix with the sulfur dioxide in the ppm (parts per million) concentration. It has been shown in the past that SO_x compounds can react with the cathode material to form sulfates, under a ppm level for SO₂ [24]. The normal level of SO₂ in the atmosphere is ~10 ppb (parts per billion) level and there seems to be a minimum level of SO₂ needed for a reaction to take place in the cathode. [24, 25]. This will be important if the SOFCs will be used in processes containing combustion byproducts or synthesis gases, because they contain traces of sulfur compounds. Also, the performance degradation depends on the contaminant concentration, which may differ depending on the cathode [24, 25].

The sulfur degradation in the cathode seems to originate from SO₂ wanting to react with the Sr component to form SrSO₄, where the amount of SrSO₄ formed is dependent on the sulfur concentration and the tendency of SO₂ to adsorb onto the cathode surface [24, 25]. Some examples are the cathodes La_{0.6}Sr_{0.4}CoO_{3-δ} (LSC) and LSCF. LSC has the A-site cations degrade into SrSO₄ and La₂O₂SO₄ on top and a cobalt phase on the bottom [26]. LSCF is similar with SrSO₄, but with a CoFe₂O₄ phase since LSCF has another B-site element [25]. This is shown in Figure 8.

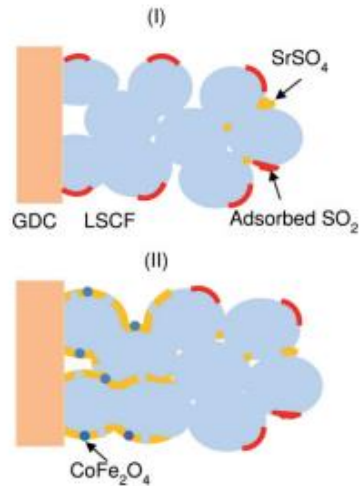


Figure 8. (I) is the adsorption of SO₂ on LSCF and SrSO₄ formation at grain boundary. (II) is SrSO₄ concentrating itself closer to the cathode/electrolyte interface [25].

In either case, the mechanism for reaction seems to originate at the active sites where SO₂ can react with half an oxygen molecule and SrO (A-site cation oxides) to form SrSO₄ [27]. This may be facilitated under humidity since Sr tends to segregate to the surface and with humidity, the A site cations that go to the surface may form oxides or hydroxides. A majority of the alkaline earth metal perovskite cathodes contain Sr, so the non-Sr cathodes may degrade differently.

2.5 Chromium

Another major source of cathode contaminant is from the materials used to create the fuel cell stacks. For commercialization, it is not feasible to use a single cell, instead multiple cells are stacked together to create a fuel cell stack. Metallic interconnect materials are used to electrically connect the anode of one cell to the cathode of the neighboring cell [28]. Due to the advance of fuel cell technology, SOFC operating temperature has been reduced to ~600-800°C, so interconnect materials are shifting from ceramics to metals.

Therefore, for largescale production of SOFCs, cheap metallic interconnects with high thermal and electronic conductivity must be used [29]. Most of these materials so far have been nickel, iron, or chromium alloys [28, 29]. The main problem with the interconnect materials is chromium and that other interconnect alloys all contain some amounts of it. At high temperatures, the chromium will form a protective layer of Cr_2O_3 and in oxidizing atmospheres, CrO_3 and $\text{Cr}(\text{OH})_2\text{O}_2$ can be formed [29]. The validity of the formation of CrO_3 and $\text{Cr}(\text{OH})_2\text{O}_2$ is still in debate, while experimental evidence has instead shown some support for a nucleation theory. Due to surface segregation of cations, most likely due to water, the cations (nuclei) can react with chromium oxide; this reduces the ohmic resistance of the fuel cell stacks [13, 29].

The chromium deposition mechanism is still being debated upon, however the effect of Cr on cathode materials is complex [13, 29]. What has been discovered so far is that the cathode degradation results from Cr compounds forming on the cathode surface, on the cathode/electrolyte interface, or homogeneous degradation [13, 30].

An example is shown in Figure 9 for LSM. For LSM, predominately, Mn ions are formed from the B-site during polarization, which can then react with Cr_2O_3 [29]. This is a spinel $(\text{Mn,Cr})_3\text{O}_4$ phase at the TPB (Triple Phase Boundary) that can divert oxygen ions away from the electrolyte to reduce performance [13]. TPB is where the electrode, electrolyte, and fuel meet to produce electricity from the electrochemical reactions. Formation of LaMnO_3 and SrCrO_4 on the LSM surface and its affects is still unclear.

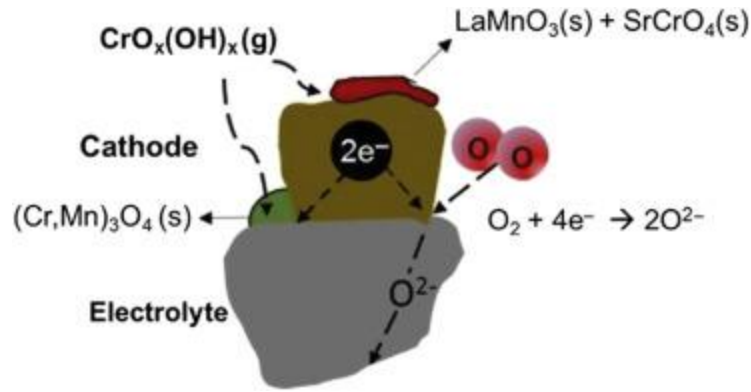


Figure 9. Cr poisoning schematic for LSM, showing places around the cathode for Cr to react with [13].

Another example, LSCF forms SrCrO₄ since it is thermodynamically favorable and kinetically fast [29]. This is not the case for BaCrO₄. As a result, a blocking layer is formed to hinder oxygen from getting to the active sites. A third cathode La₂NiO_{4+δ} (LNO), undergoes homogeneous degradation under Cr poisoning by forming La(Cr,Ni)O₃ [29]. Studies have also shown that humidity will speed up the rate of Cr deposition [13, 31].

2.6 Silicon

The last contaminant reviewed is glass-based sealing materials, which are used to seal the fuel cell stacks. These glass-based materials contain silicon that can be released into the gas stream, causing cathode poisoning and the Si concentration has been observed to increase over time [13, 31]. The silicon poses several issues. It has been reported that the silicon can react with the electrolyte to form an insulating phase that segregates the grain boundaries. This would lower the conductivity of the cell [13]. In addition, recent cathode studies have found a thin silicate layer on the cathode, and it is assumed that the layer can hinder ORR by blocking the active sites [13].

Like chromium, the formation of silicon (Si) species is increased with the presence of humidity and even a thin silicate layer can block the active sites needed for ORR [13]. The mechanism starts with the glassy sealing material under humid temperatures. Solid SiO_2 can react with two gaseous water molecules to form gaseous Si(OH)_4 [13]. A possible corrosion mechanism is the segregated Sr on the cathode surface, which can exist as an oxide or hydroxide, can react with Si(OH)_4 to form Sr-silicates [13]. Schrodler, Nina et al. confirmed the presence of Sr/La-silicates on LSC and LNO [30, 31]. Therefore, to reduce cathode degradation due to contaminants, prevention of A-site cations segregating to the surface and preventing the cathode from reacting is a critical factor.

2.7 Material Selection for this work

Of the perovskite type cathodes, double perovskite cathodes have recently shown interesting results in literature. The double perovskite cathodes chosen to be analyzed in this research are $\text{Pr}_1\text{Ba}_{0.8}\text{Ca}_{0.2}\text{Co}_2\text{O}_{5+\delta}$ (PBCC), $\text{Pr}_1\text{Ba}_{0.5}\text{Sr}_{0.5}\text{Co}_{1.5}\text{Fe}_{0.5}\text{O}_{5+\delta}$ (PBSCF), and $\text{Nd}_1\text{Ba}_{0.5}\text{Sr}_{0.5}\text{Co}_{1.5}\text{Fe}_{0.5}\text{O}_{5+\delta}$ (NBSCF). Regular perovskites for SOFCs follow the general ABO_3 formula where A is a rare earth or alkaline earth metal ion, B is the transition metal ion, and O is oxygen [32]. The schematic for an ABO_3 perovskite is shown in Figure 10 where the yellow atom is the A-site ion, the green atom is the B-site ion, and the red atom is oxygen.

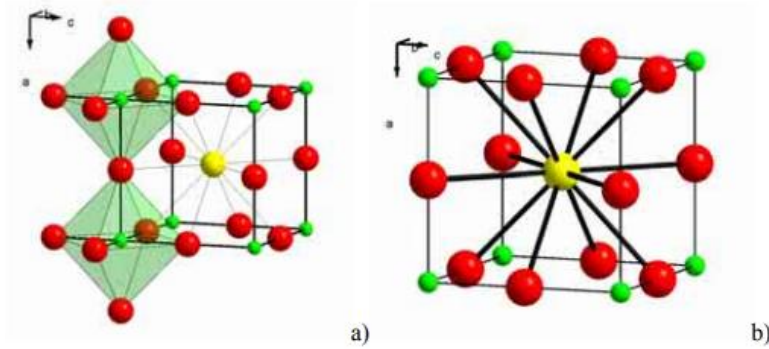


Figure 10. Schematic of a cubic ABO_3 perovskite with (a) showing a $[BO_6]$ octahedra at the corner of the cube and (b) showing the A ion with a 12-sided polyhedral [33].

Double perovskites generally have the form $AA'B_2O_{5+\delta}$ and are the result of doping A' or B' site cations into perovskites [32]. The ideal schematic of a double perovskite ($PrBaCo_2O_{5+\delta}$) is $[BaO]-[CoO_2]-[PrO_\delta]-[CoO_2]-[BaO]$ and the schematic in Figure 11 below is specifically for PBSCF [32].

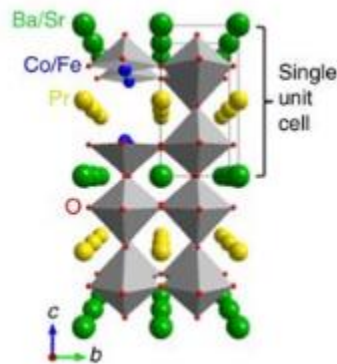


Figure 11. Schematic of the PBSCF double perovskite crystal structure [32].

Unlike LSCF, PBCC was shown to have improved performance in the presence of ambient air (3% moisture) from previous studies done in the group. In PBSCF and NBSCF, the substitution of Sr and Fe was made into the A and B sites. By inserting Sr into the A

site of the ABO_3 perovskite, there would be less Ba, which has a higher tendency to segregate out. Replacing some Co with Fe would increase the stability of the material as well as increase ion diffusivity and ORR activity [34, 35]. The perovskite PNM ($Pr_2Ni_{0.5}Mn_{0.5}O_{4+\delta}$) was composed of a mix of perovskite PNM and PrO_x phases was chosen because it showed great stability in 3% humidified air and hydrogen [36].

CHAPTER 3: METHODOLOGY

3.1 Technical Approach Overview

Figure 12 shows a diagram of the techniques used to analyze the cathode performance and stability before and after exposure to % water vapor. To analyze the structural stability of the cathodes, XRD (Panalytical XPert PRO Alpha-1 XRD) is used to get the bulk phase composition while Raman (1998 Renishaw InVia Raman spectrometer) is used to get the surface composition and structure of cathode powders. Raman is also taken on the tape casted cathodes after symmetric cell testing to compare with the data from the cathode powders. SEM (Hitachi SU8230) is used to characterize the morphology of the bulk and surface of the cathode. Lastly, EIS using symmetric cells are tested to characterize the ORR/OER activity (electrochemical performance) of the cathodes.

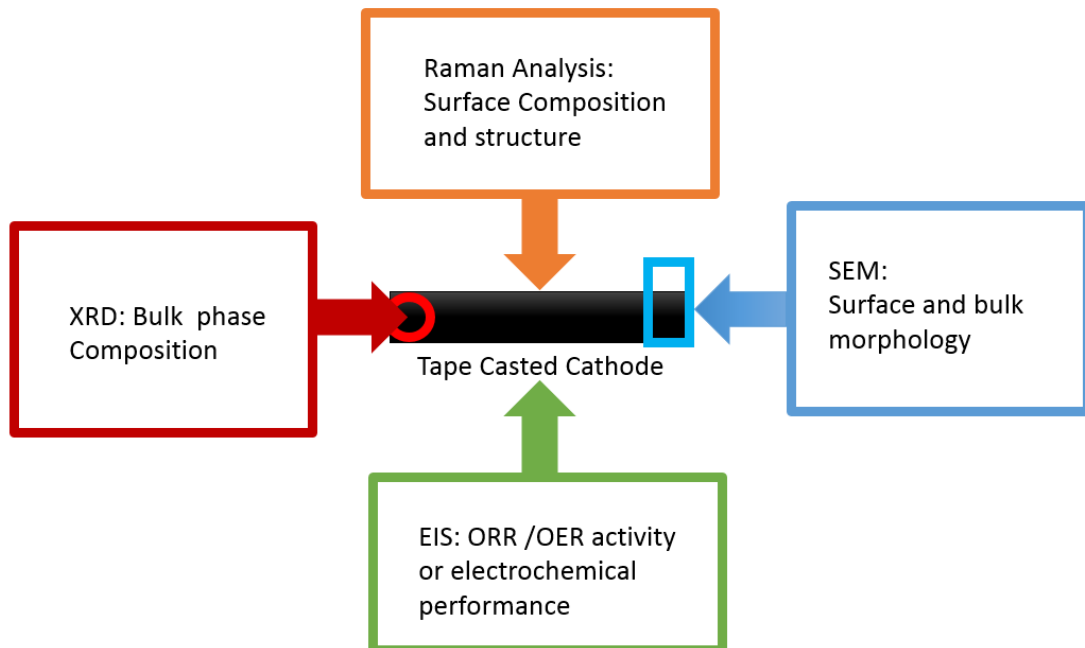


Figure 12. Diagram of techniques used to analyze the cathode performance and stability.

A schematic of symmetric cells fabricated for testing of the cathode performance and stability is shown in Figure 13 below. They are fabricated with a dense electrolyte with 2 porous cathodes on each side. The atmosphere the cell will be exposed to are % water vapor/moisture and balance air. The fabrication process for the symmetric cells will be explained in the following sections of this chapter.

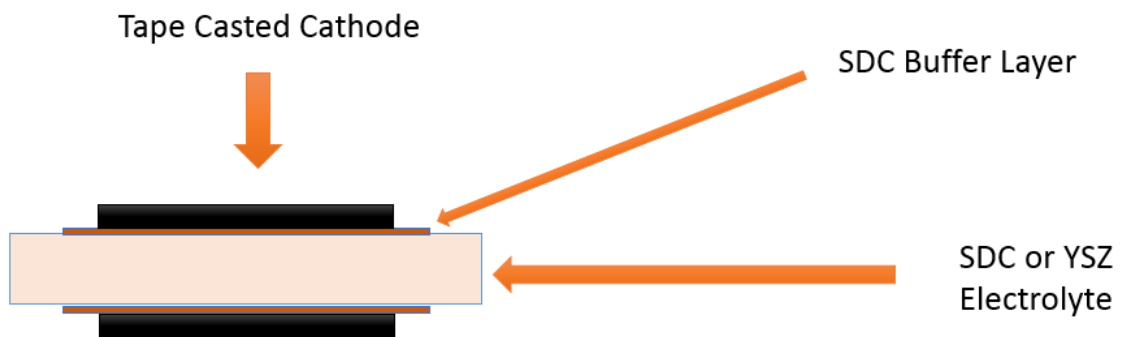


Figure 13. Schematic of the symmetric cell used for testing.

Shown in Figure 14, the green arrow shows cells of good performance while the red arrow shows cells of bad performance. Good performance is characterized by little to no change in the ASR value or in the R_p values on the semicircles top right of Figure 14. Information on calculating the ASR and on reading EIS data will be explained in the next chapter. Bad performance is characterized by the red arrow, which means cathode degradation occurs, thus there is a big increase in ASR.

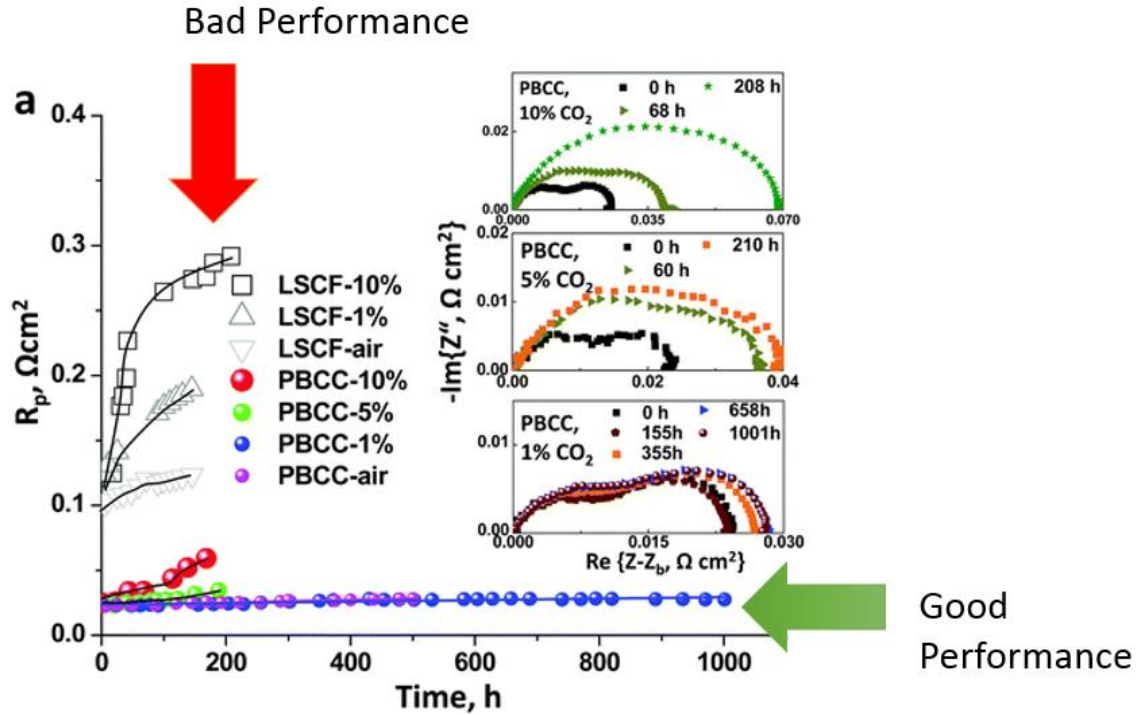


Figure 14. An example how EIS is used to measure durability of cathodes by showing cells with good (green arrow) and bad (red arrow) performance. LSCF and PBCC symmetric cells using SDC under OCV with various CO_2 concentrations at 750°C . ASR vs time (hr) [37].

When cathode degradation occurs, typically an insulating phase is formed on the cathode surface or the new phase is less active for ORR/OER as shown in Figure 15. In Figure 15, SrO is formed from cation segregation (discussed in Chapter 4), which can already hinder the ORR by blocking oxygen from the cathode [38]. It also has a high tendency to react to form other phases. An example is in CO_2 atmospheres, where SrCO_3 is formed due to thermodynamic favorability [23]. Therefore, it is reasonable to use Raman to see if there are any new phases formed on the surface after testing. XRD is also used because the surface and bulk may have different degradation pathways because the cathode surface is the interface where the high % water vapor can react with. If degradation does occur, there may be a new morphology that formed, which can be seen using SEM.

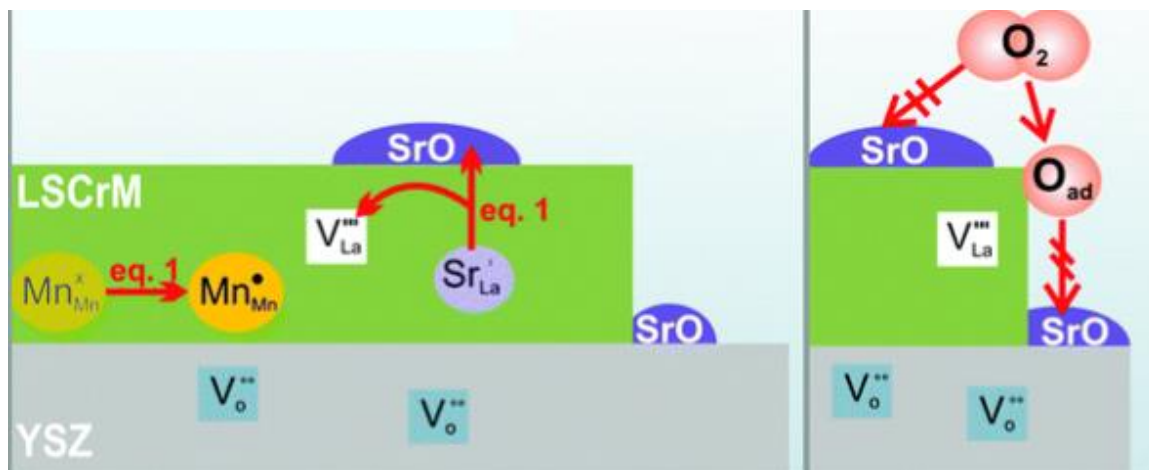


Figure 15. An example of a possible degradation mechanism for cathodes. Here, Strontium can segregate to the surface under strong oxidizing conditions to form SrO, which can react with other contaminants in the atmosphere [38].

3.2 Powder Synthesis

The experiments needed to test the stability of the cathode powders and their electrochemical impedance performance in high moisture. The cathode powders were synthesized by the combustion method by using citric acid and ethylene glycol as fuel (pechini method). ACS reagent grade with over 99.5% purity citric acid from Sigma-Aldrich and laboratory reagent grade 99+% ethylene glycol from VWR Chemicals were used. Metal Nitrates of the A and B site cathodes were added to a 1000ml beaker based on the A and B site elements in the cathode composition of PBCC, PBSCF, and NBSCF. The amount of citric acid added was equal to the total moles or total composition of metal nitrate precursors. Citric acid and ethylene glycol were added in a 1:1 weight ratio. Enough distilled water was added to dissolve all the compounds on a hotplate with a stir bar.

The precursors for combustion are listed below. Precursors from Sigma-Aldrich were 99.9% purity Praseodymium(III) nitrate hexahydrate, ACS 98+% Cobalt(II) nitrate

hexahydrate from, ACS 98+% Iron(III) nitrate nonahydrate, 99% Calcium nitrate tetrahydrate, and 99% Manganese(II) nitrate tetrahydrate Precursors from Alfa Aesar were 99.9% Neodymium(III) nitrate hexahydrate, ACS 99+% Barium Nitrate, and 98% Nickel(II) nitrate hexahydrate. The Strontium Nitrate used was from Johnson Matthey Chemical Company.

Once the solution is homogeneous, the hotplate is heated to ~450°C for combustion. The resulting powder is then calcined at 900°C for 2 hours and ball milled for 24 hours in ethanol to achieve homogenous particle size. For XRD and Raman analysis, the initial powders are calcined again at 1100°C for 2 hours at a ramp rate of 2°C/minute to achieve the double perovskite phase.

3.3 Fabrication of the Cathodes

To create cathodes for symmetric cell testing, the cathode powders are tape casted.

The initial mixture in a small bottle is:

- 10grams of cathode powder
- 1g of graphite(solid)
- 0.36g of fish oil
- 2.88g of ethanol (or 3.6ml)
- 3.2g of xylene (or 4 ml)
- 30 zirconia balls in bottle

0.66g of Polyalkylene glycol, 0.34g of Butyl Benzyl Phthalate, and 0.62g of Polyvinyl Butyral (PVB) are added to the bottle after each 12-hour intervals. Lastly, the bottle is ball milled for another 12 hours, for a total of 48 hours to complete the tapecasting cathode

slurry. The top of the bottle is cut off and then degassed at ~25-30mmHg to remove the air bubbles. The tapecasting blade is set to a height so that the cathode tape is 50 microns thick. A mesh is used to catch the zirconia balls so only the slurry gets tapecasted. To prevent dust from sticking to the wet tape, a cover is used after the tape is completely tape casted. Once the tape is dried, a hole of the desired size is punched out to produce coin cells. Here, 0.25in cathode coin cells are punched out.

3.4 Fabrication of Dense Electrolyte

The electrolyte used for symmetric cell testing was SDC since it is humidity resistant. Commercial mid-grade SDC is bought from Fuel Cell Materials. 0.24grams of SDC is pressed in a 10mm die press to about 4-5 tons. SDC pellets are then sintered at:

- Ramp 1°C/min to 600°C
- Hold 600°C for 1 hour
- Ramp 5°C/min to 1450°C
- Hold 1450°C for 5 hours
- Cool to 600°C at 3°C/min

Sintered SDC pellets are cleaned with ethanol and kimtech science wipes. An SDC buffer layer is used to adhere the cathode tapes onto the SDC electrolyte. The SDC buffer layer solution was made of 1g of Co-precipitated SDC, 4g V006 from Heraeus or ink vehicle SKU: 311237 from Fuel Cell Materials, and 20g of acetone that was ball milled for at least 2 weeks and is continuously ball milled when not in use. Here, ball milling refers to a bottle rolling.

3.5 Carbon Co-Precipitated SDC

For double perovskite cathodes, the buffer layer must be more homogenous and of finer particle size to better adhere the cathode to the electrolyte. Therefore, carbon co-precipitated (CCP) SDC is used in the SDC buffer layer solution. The reagents used were 99% Ammonium hydrogen carbonate (NH_4HCO_3) from Alfa Aesar, and 99% Cerium(III) nitrate hexahydrate and 99.9% Samarium(III) nitrate hexahydrate from Sigma-Aldrich.

1.5812 grams of NH_4HCO_3 and distilled water is used to prepare a 200ml solution of 0.1 molarity ammonium bicarbonate solution. A second solution of 100ml of 0.1 molarity of ceria and samarium is also prepared. The ceria and samarium are added in a 4:1 ratio by weight with the ceria and samarium added having a concentration of 0.5 and 0.25 mol/L respectively. Distilled water is used to dissolve the ceria/samarium nitrates to 100ml. A stir bar is placed into the bicarbonate solution and a pump is used to titrate the ceria/samarium solution into the bicarbonate solution at a rate of 10ml/min. It is okay if the pump is too slow and the rate is at least 7.5ml/min. After titration, let the solution mix for 30 minutes, then stop the stir bar and let the solution sit for 15 minutes. Decant the top opaque liquid and pour the milky white solution into 4 centrifuge tubes. Make sure each tube has the same weight. Centrifuge the tubes at 6000rpm for 5 minutes. Repeat these 3 times in distilled water. Between each centrifuge, decant the liquid and refill with fresh distilled water. Make sure the white mixture on the sides are fully mixed, i.e. no floating particles, before centrifuging again. Repeat the centrifuge steps 2 more times, but this time with ethanol. The result is that the mixture on the side should turn into a pale white-yellowish color. Dry the mixture on the side of the centrifuge vials, then calcine the SDC powder at 900°C for 2 hours.

3.6 Symmetric Cell Fabrication

A pipette was used to add 15 microliters of SDC buffer solution to one side of the electrolyte. The buffer solution was dried for 10 minutes in air. Then one piece of cathode tape is stuck onto the electrolyte. A small flat surface was used to press the cathode tape onto the SDC to make sure the entire tape is stuck onto the electrolyte. The resulting half-cell was dried in an oven at ~65-80°C for one hour. Depending on the drying oven temperature, make sure to check that the cathode and electrolyte is fully dried before flipping over. The previous steps are repeated to add another cathode tape onto the electrolyte to create a symmetric cell. A sample holder that can have the symmetric cells face up vertically are used to fire the symmetric cells at:

- Ramp 1°C/min to 400°C
- Hold 400°C for 1 hour
- Ramp 2°C/min to 1080 °C
- Hold 1080°C for 2 hours
- Cool at a rate of 3°C/min

3.7 Testing Apparatus

The symmetric cell testing components is shown in Figure 16. Symmetric cells are inserted in-between two silver wires that are pressed to the side by a small alumina rod shown in Figure 16a. The components used to hold the symmetric cell are shown in Figure 16b.

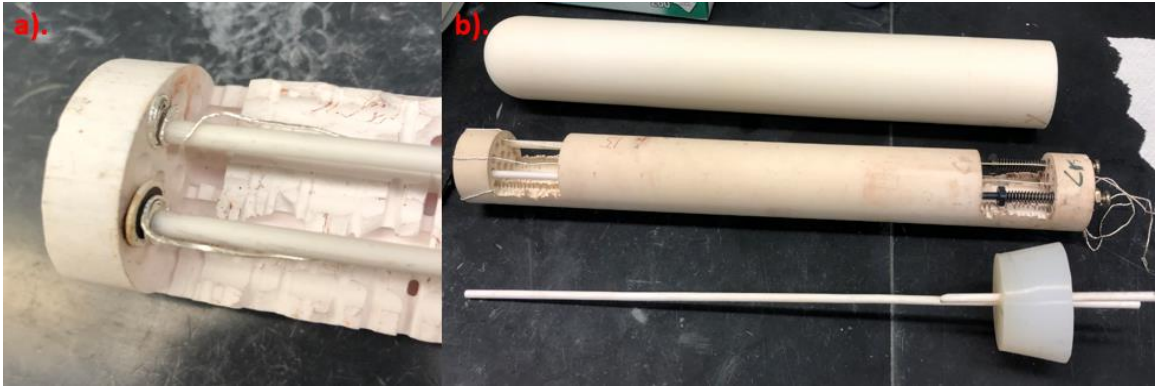


Figure 16. a). Location where symmetric cell is placed between 2 silver wires. b). testing components: alumina tube, alumina rod, and rubber stopper.

The alumina rod is then placed into an alumina tube and then plugged with a rubber stopper shown in Figure 17. Three holes are drilled into the rubber stopper. Two holes are for single bored alumina rods to be inserted to allow gas/moisture to flow into the tube and out of the tube. The last hole drilled is an extra hole to prevent gas build up, which would cause the internal pressure to increase and pop out the rubber stopper from the alumina rod during testing.

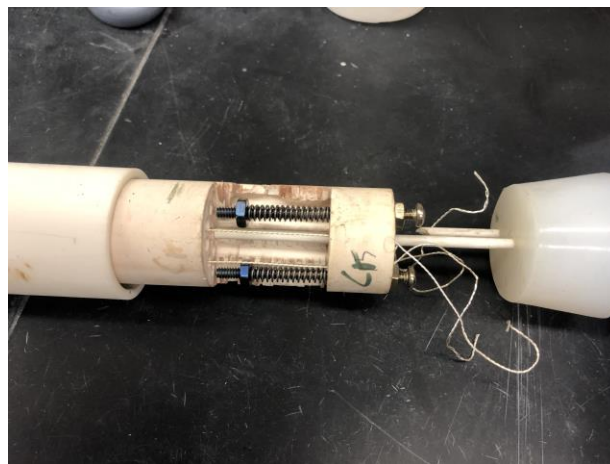


Figure 17. Shows how the symmetric cell testing apparatus is assembled into the alumina rod.

The alumina tubes with one side closed had a length of 1 foot with an outer diameter of 38mm and an inner diameter of 32mm. High-Temperature tapered round silicone rubber plugs were bought from McMaster-Carr with the small end being 1.265625in and the larger end being 1.53125in. The holes in the rubber stopper were made with a 1/8in drill bit. Symmetric and fuel cells are tested in our custom testing rack shown in Figure 18.



Figure 18. Fuel Cell Testing Rack.

LabView was used to control the furnace temperature. To make sure that the % moisture fed into the system is correct, a humidification system is used so that 40% moisture and balance air is fed into the alumina test tubes, which is shown in Figure 19. Table 1 below shows the temperature in Celsius of the bubbler in the humidification system to get 10-40% moisture calculated from Lange's Handbook [39]. The vapor pressure of water was based on 1 atm or 760 torr. Air gas at a rate of about 100 sccm is fed into the back of the humidification system and heat tape is used to make sure that the output of the humidification system is kept at 40% moisture and balance air.

Table 1: Humidification System Temperature to get % Moisture.

% Moisture	Pressure (torr)	Bubbler Temp.
10%	76	46.1 °C
20%	152	60.4 °C
30%	228	69.4 °C
40%	304	76.2 °C



Figure 19. Humidification System from Fuel Cell Technologies, Inc.

PTFE tubing and Swagelok is used to connect the humidifier system output to the sample chambers shown in Figure 20. The heat tape was set to 110°C to ensure that the humidified air did not condense back to water. Extreme-Temperature PTFE semi-clear tubing for chemicals were ordered from McMaster-Carr with an inner diameter of 0.1875in and an outer diameter of 0.25in.



Figure 20. PTFE wrapped in heat tape that connects the humidification system output into the alumina rods to prevent water from condensing.

The impedance was measured using a Parstat MC multichannel potentiostat from Ametek scientific instruments using the software VersaStudio. Constant voltage was applied, and current was measured using Arbin Instruments and the software MITS Pro.

CHAPTER 4: RESULTS AND DISCUSSION

4.1 Symmetric Cell Characteristics

The dimensions of the symmetric cells were found by using SEM for later calculations. Since the diameter of the cathode tape is 0.25in or 0.635cm, the active surface area of the cathode can be calculated using the area of a circle shown in Equation 1 below.

$$\text{Cathode area} = \pi \times \text{radius}^2$$

Equation 1

This gives the area of the cathode to be 0.31669191 cm², which is the area that the current flows through. For a symmetric cell the area must be divided in half due to symmetry because the measured R_p from EIS is for both cathode electrodes, so the symmetric cell cathode area is 0.158346cm². Due to the small cathode area, there may be greater error in calculating the area specific resistance (ASR). Figure 21 shows the dense SDC electrolyte having a thickness of 500 microns.

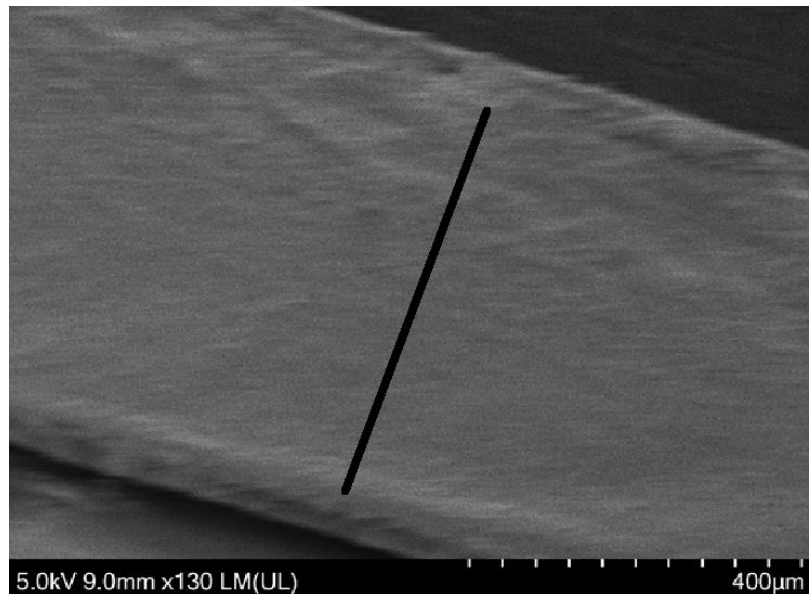


Figure 21. Cross-section of the cathode symmetric cell, black line indicates the SDC pellet thickness of 500 microns.

The cathode thickness shown in Figure 22 is 50 microns with the SDC buffer layer between the cathode and the electrolyte being a few microns thick, so the total thickness of the Cathode/SDC/Cathode symmetric cell is about 600 microns or 0.6mm thick.

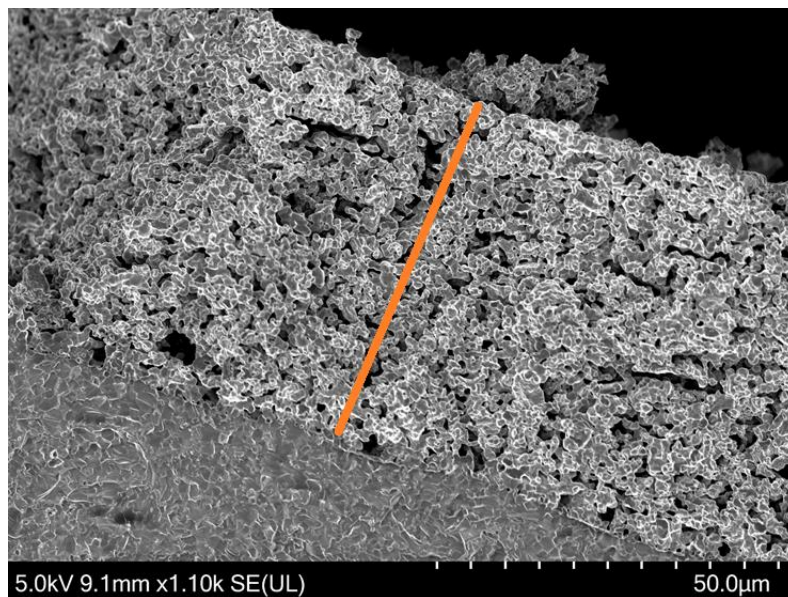


Figure 22. Porous cathode with the orange line showing the cathode thickness of 50 microns.

4.2 How to Interpret EIS and Activation Energy

To get the activation energy, it is important to know how to read the impedance data measured from EIS. A sample figure on how to determine R_p and R_{ohmic} is shown in Figure 23. Electrolyte resistance or R_{ohmic} is found in the location where the semicircle first crosses the x-axis or the length of the x-axis from zero to the green arrow. If the electrolyte resistance increases, the distance from zero on the x-axis will increase by shifting the first location the semicircle crosses the x-axis to the right shown in Figure 24. This typically occurs when the electrodes delaminate from the electrolyte. The cathode polarization resistance or R_p is the length of the semicircle shown in blue. Cathode degradation is shown

by increasing the length of the semicircle when impedance is measured. An example was shown back on the right side of Figure 14. Total resistance is R_p and R_{ohmic} added together.

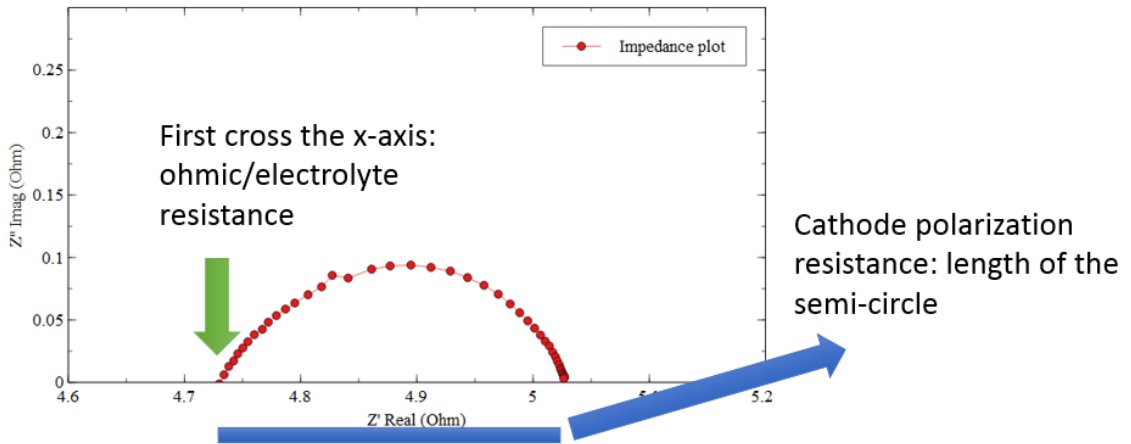


Figure 23. Sample impedance plot on how to determine R_{ohmic} and R_p .

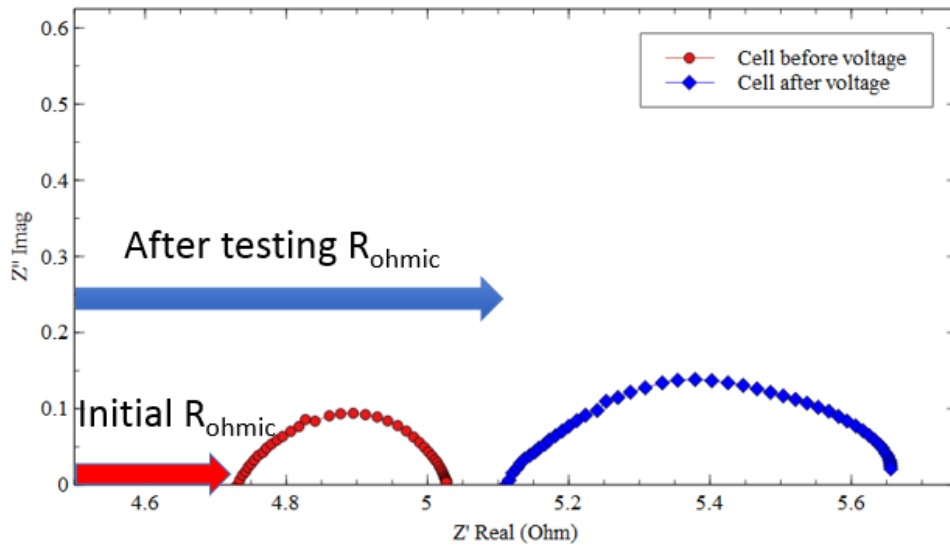


Figure 24. Shows what happens to the measured EIS data if the electrolyte/ohmic resistance increases after testing.

The activation energy was found by measuring the impedance at 50°C intervals from 550 to 750°C. 1000 divided by the temperature converted to Kelvin (K) is plotted on the x-axis. The y-axis plots the natural log of the cathode polarization resistance. From the points plotted on the graph, a fitted line is generated, and the slope is then converted into activation energy in terms of eV. Slope is related to the activation energy through the Arrhenius equation in Equation 2 where:

$$slope = \frac{E_a}{gas\ constant}$$

Equation 2

The activation energy in eV is shown in the Equation 3 below where 8.314 is the gas constant in $\frac{J}{mol \cdot K}$ and the 1000 multiplier is from the x-axis conversion.

$$E_a = slope * 8.314 \frac{Joule}{Mole * K} * \frac{6.242 * 10^{18} eV}{Joule} * \frac{1mole}{6.022 * 10^{23}} * 1000$$

Equation 3

The converted cathode polarization data is shown in Figure 25 below while the summary of the activation energies for the cathodes are shown in Table 2. From Table 2, PBCC had the lowest activation energy.

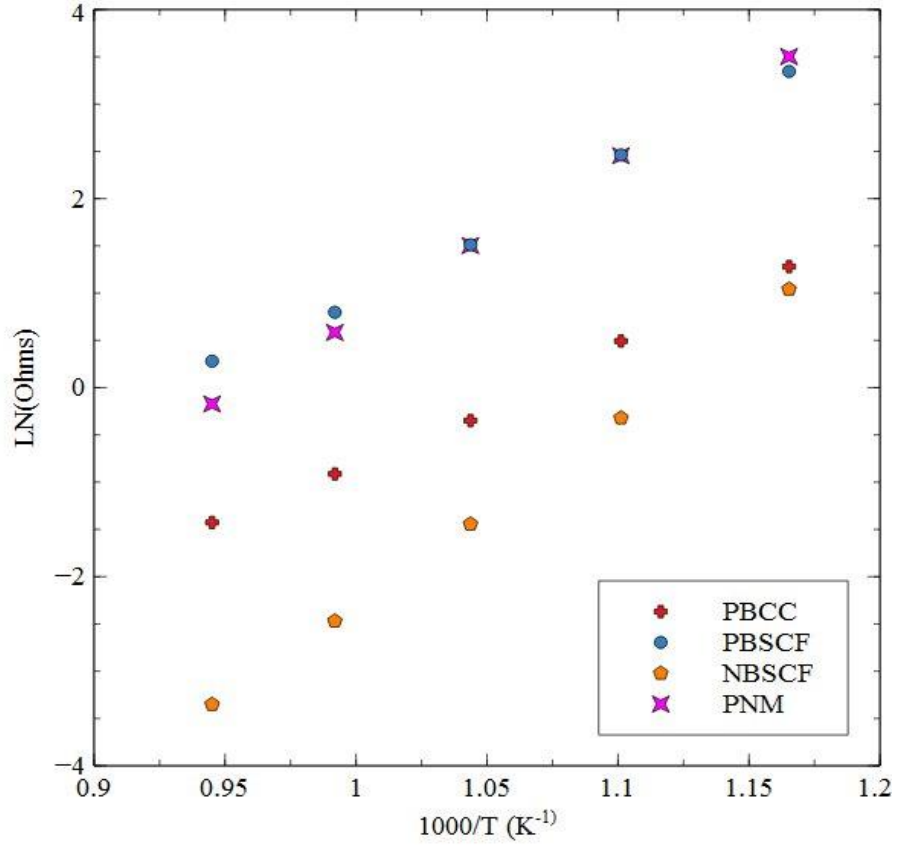


Figure 25. Plots for cathode activation energy. Fitted lines for each cathode can be used to get a slope to calculate activation energy based on Equation 3.

Table 2. List of cathode activation energies in eV

PBCC	1.07 eV
PBSCF	1.22 eV
NBSCF	1.72 eV
PNM	1.27 eV

Activation energy is the minimum amount of energy required for a specific reaction to occur. Since PBCC requires less energy, its cathode R_p is less sensitive to temperature, which means that its ORR kinetics is expected to be faster at lower temperatures. This would also help with commercialization by reducing the operation temperature. By reducing the operating temperature there is also less corrosion to the material components.

4.3 Structural Stability

First the cathode powders before and after 40% moisture (% water vapor) with balance air were analyzed. XRD and Raman Spectroscopy were used to analyze the bulk and surface structural changes if any, respectively. It can be seen in Figure 26 below that all the double perovskites appear to be chemically stable. There is also some sharpening of peaks in the after data, which may signify grain growth. This also occurs in PNM, however in Figure 27 there are several small peaks that disappear and form due to the high moisture exposure, which may indicate phase separation. While the initial PNM structure is reported to possess good catalytic properties for ORR, it is unknown if the new phase or phases that formed also possess good properties for ORR [36, 40]. EIS can be used to measure the ORR activity, which is verified in Figure 40 for PNM. PNM degrades rapidly under high moisture shown in the EIS measurements. This suggests that PNM degrades severely under high water vapor content and that the new phase forming is less active for ORR.

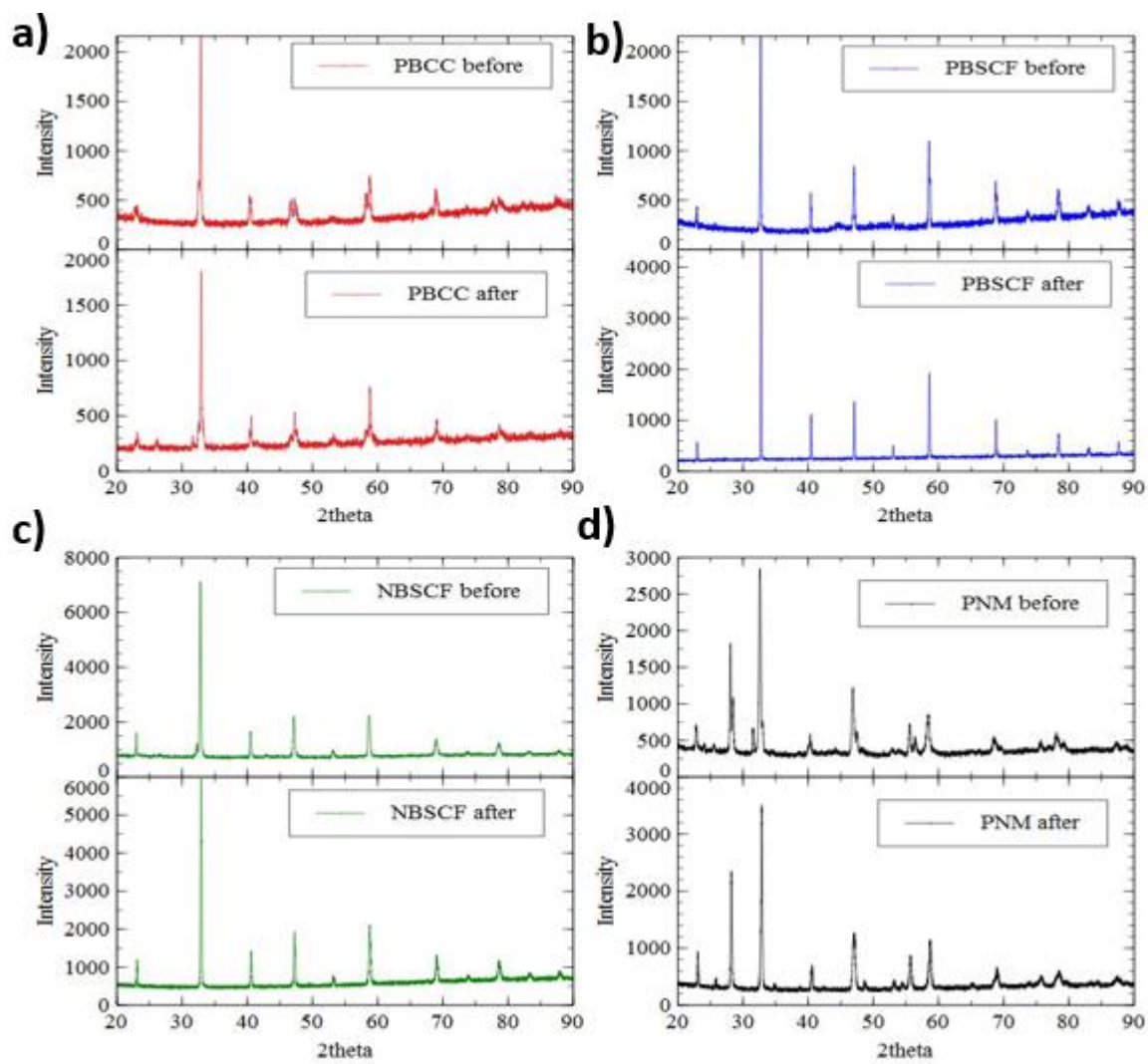


Figure 26. XRD showing the chemical stability of the cathodes: a). PBCC, b). PBSCF, c). NBSCF, and d). PNM before and after 500hrs in 40% moisture at 700°C.

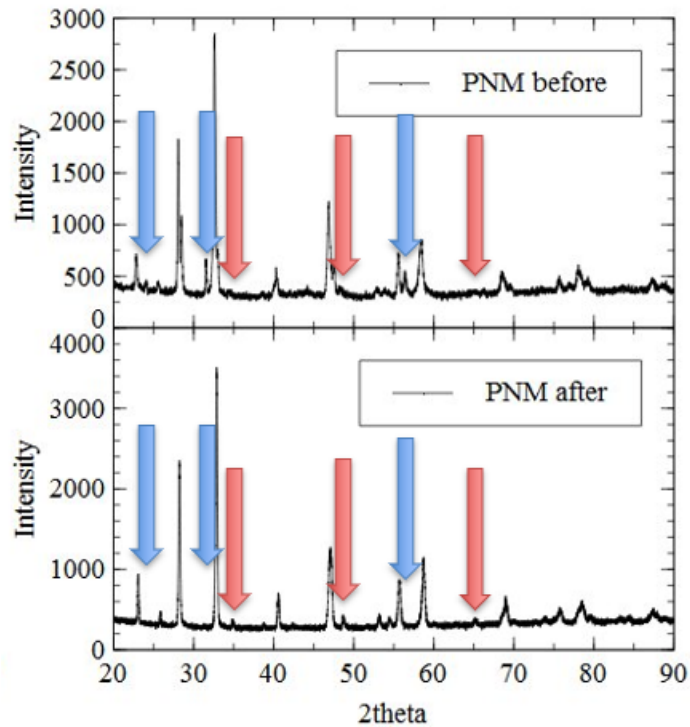


Figure 27. XRD on PNM after 500hrs in 40% moisture at 700°C with blue arrows show peak disappearances and red arrows show new peaks.

Shown in Figure 28 is the NBSCF initial Raman scan. The other double perovskites all had the same initial Raman scan as NBSCF, where there is no Raman signal. After 500 hours of testing, both NBSCF and PBSCF did not show any change in the Raman data shown in Figure 29. The sharp lines in PBSCF in Figure 29 are due to artifacts or some other interference in the machine and are not peaks.

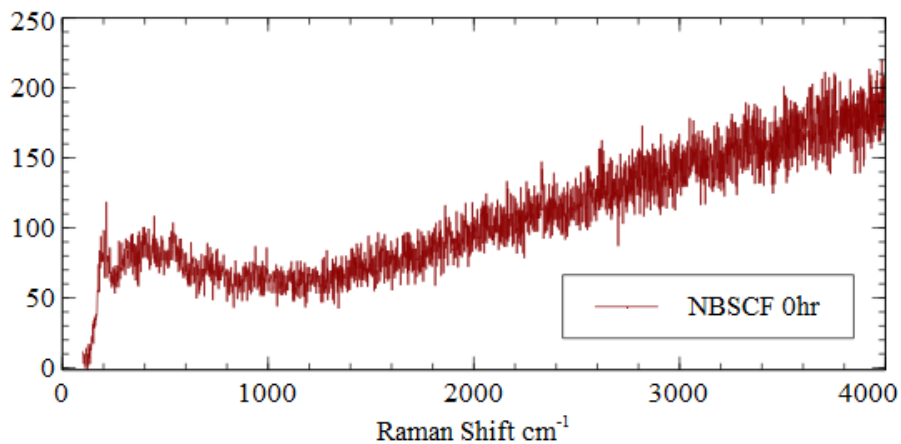


Figure 28. NBSCF powder initial Raman scan.

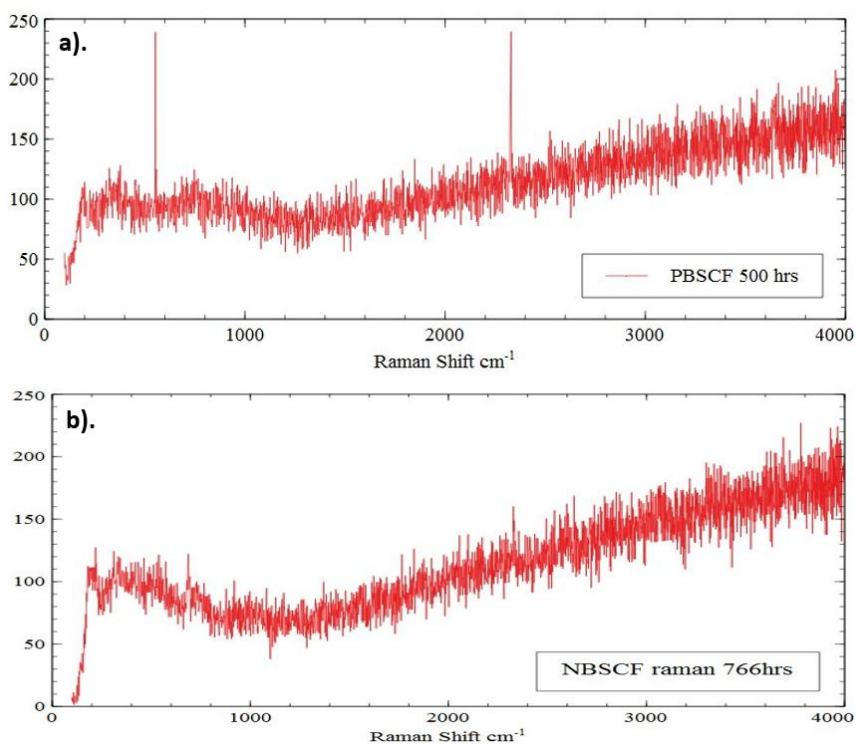


Figure 29. a). PBSCF powder and b). NBSCF powder Raman scan after 500hr in 40% moisture at 700°C.

The other 2 cathodes, PBCC and PNM, showed a change in the Raman data. PNM had 2 initial peaks shown in Figure 30. PNM is not a pure perovskite, it is composed of the perovskite and fluorite PrO_x , therefore the two peaks possibly represent PrMnO_x and PrO_x

[40]. Figure 31 shows the PNM Raman data after 40% moisture exposure, which shows several new peaks signifying that something changed on the surface. However, PNM is not further analyzed due to the poor EIS performance shown later.

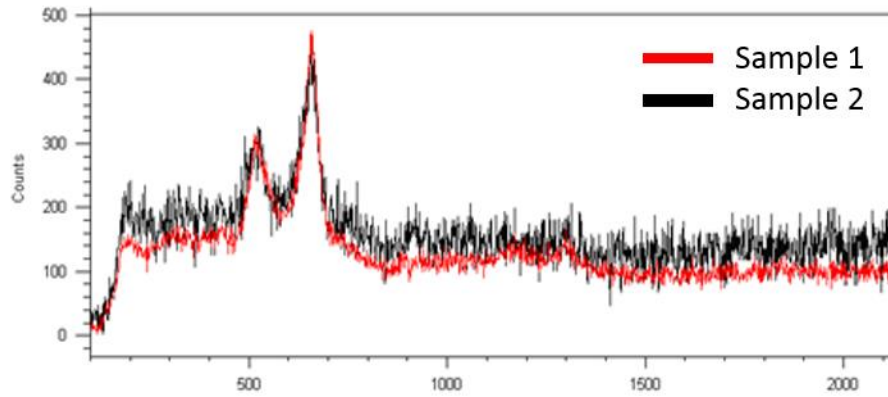


Figure 30. Raman shift for initial PNM powder for 2 samples. The two peaks represent PrMnO_x and PrO_x .

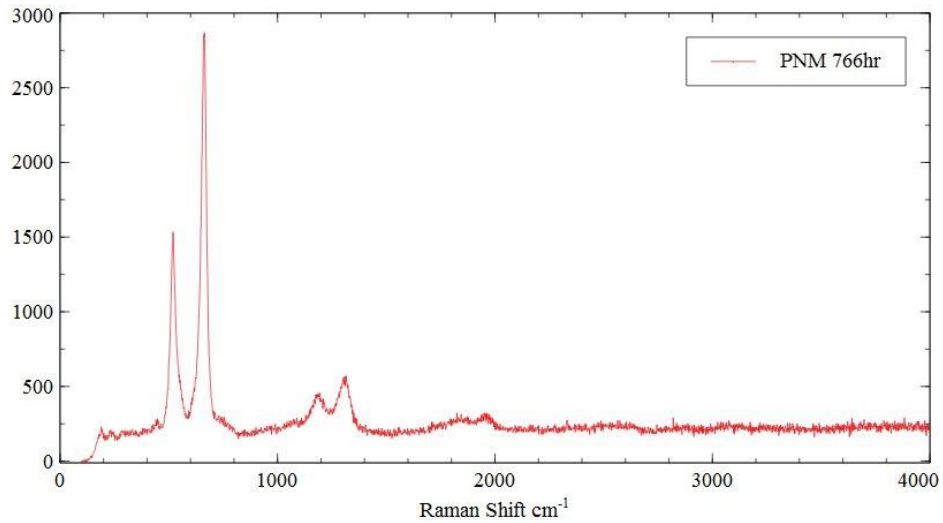


Figure 31. PNM powder Raman shift after 40% moisture exposure for 766 hours at 700°C.

Figure 32 shows the emergence of a new peak for PBCC after testing. From literature sources, the orange arrows signify that the newly formed peak is BaCoO_3 based on Milt et al [41]. Considering cation segregation mentioned above, Barium will segregate to the surface. For LSCF, Cobalt Oxide has been observed to segregate to the surface by Ling Zhao et al [42]. Considering the high moisture content, it is likely for the Barium to react with the Cobalt Oxide to form BaCoO_x because once enough Barium segregates to the surface, some cobalt and oxygen must also segregate to maintain the lattice charge balance.

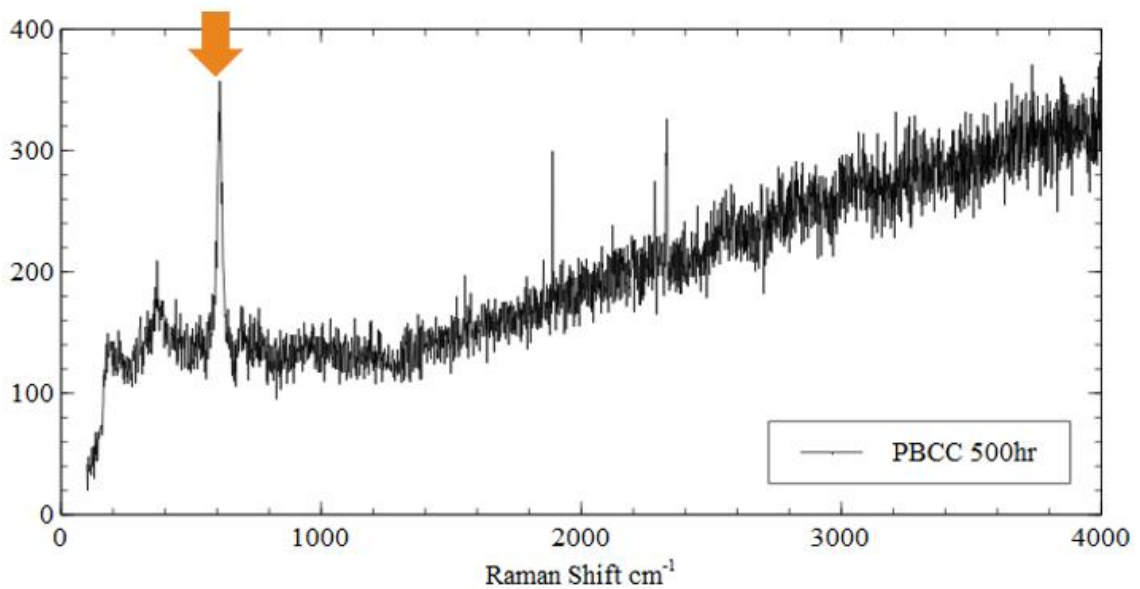


Figure 32: a). PBCC powder Raman scan after 500hr in 700°C with 40% moisture exposure. Sharp lines due to cosmic rays/artifacts. Orange arrows represent BaCoO_3 at around 610 cm^{-1} .

4.4 Cell Fabrication Verification

Before long-term testing is done, the repeatability of the fabricated cells must be determined by using EIS measurements. First the initial R_p in dry air is tested for repeatability then the repeatability of the symmetric cells in 40% moisture is tested. The initial R_p in dry air repeatability is shown in Figure 33, Figure 34, and Figure 35 below for the double perovskites. PNM is excluded, due to its poor performance in moisture. The figures show the ASR by multiplying the R_p by the symmetric cell cathode area shown in Equation 4.

$$ASR = R_p * 0.158346\text{cm}^2$$

Equation 4

PBCC showed great repeatability in Figure 33 even with different buffer layer solutions. Cells 1 and 2 used the same buffer layer (BL) while cells 3+ were made using a different SDC buffer layer (NBL). The SDC used in BL and NBL are from two different CCP SDC catches.

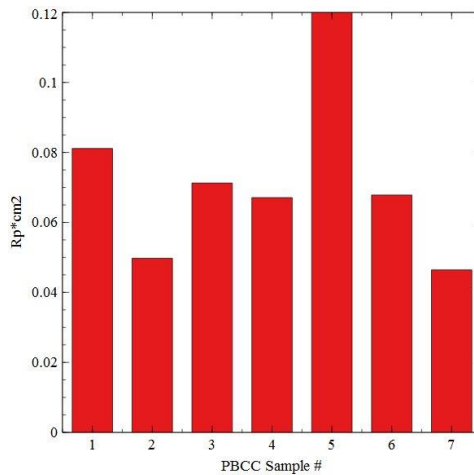


Figure 33. Initial PBCC/SDC/PBCC symmetric cell ASR EIS data in ambient air at 700°C under OCV conditions. Cells 1-2 made with BL and Cells 3+ with NBL.

However, this is not the case for NBSCF and PBSCF. The difference in R_p for the cells in NBSCF and PBSCF are also shown in Figure 34 and Figure 35. This may be due to different batches of SDC buffer layer solutions, which can lead to difference performances due to the differences in the SDC particle sizes. Different cathodes may have different compatibility with the buffer layer solutions depending on the morphology and size of the SDC powder used.

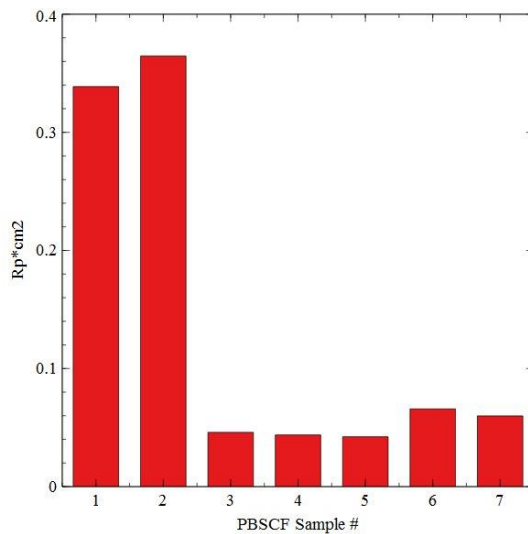


Figure 34. Initial PBSCF/SDC/PBSCF symmetric cell ASR EIS data in ambient air (~3% H₂O) at 700°C under OCV. Cells 1-2 made with BL and Cells 3+ with NBL.

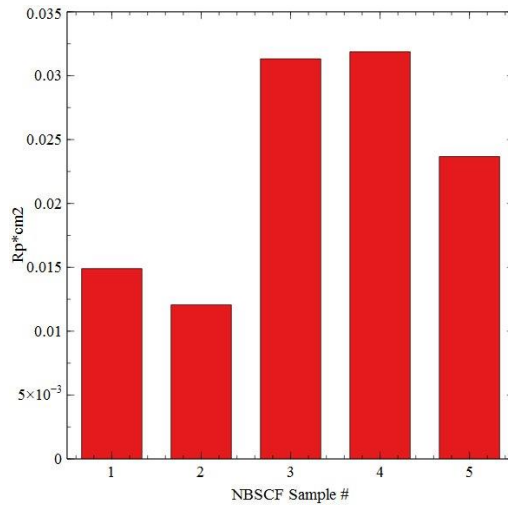


Figure 35. Initial NBSCF/SDC/NBSCF symmetric cell ASR EIS data in ambient air (~3% H₂O) at 700°C under OCV. Cells 1-2 made with BL and Cells 3+ with NBL.

However, it is shown that once the cells are exposed to high humidity, the R_p of the cells become very similar due to the water promoting effect on PBSCF shown in Figure 36. This phenomenon could be that the moisture helps further bond the buffer layer with the cathode and electrolyte on top of the water promoting effect due to the differences in the SDC buffer layer solution. Moisture could also enhance the cathode's catalytic function [43]. Other possibilities include an error in the EIS testing equipment or not giving enough time for the samples to heat up.

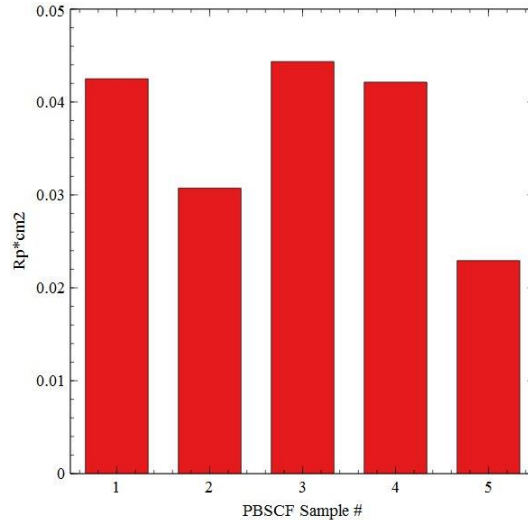


Figure 36. PBSCF/SDC/PBSCF symmetric cell ASR EIS data after water promoting effect. Shows lowest ASR after moisture exposure. Testing conditions are 40% moisture and balance air at 700°C under OCV. Cells 1-2 made with BL and Cells 3+ with NBL.

Figure 37, Figure 38, and Figure 39 below show the repeatability of the experiments in heavy moisture. Figure 37 shows that the PBCC cells have about the same R_p regardless of the CCP SDC batch with the only difference being how big the initial water promoting effect is. PBSCF shows less resistance with the NBL, but the stable performance matches the BL cells. NBSCF shown in Figure 39 seems to be undergoing exponential degradation in 40% moisture that decays over time. It seems like the NBL cells undergoes exponential degradation at a faster rate than the BL cells.

A possibility is that the compatibility of the two different batches of CCP SDC to the cathode is different. For PBSCF, the NBL is more compatible with the PBSCF, which leads to better adhesion of the PBSCF and SDC. As a result, a strong interface is created between the PBSCF and SDC that lowers the cathode resistance. This may be why the NBL PBSCF has better performance than the BL PBSCF. For NBSCF, it is the opposite and the weaker interface in the NBL NBSCF leads to great degradation of the NBSCF cathode. Therefore,

since the SDC buffer layer solution is the only difference, it may be something to further look at for another study.

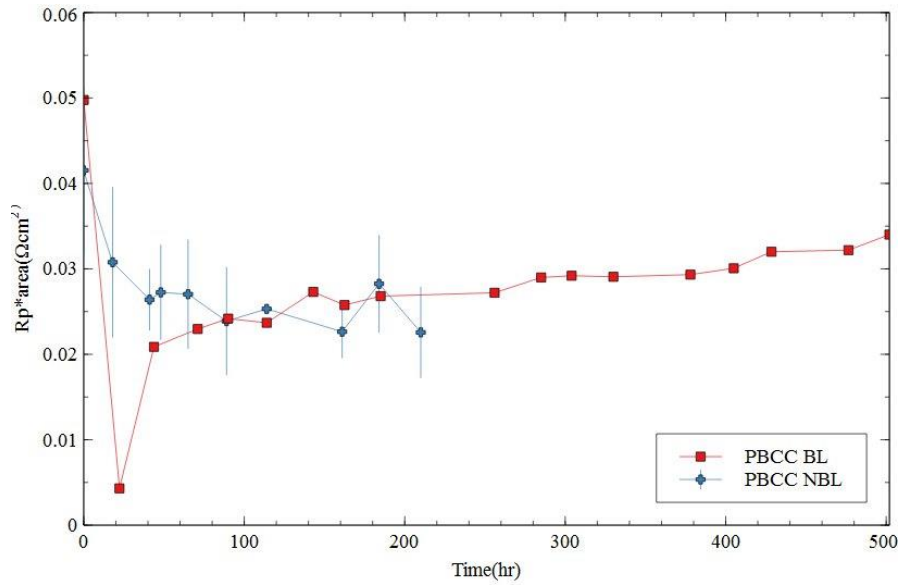


Figure 37. PBCC/SDC/PBCC symmetric cells short term repeatability in 40% moisture and balance air at 700°C under OCV conditions. NBL error bars average 2 cells.

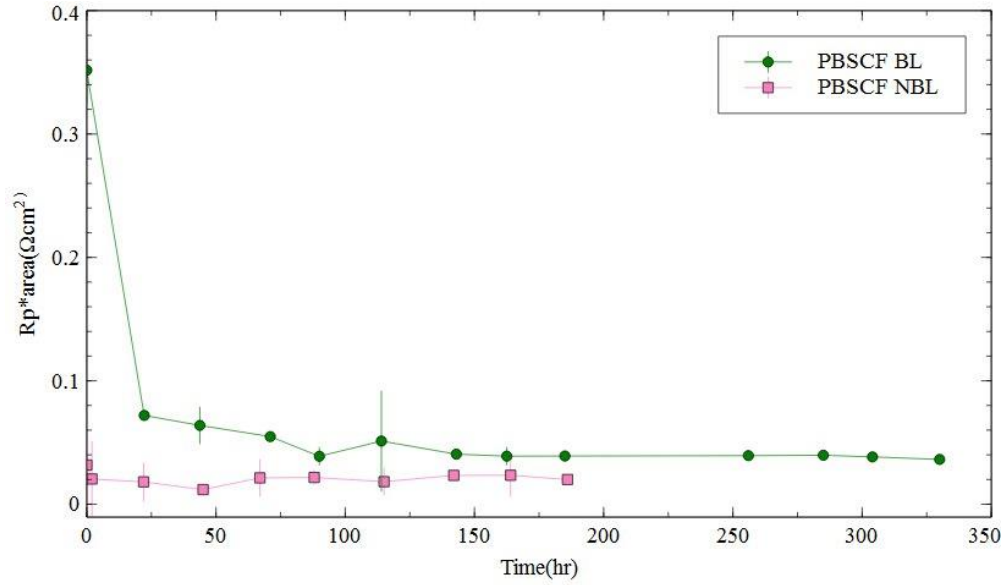


Figure 38. PBSCF/SDC/PBSCF symmetric cell short term repeatability in 40% moisture and balance air at 700°C under OCV. BL error bars average 2 cells and NBL error bars average 3 cells.

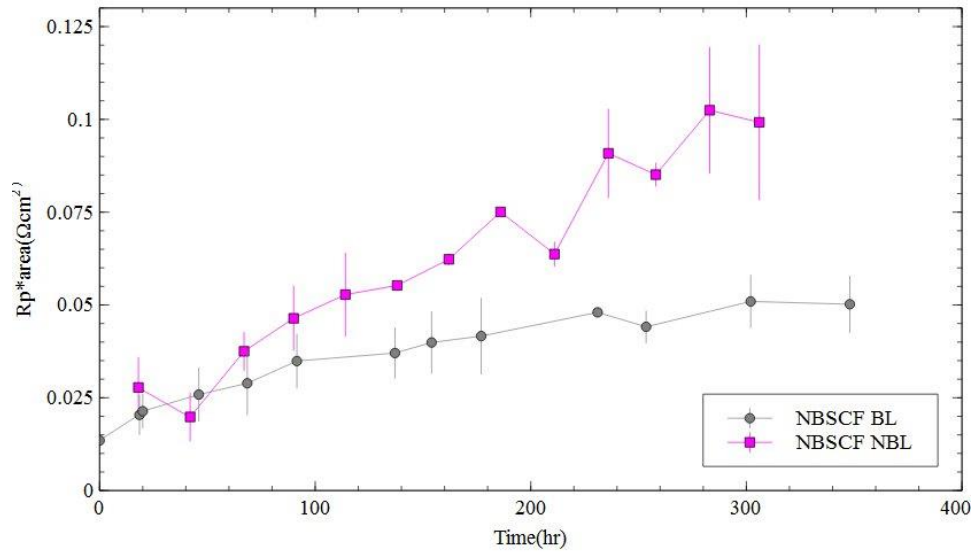


Figure 39. NBSCF/SDC/NBSCF symmetric cell short term repeatability in 40% moisture and balance air at 700°C under OCV. BL error bars average 2 cells and NBL error bars average 2 cells.

4.5 EIS Long-term Performance

Figure 40 below shows how fast the PNM symmetric cell degrades under heavy moisture, therefore PNM is removed from consideration. The remaining 3 cathodes are then plotted together to compare the long-term testing data as shown in Figure 41. All 3 cathodes are still operable even after exposure to 40% moisture after 750 hours. PBSCF showed great stability the first 500 hours, but heavily degraded later until the rate became constant. NBSCF showed an exponential decay in R_p with fast degradation when initially exposed to humidity. The great initial cathode performance of NBSCF may suggest that NBSCF would be a great cathode for conditions involving little to no % water vapor. Also, NBSCF did not show a water promoting effect. Finally, PBCC had the lowest R_p at the end of testing in moisture. This suggests that PBCC in 40% H_2O is more resistant to high % water vapor than PBSCF/NBSCF. All three cathodes are further tested under applied voltage/current because the microstructure may not be stable under voltage/current and high moisture.

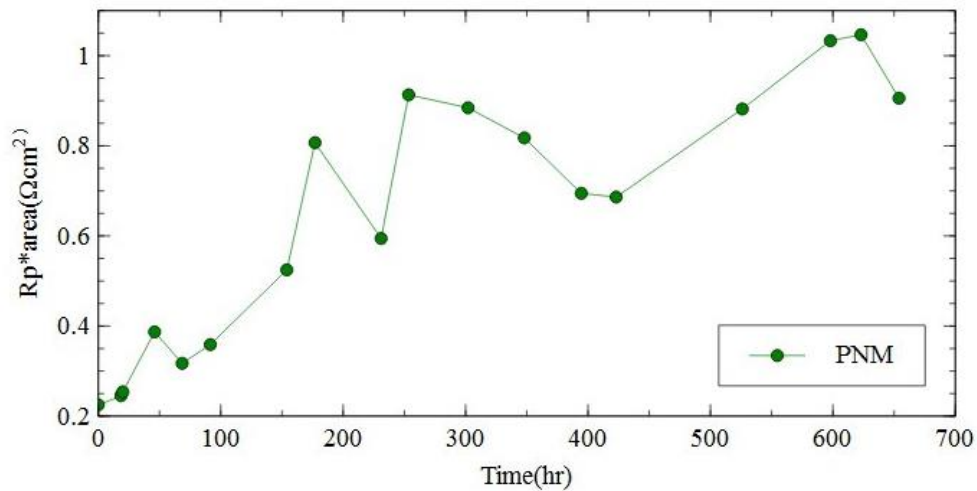


Figure 40. PNM/SDC/PNM symmetric cell long-term data in 40% moisture and balance air for 650hrs at 700°C under OCV.

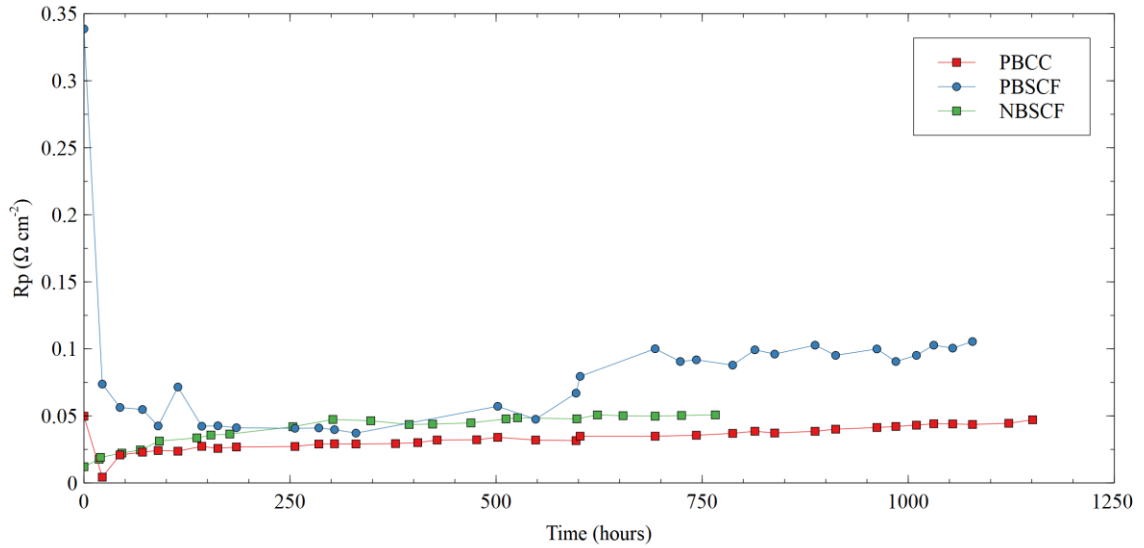


Figure 41. Long-term cathode/SDC/cathode ASR vs time(hr) in 40% moisture and balance air at 700°C for double perovskites under OCV.

Since PBCC performed the best, SEM was used to see if any morphological changes could be uncovered and to see if it supports the Raman and XRD data. Figure 42 and Figure 43 show the SEM images of PBCC before and after testing. The grains are clearly larger after testing, which could slow down oxygen ion transport and result in a larger R_p . Figure 43 shows that the morphology largely remains the same for the bulk phase, being porous spherical particles. However, the surface looks denser and more angular in Figure 42. A closer look is taken in the next section.

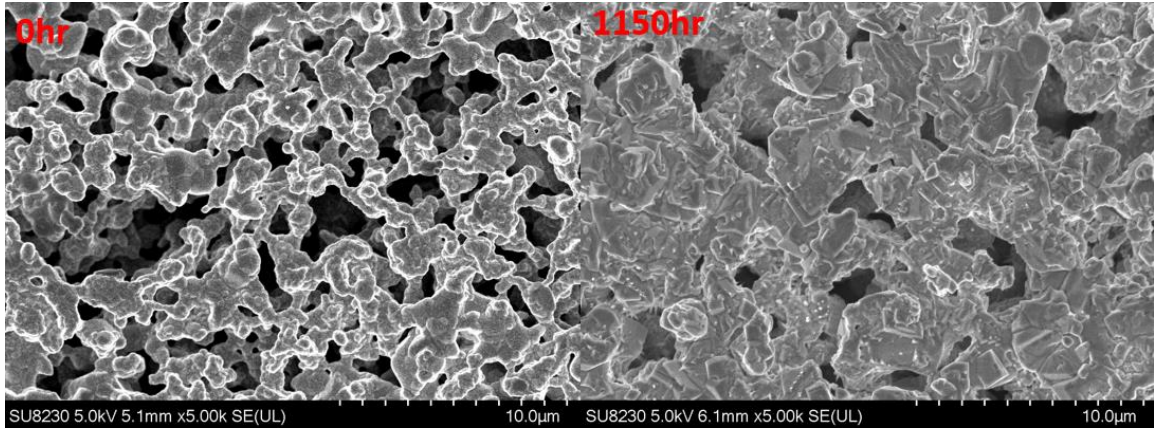


Figure 42: SEM image of PBCC on the surface before and after symmetric cell testing (40% moisture and balance air) at 700°C under OCV.

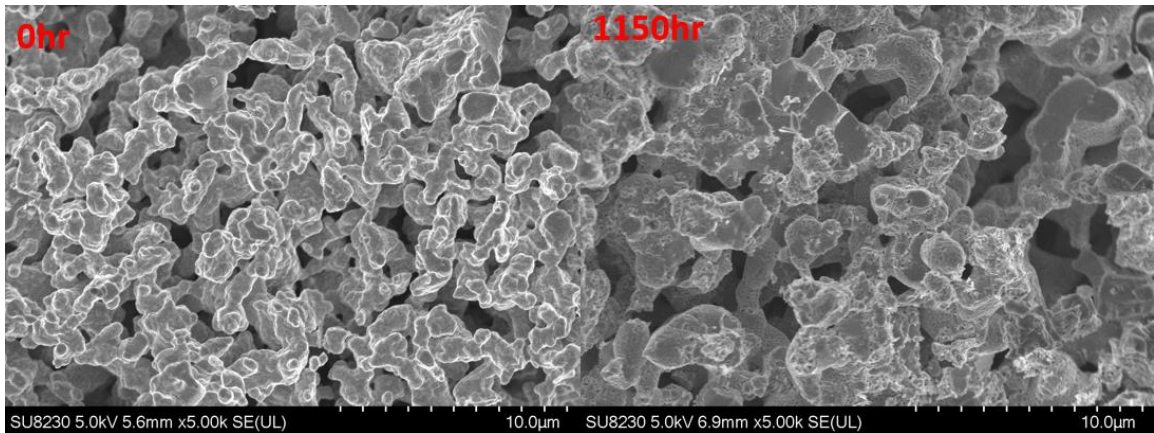


Figure 43: SEM image of PBCC cross-section before and after symmetric cell testing (40% moisture and balance air) at 700°C under OCV.

Table 3 and Table 4 shows the summary of the long-term impedance data. PBCC has the lowest degradation rate per hour compared to NBSCF and PBSCF.

Table 3. Degradation Comparison Rate for the cathodes using similar time frames.

Rp*Area (Ohm*cm ²)	PBCC	PBSCF	NBSCF
Activated Initial Rp	0.004	0.039	0.013
End Rp	0.037	0.085	0.055
Time (hr)	765	797	766
Degradation (Rp*Area)/hr	4.268E-05	5.846E-05	5.389E-05

Table 4. Long-term Impedance data summary

Rp*Area (Ohm*cm ²)	PBCC	PBSCF	NBSCF
Initial Dry Air	0.050	0.352	0.013
Fully Water Activated	0.004	0.039	N/A
End Rp	0.044	0.0984	0.055
Start Time Activated (hr)	22	90	0
End time (hr)	1122	1031	766
Duration	1100	941	766
Degradation (Rp*Area)/hr	3.654E-05	6.331E-05	5.389E-05

4.6 Degradation Mechanism

The EIS data shows that the R_p for NBSCF and PBSCF does degrade under 40% moisture, however the XRD and Raman data do not show any structural change after 500hrs. XRD does show some lattice change with the very slight peak shifts. For PBCC, the Raman data showed the formation of $BaCoO_3$ as discussed in a previous section. Figure 44 shows the PBCC surface cross-section after testing. There is a change in the surface morphology, where the surface is more crystalline and angular compared to the porous bulk. This lends evidence along with Figure 42 to the possible formation of a new phase on the PBCC surface due to the different morphologies.

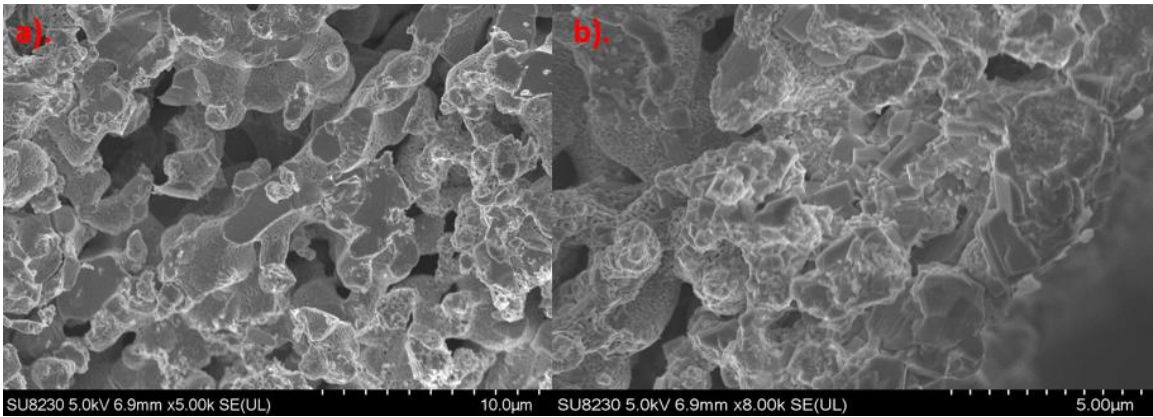


Figure 44. a). bulk and b). surface of PBCC both after 1150hr symmetric cell testing in 40% moisture and balance air at 700°C under OCV.

It is known that humidity promotes cation segregation, especially in alkaline earth metals, to the surface, therefore the Barium near the surface could react with oxygen adsorbed on the cathode surface and Cobalt from the bulk. The Barium could also first react with a water molecule to form a barium hydroxide compound. This would also explain why the $BaCoO_3$ is found on the surface using Raman, but not in the bulk using

XRD. BaCoO₃ has been used recently as a catalyst to suppress cation segregation and boost ORR on LSCF cathode surfaces [44]. BaCoO₃ is a very good catalyst for ORR activities, so it is hard to conclude if it is the cause of the EIS performance degradation in PBCC. If BaCoO₃ has worse ORR activity than PBCC, it could explain the why the PBCC symmetric cell has a slow R_p degradation even in 40% moisture. However, it is more likely there may be another insulting phase forming on the PBCC surface that is not Raman active like Barium Oxide. Other techniques would need to be used to uncover a more detailed degradation mechanism for PBCC and the cause of PBCC degradation in 40% H₂O.

4.7 Applied Voltage

The cathodes stability when exposed to voltage and current must also be evaluated when the cathode is used in full cell testing. If the cathode is not stable when exposed to voltage/current, the power density of the full cell will suffer and/or degrade. Here, constant voltage is applied, so if any degradation occurs only the current will drop, which would not destroy the cell unlike if current was kept constant. Alternating positive and negative constant voltage will be applied to evaluate the stability of the cathodes in both SOFC and SOEC modes. When the applied voltage is negative, it is modeling ORR for SOFCs and when the applied voltage is positive, it is modeling OER for SOECs.

From the constant voltage applied, the Arbin collected the measured current data. The current density applied to the cell was calculated by Equation 5 below.

$$\text{Current Density} = \frac{\text{Measured Current}}{0.31669191} \frac{\text{Amps}}{\text{cm}^2}$$

Equation 5

The voltage applied to the electrodes is calculated using the measured current and the measured R_p from EIS shown in Equation 6, which is derived from Ohm's Law Voltage = Current*Resistance.

$$\text{Cathode Voltage} = R_p * \text{Measured Current}$$

Equation 6

To get the overpotential on one cathode/electrode for the symmetric cell, the cathode voltage is divided by 2 shown in Equation 7 below.

$$\text{Overpotential} = \text{Cathode voltage} / 2$$

Equation 7

The symmetric cells at 40% moisture with constant current were first tested to see the response of the cells shown in Figure 66 to Figure 69 in Appendix A. When the moisture is set to 40% at 93hrs, the PBCC and PBSCF symmetric cells encounter severe oscillation in the measured current. This is accompanied by an increase in R_p in the cathode, which would mean that the cathode is structurally degrading.

Next is to evaluate what moisture content the cathodes can withstand while applying constant voltage. Most small button cells apply a current density of 1 Amp/cm². Here, the target is to apply an initial constant voltage that gives a current density of 1 to 1.2 Amp/cm² because of the initial data from Figure 66 to Figure 69 in Appendix A, the current decreases due to the increase in total resistance of the symmetric cell. This is due to corrosion in the cell from long-term moisture exposure. It is expected that as we increase the percent moisture from 10% to 30% that the total resistance will increase, thus lowering the current density.

Figure 45 to Figure 53 show constant applied voltage on PBSCF cells at $\pm 1.65\text{V}$, NBSCF cells at $\pm 1.7\text{V}$, and PBCC cells at $\pm 1.5\text{V}$. In the initial hours, the applied voltage was continuously reduced to account for the water promoting effect, which reduced the total resistance of the symmetric cells. This caused the measured current to increase during this time. For PBSCF and NBSCF, both are stable for the measured current at 20% humidity shown in Figure 45 to Figure 50 despite some oscillation. NBSCF is far more sensitive to moisture compared to PBSCF as shown in the cathode degradation in Figure 50. However, once moisture is increased to 30%, PBSCF and NBSCF symmetric cells start to experience heavy oscillation in the measured current data. This is accompanied by an increase in the total resistance in the EIS measurements. The 30% moisture with applied voltage is too caustic to the cathode, which is shown by the current decreasing over time as the resistance increases. Eventually the heavy degradation of the cathode will cause the cell to ultimately fail. The degradation of the symmetric cell may be the cause for the huge oscillation in the current data collected.

In Figure 47 and Figure 50, it is shown that the R_{ohmic} rapidly rises once we see the cathode R_p degrade. The electrolyte will not have a great change in value unless the contact area changes. Therefore, for PBSCF/NBSCF the cathode is starting to delaminate from the electrolyte at 30% moisture. Delamination of the cathode from the electrolyte is shown in Figure 71 for PBSCF and Figure 72 for NBSCF in Supplementary Appendix A. This also means that the high-water vapor and current is weakening the buffer layer that adheres the cathode to the electrolyte and is further verified in Figure 53. For future experiments, new binders that are more resistant to high % H_2O is required so that the adhesion layer does not allow delamination.

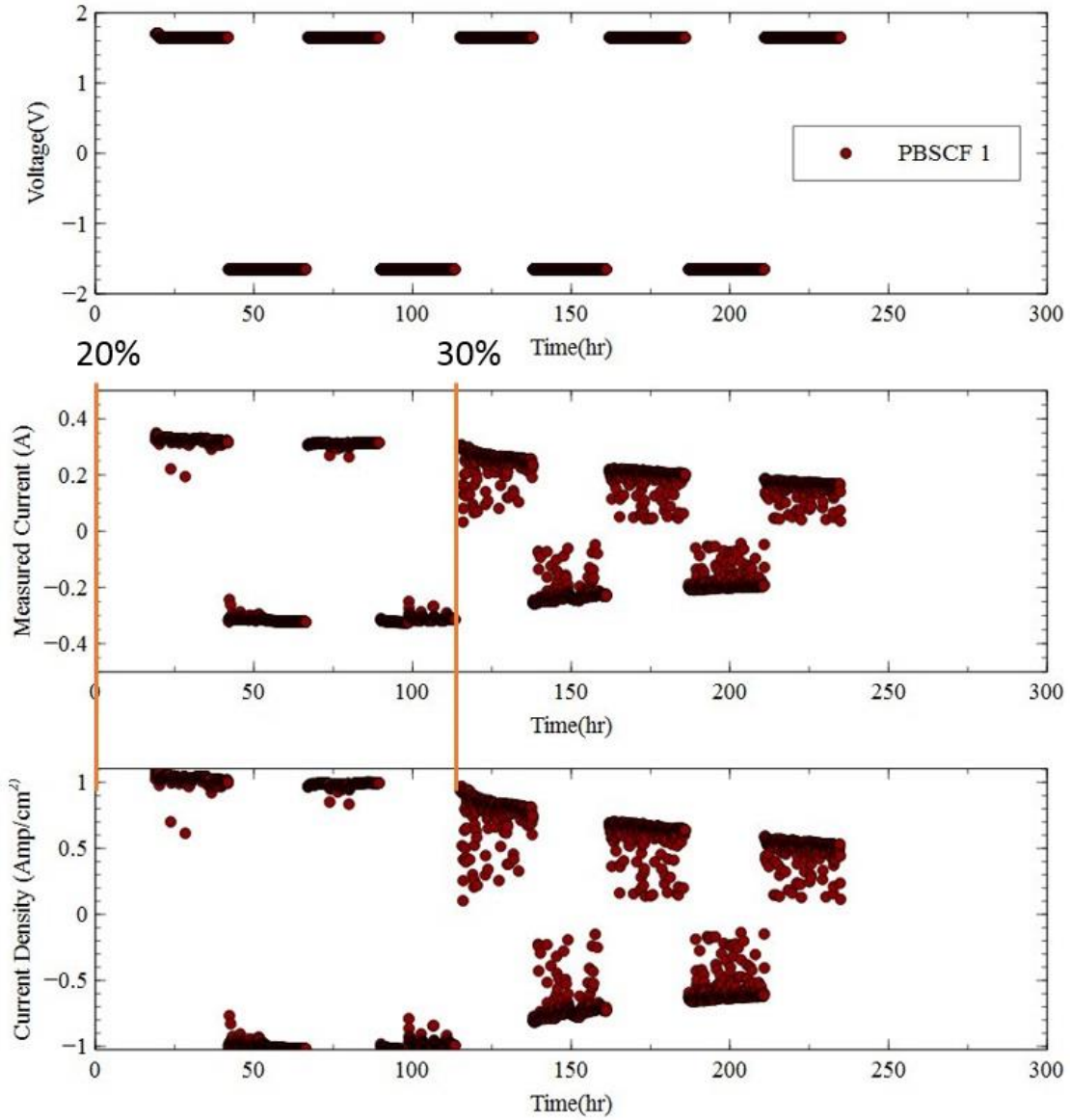


Figure 45. PBSCF/SDC/PBSCF symmetric cell under constant alternating +/- 1.65 Volts at 18hr. Switch to 20% moisture at 0hr, and 30% moisture at 114hr. Balance air at 700°C. Plots voltage, current, and current density vs time (hr).

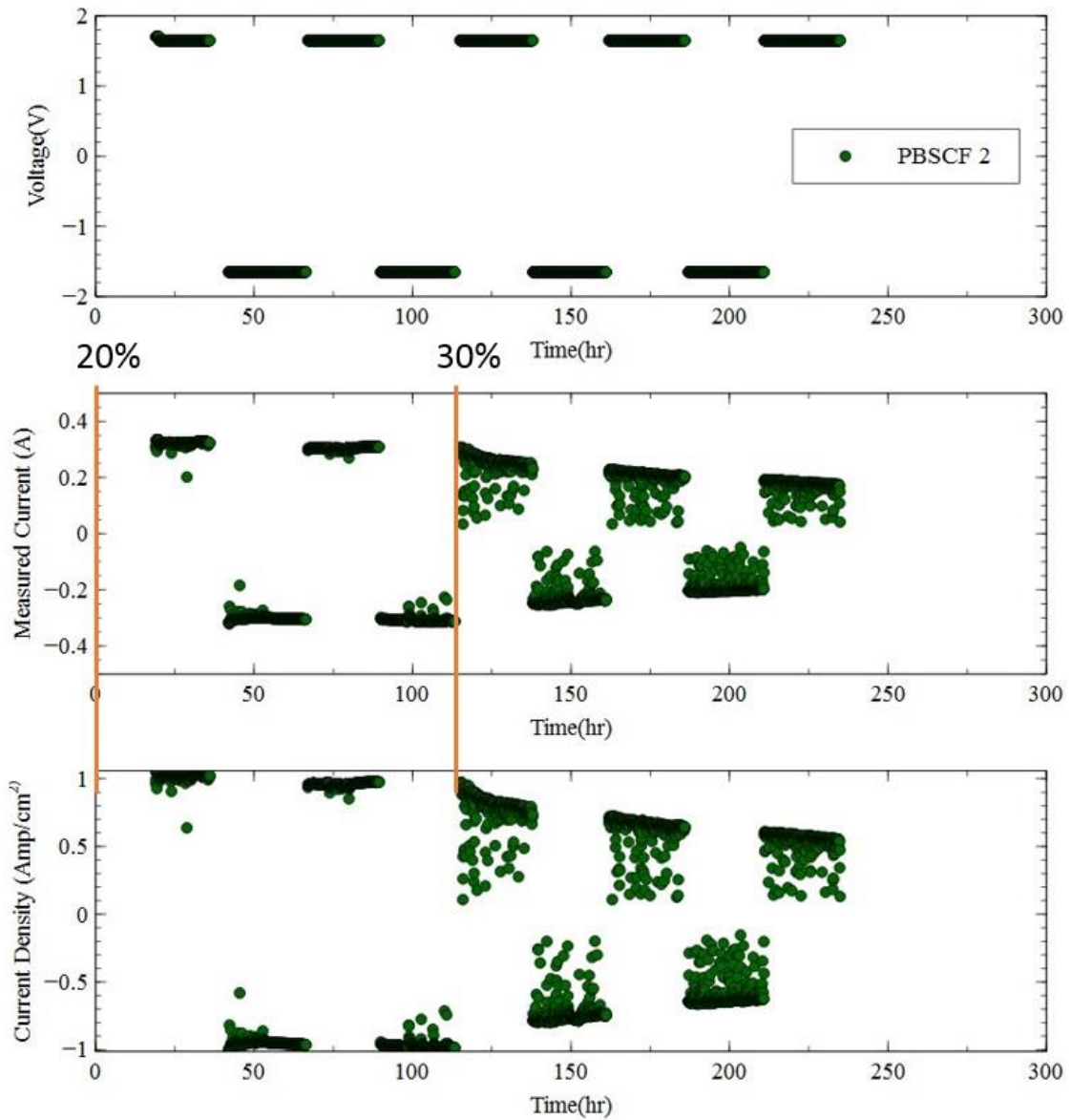


Figure 46. Another PBSCF/SDC/PBSCF symmetric cell under constant alternating +/- 1.65 Volts at 18hr. Switch to 20% moisture at 0hr, and 30% moisture at 114hr. Balance air at 700°C. Plots voltage, current, and current density vs time (hr).

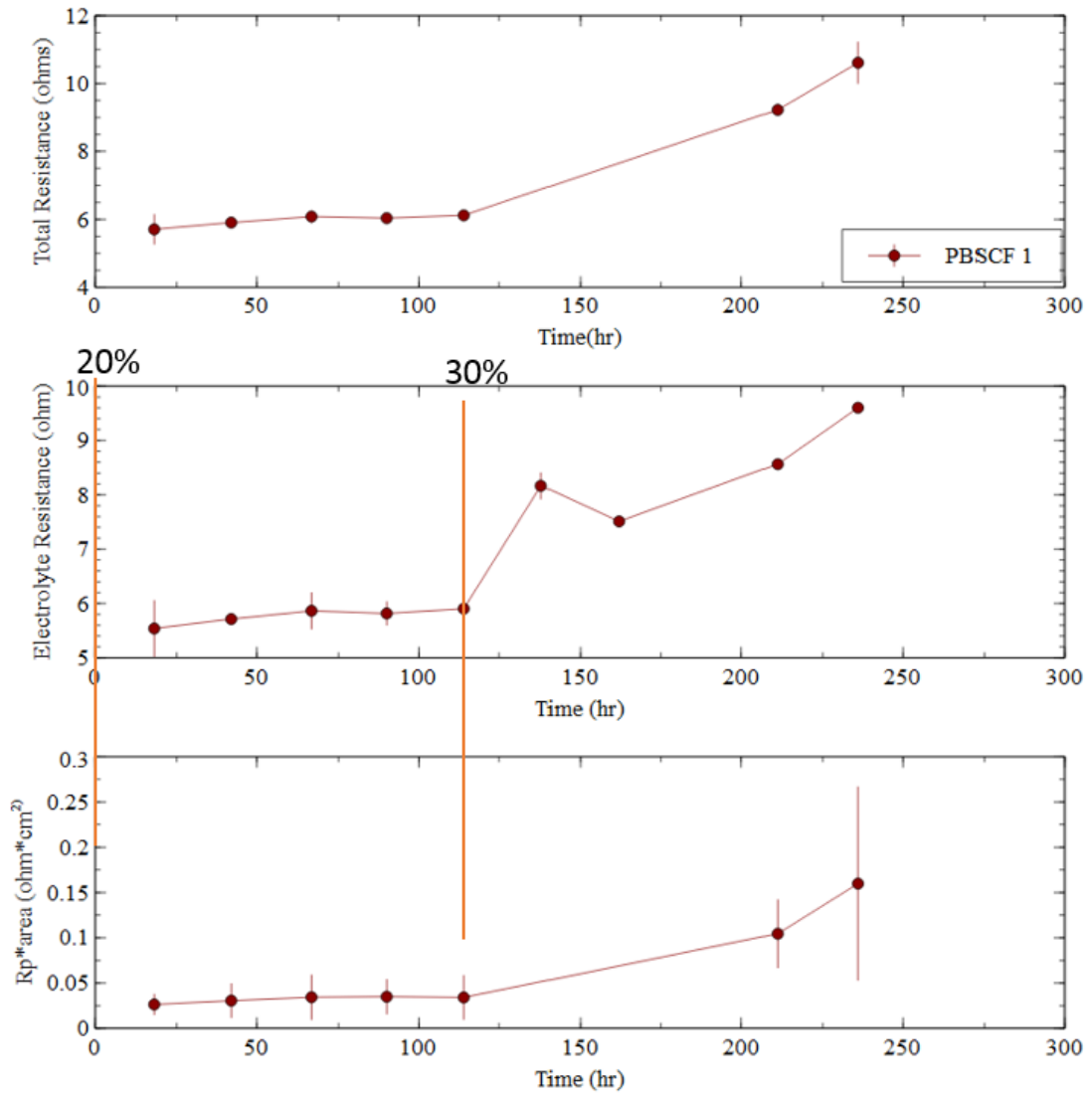


Figure 47. PBSCF/SDC/PBSCF EIS data under constant +/- 1.65 Volts at 18hr. Switch to 20% moisture at 0hr, and 30% moisture at 114hr. Balance air at 700°C. Shows error bars for 2 cells tested. Plots total resistance, ohmic resistance and ASR vs time (hr).

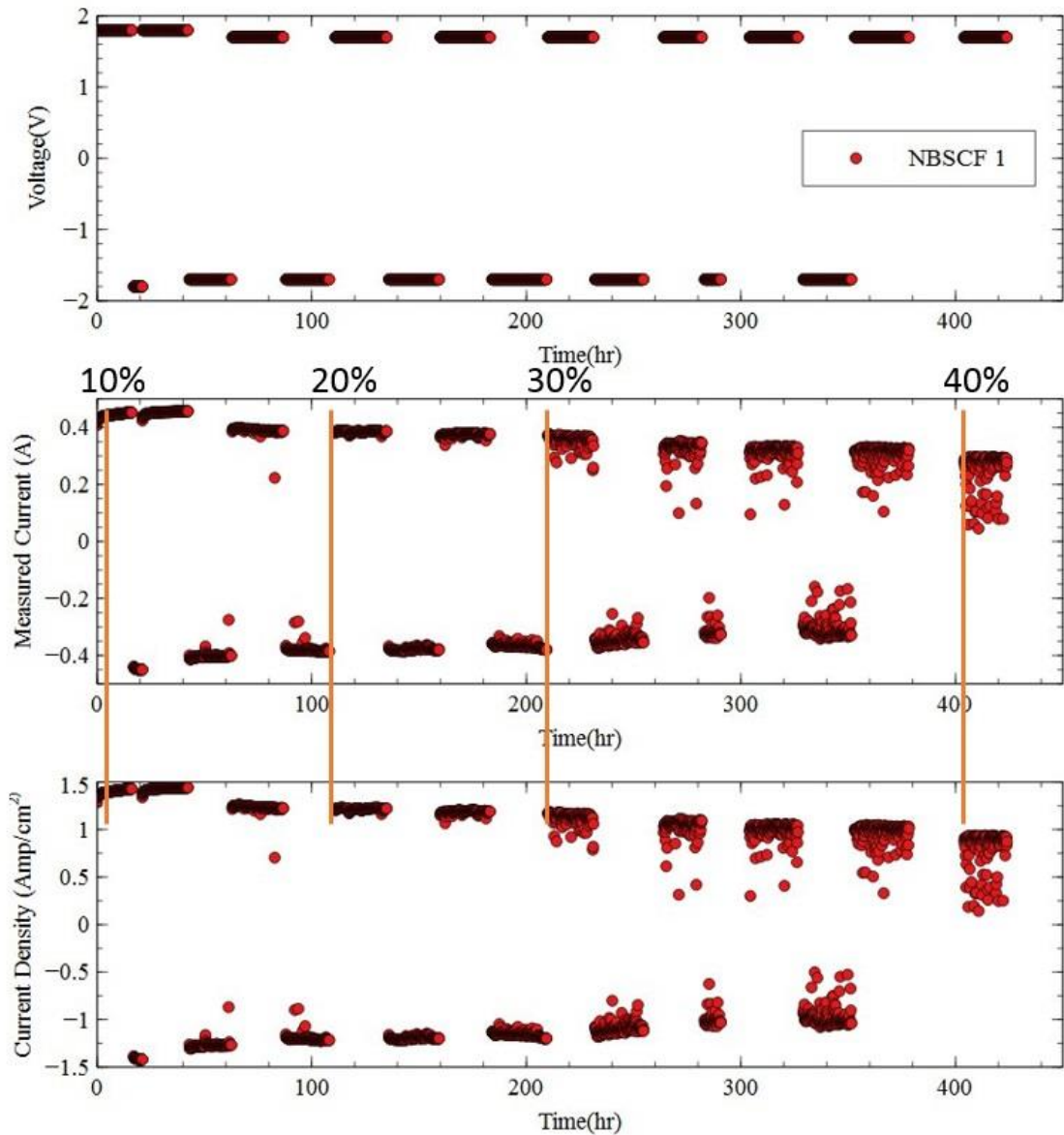


Figure 48. NBSCF/SDC/NBSCF symmetric cell under constant alternating +/- 1.7 Volts at 43hr. Initial 10% moisture at 0hr, switch to 20% moisture at 109hr, 30% moisture at 209hr and 40% moisture at 403hr. Balance air at 700°C. Plots voltage, current, and current density vs time (hr).

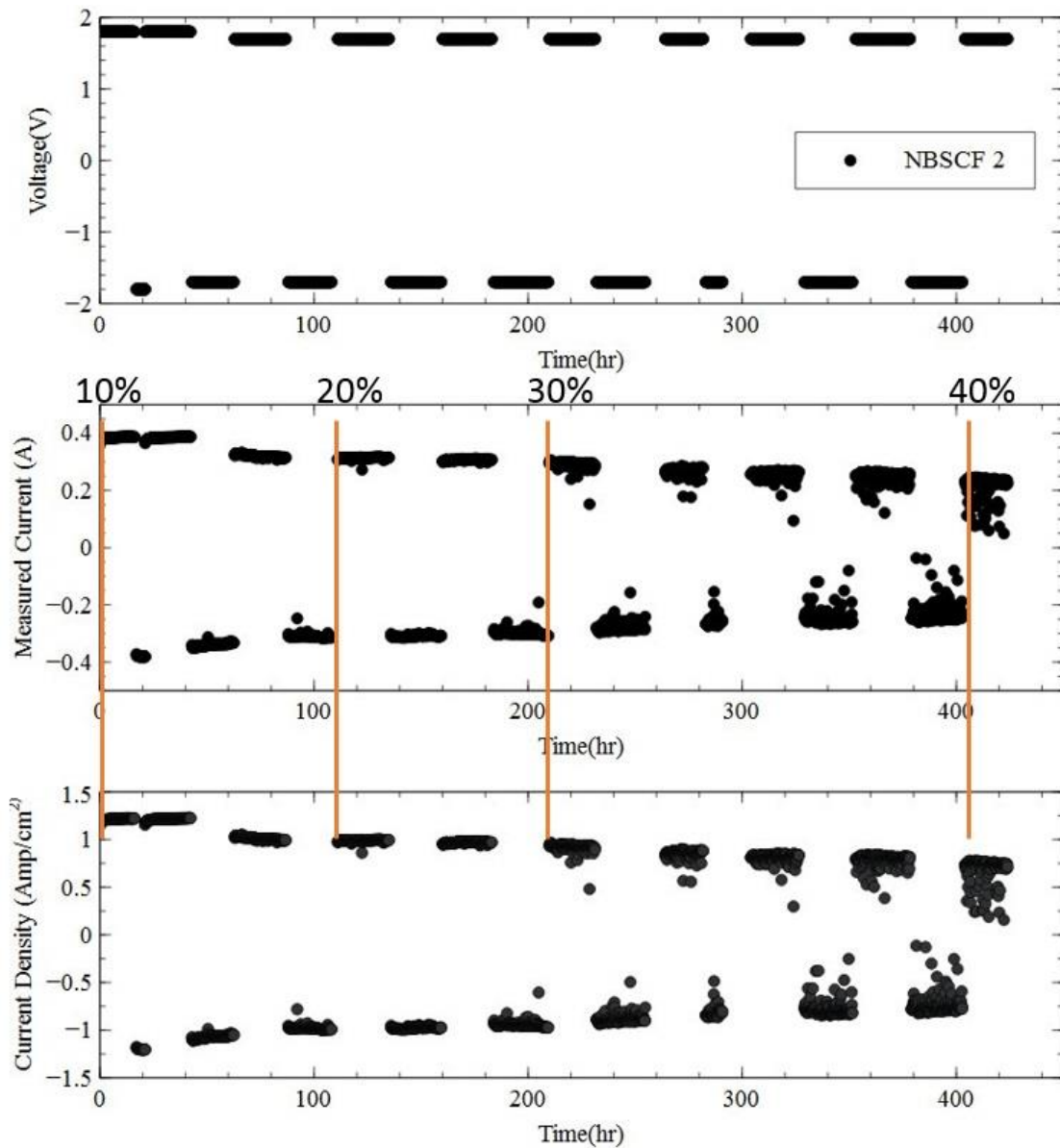


Figure 49: Another NBSCF/SDC/NBSCF symmetric cell under constant alternating ± 1.7 Volts at 43hr. Initial 10% moisture at 0hr, switch to 20% moisture at 109hr, 30% moisture at 209hr and 40% moisture at 403hr. Balance air at 700°C. Plots voltage, current, and current density vs time (hr).

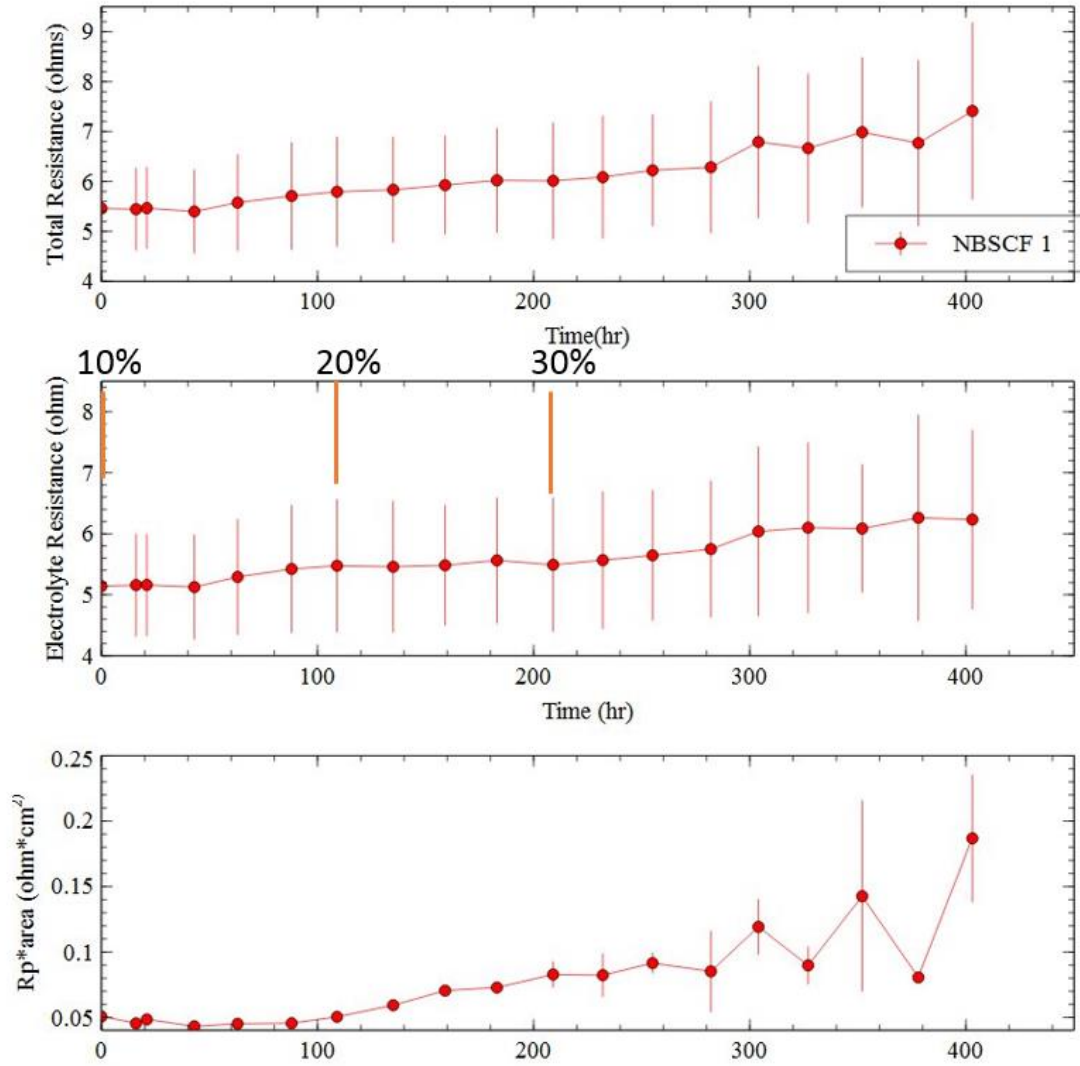


Figure 50. NBSCF/SDC/NBSCF EIS data under constant +/- 1.7 Volts at 43hr. Initial 10% moisture at 0hr, switch to 20% moisture at 109hr, 30% moisture at 209hr and 40% moisture at 403hr. Balance air at 700°C. Shows error bars for 2 cells tested. Plots total resistance, ohmic resistance and ASR vs time (hr).

PBCC shows some oscillation at 30% moisture near the end of testing for Figure 52 while Figure 51 showed even greater oscillation, but it is far more stable than PBSCF and NBSCF. The 30% moisture caused the current (also current density) to slowly decrease, which may be attributed to the small increase in electrolyte resistance (delamination). The EIS shows near steady R_p in Figure 53 for the PBCC cathodes in 30% moisture under a current density of 1 Amp/cm². Unlike PBSCF and NBSCF, this means that PBCC is more resistance to high concentrations of water vapor and is more stable under 30% moisture. As shown in the supplementary Appendix A in Figure 70, PBCC under applied voltage is unstable in 40% moisture, like PBCC in 40% moisture under OCV.

Under 30% moisture, PBCC's ohmic resistance is largely unchanged until the end where one of the cells starts to delaminate slightly. The effect of delamination was shown in Figure 71 and Figure 72 of the Supplementary Appendix A. PBCC is different from the degradation in PBSCF and NBSCF where both R_p and R_{ohmic} degraded under the same conditions. Perhaps this is because PBCC is resistant to 30% moisture with applied voltage, however it does not mean that the binder used in the buffer layer solution is resistant to high steam content. From the PBCC results, it seems suggests that the high-water vapor concentration is corroding the buffer layer solution that adheres the cathode to the electrolyte. This supports the delamination findings in PBSCF and NBSCF. Regardless, the great stability of ORR and OER performance shown by stable ASR for PBCC at 30% moisture makes it a great candidate for SOFC/SOEC systems.

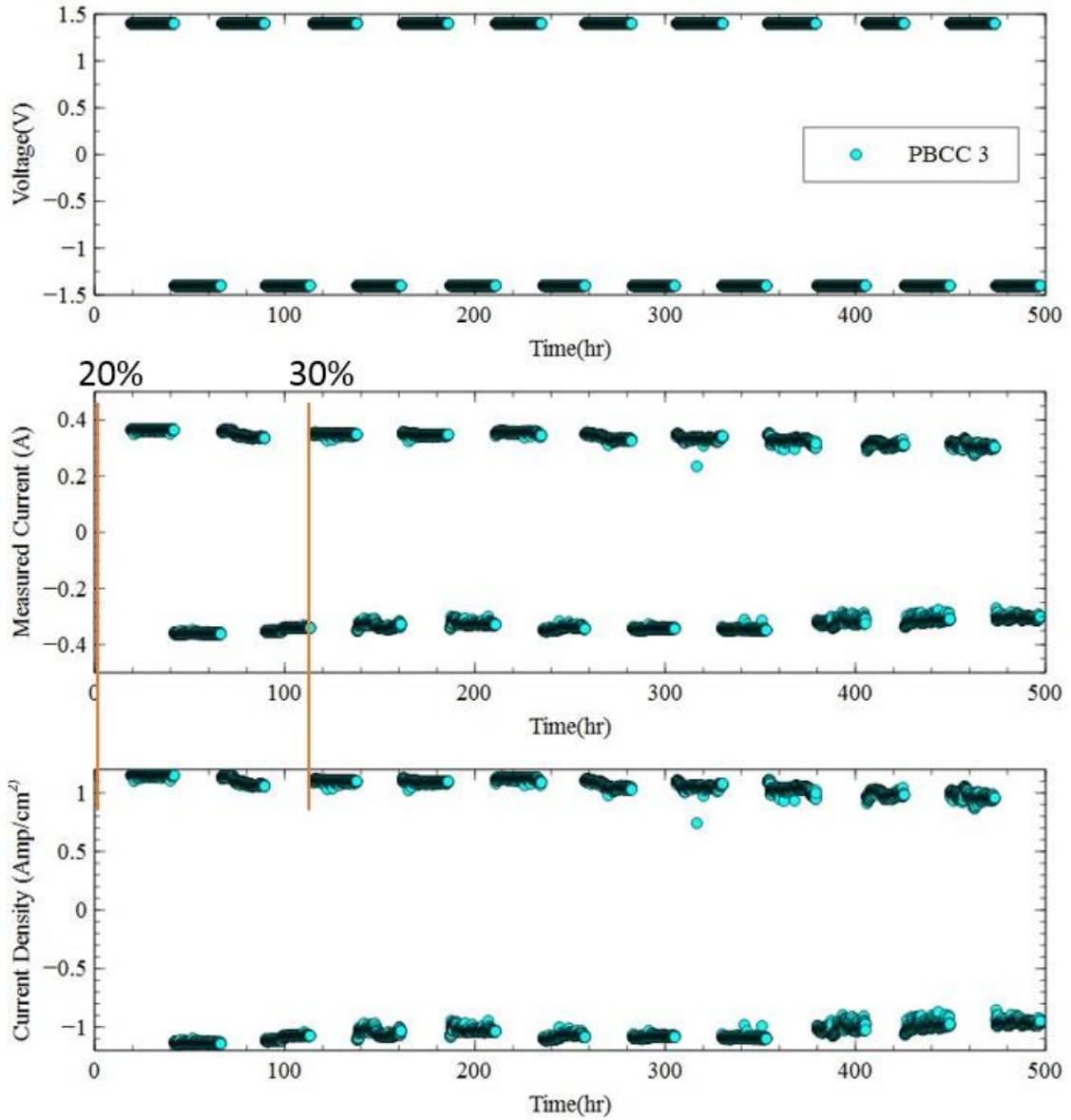


Figure 51. PBCC/SDC/PBCC long-term stability under constant alternating +/- 1.4 Volts at 18hr. Initial 20% moisture at 0hr, switched to 30% moisture at 114hr. Balance air at 700 °C. Plots voltage, current, and current density vs time.

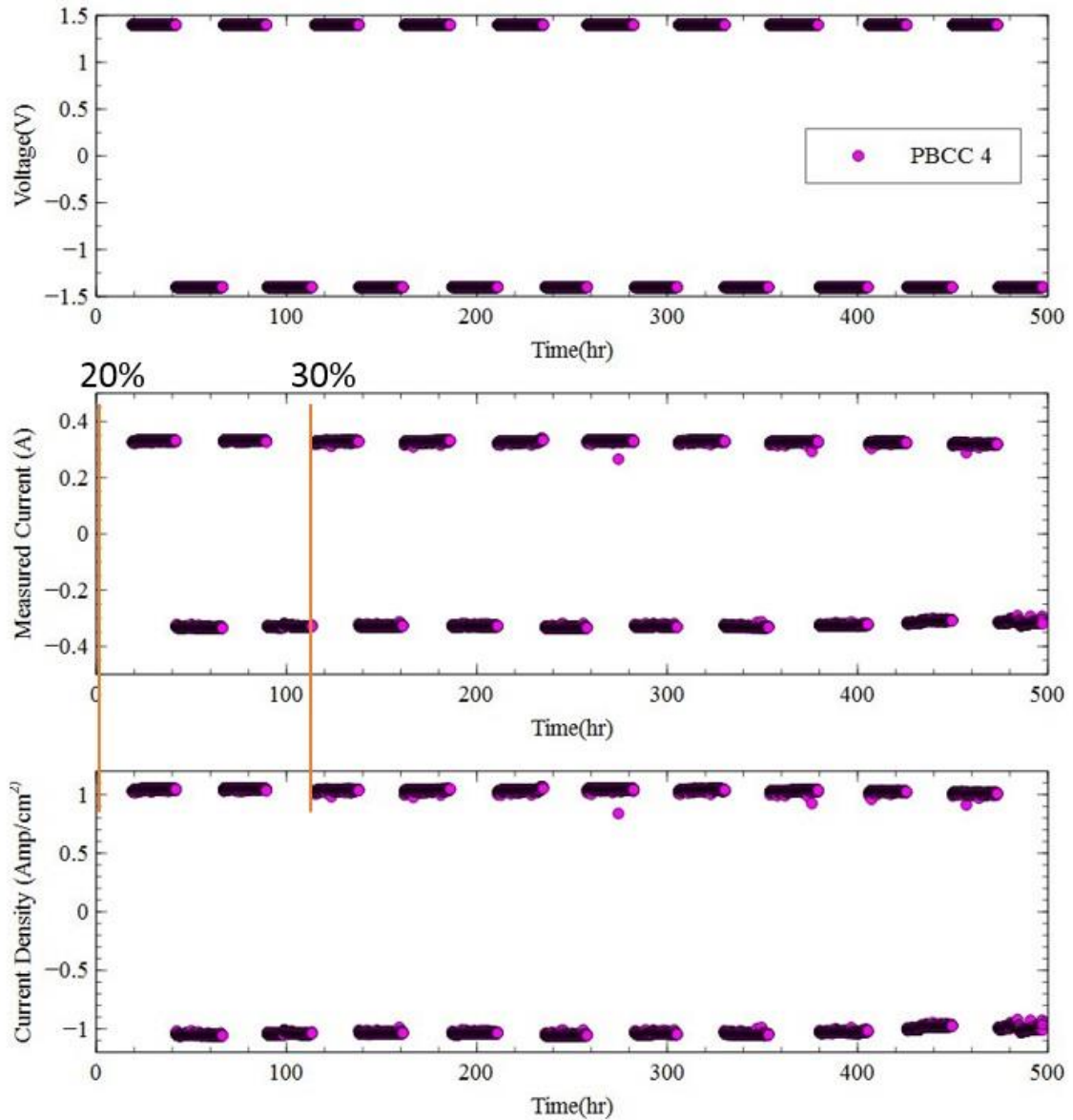


Figure 52. Another PBCC/SDC/PBCC long-term stability under constant alternating +/- 1.4 Volts at 18hr. Initial 20% moisture at 0hr, switched to 30% moisture at 114hr. Balance air at 700 °C. Plots voltage, current, and current density vs time

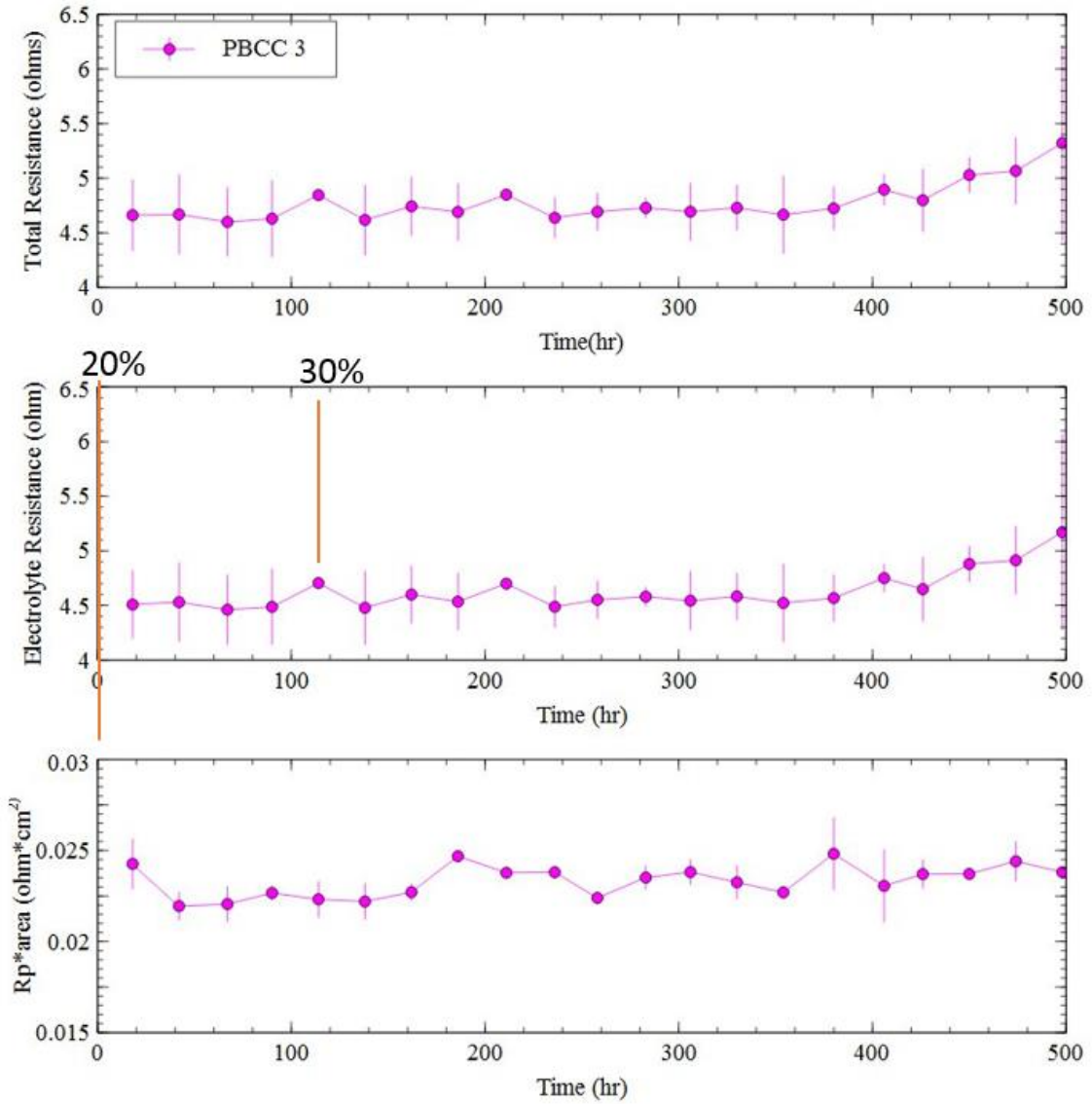


Figure 53. PBCC/SDC/PBCC EIS long-term stability under constant +/- 1.4 Volts at 18hr. Initial 20% moisture at 0hr, switched to 30% moisture at 114hr. Balance air at 700°C. Shows error bars for 2 cells tested. Plots total resistance, ohmic resistance and ASR vs time.

Overpotential was also used to keep track of the performance of the cathode, which is shown in Table 5, Table 6, and Table 7 for PBSCF, NBSCF and PBCC, respectively. These tables show the change in overpotentials as the moisture level is increased. The voltage sign shows after which + or - voltage the R_p was taken by the EIS machine. NBSCF and PBSCF shows a great increase in overpotential due to the degradation in the cathode, whereas PBCC's change in overpotential is almost negligible.

Table 5. Overpotential (V) on electrode for applied voltage on PBSCF symmetric cells.

	Time (hr)	Volt	Moisture	Amp/cm2	Current(A)	Rp	Vcathodes	Overpotential
PBSCF 1	42	+	20%	1	0.317	0.253	0.080	0.040
PBSCF 1	67	-	20%	1.02	0.323	0.296	0.096	0.048
PBSCF 1	211	-	30%	0.622	0.197	0.779	0.153	0.077
PBSCF 1	236	+	30%	0.524	0.166	1.348	0.224	0.112
PBSCF 2	42	+	20%	1.01	0.320	0.132	0.042	0.021
PBSCF 2	67	-	20%	0.964	0.305	0.138	0.042	0.021
PBSCF 2	211	-	30%	0.62	0.196	0.540	0.106	0.053
PBSCF 2	236	+	30%	0.55	0.174	0.671	0.117	0.058

Table 6. Overpotential (V) on electrode for applied voltage on NBSCF symmetric cells.

	Time (hr)	Volt	Moisture	Amp/cm ²	Current(A)	Rp (ohm)	Vcathodes	Overpotential
NBSCF 1	63	-	10%	1.23	0.3895	0.2771	0.1079	0.0540
NBSCF 1	88	+	10%	1.22	0.3864	0.2757	0.1065	0.0533
NBSCF 1	183	+	20%	1.1864	0.3757	0.4465	0.1678	0.0839
NBSCF 1	209	-	20%	1.2	0.3800	0.4905	0.1864	0.0932
NBSCF 1	352	-	30%	1.04	0.3294	0.6699	0.2206	0.1103
NBSCF 1	378	+	30%	1.02	0.3230	0.52094	0.1683	0.0841
NBSCF 2	63	-	10%	1.05	0.3325	0.2637	0.0877	0.0438
NBSCF 2	88	+	10%	1	0.3167	0.2999	0.0950	0.0475
NBSCF 2	183	+	20%	0.97	0.3072	0.4734	0.1454	0.0727
NBSCF 2	209	-	20%	0.97	0.3072	0.5555	0.1706	0.0853
NBSCF 2	352	-	30%	0.833	0.2638	1.1318	0.2986	0.1493
NBSCF 2	378	+	30%	0.82	0.2597	0.4968	0.1290	0.0645

Table 7. Overpotential (V) on electrode for applied voltage on PBCC symmetric cells.

	Time (hr)	Volt	Moisture	Amp/cm ²	Current(A)	Rp	Vcathodes	Overpotential
PBCC 3	42	+	20%	1.15	0.3642	0.1361	0.0496	0.0248
PBCC 3	67	-	20%	1.14	0.3610	0.1424	0.0514	0.0257
PBCC 3	283	+	30%	1.028	0.3256	0.1464	0.0477	0.0238
PBCC 3	306	-	30%	1.085	0.3436	0.1526	0.0524	0.0262
PBCC 3	474	+	30%	0.959	0.3037	0.1506	0.0457	0.0229
PBCC 3	498	-	30%	0.946	0.2996	0.1502	0.0450	0.0225
PBCC 4	42	+	20%	1.047	0.3316	0.1411	0.0468	0.0234
PBCC 4	67	-	20%	1.058	0.3351	0.1362	0.0456	0.0228
PBCC 4	283	+	30%	1.041	0.3297	0.1506	0.0496	0.0248
PBCC 4	306	-	30%	1.046	0.3313	0.1482	0.0491	0.0245
PBCC 4	474	+	30%	1.007	0.3189	0.1577	0.0503	0.0251
PBCC 4	498	-	30%	1.009	0.3195	0.1506	0.0481	0.0241

4.8 Raman on Applied Voltage Cells

To verify to structural stability results, Raman is done on the symmetric cells tested under applied voltage. The symmetric cells from Figure 47 (PBSCF), Figure 50 (NBSCF), and Figure 53 (PBCC) were analyzed using Raman. From Figure 54, PBCC powder and the PBCC symmetric cell exposed to 40% water vapor both show the same peak at 614cm^{-1} which is close to Milt et al.'s peak at 607cm^{-1} for Barium Cobaltite [41]. The slight shift may be that the Barium Cobaltite formed on the PBCC surface is not the pure cubic BaCoO_3 phase. However, more experiments would need to be done to verify the mechanism of formation of BaCoO_3 on PBCC surface and what was discussed in the degradation mechanism section.

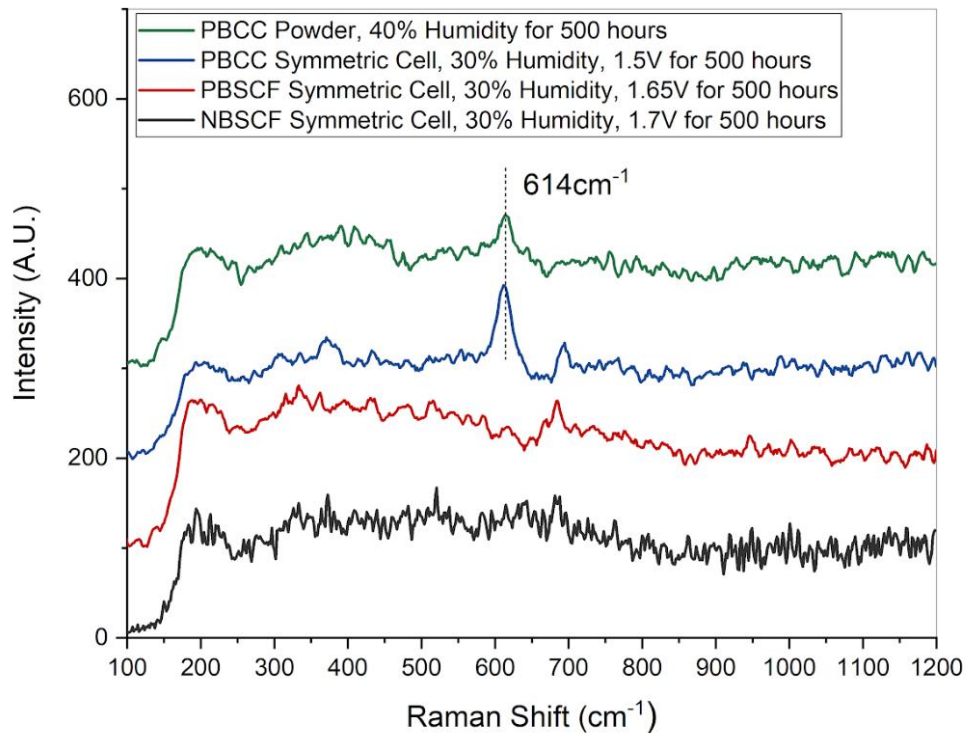


Figure 54. Raman spectra of PBSCF from Figure 47, NBSCF from Figure 50, and PBCC from Figure 70 symmetric cells after alternating voltage tests, and PBCC powder after moisture exposure for 500hrs at 700°C.

CHAPTER 5: CONCLUSION

PNM was removed from consideration due to the fast degradation in R_p . Under ROCs, NBSCF and PBSCF had unstable microstructures in 30% H_2O resulting in delamination of the cathode from the electrolyte and suffered from severe cathode corrosion. NBSCF and PBSCF did not show any structural change in the XRD and Raman data before and after testing even though EIS showed degradation. There may be an insulating phase forming that is not Raman active or there is something else happening to NBSCF and PBSCF.

Meanwhile PBCC under ROCs as symmetric cells showed stable performance for about 400hrs when tested at a current density of 1 Amp/cm² and 30% H_2O at 700°C. There was little to no change in the EIS for the cathode R_p and in the reversible ORR/OER performance. Therefore, PBCC is a great cathode candidate for SOECS/SOFCs under high moisture content.

Under 700°C in 40% H_2O under OCV, the PBCC symmetric cells had the lowest ASR, but had a slow degradation rate in ASR/hr. The cause for the degradation under 40% H_2O was investigated and from the Raman data, it is likely that $BaCoO_3$ formed on the surface. However, $BaCoO_3$ is a good catalyst for ORR, thus it is hard to conclude that the slow EIS degradation in 40% H_2O under OCV is due to $BaCoO_3$ formation. The cause of degradation may be from a Raman inactive phase forming. For SOFC/SOEC operation at 40% or higher with PBCC, infiltration of a good catalyst to block surface degradation could be used. Further experiments should be done to verify the exact mechanism for $BaCoO_3$ formation and if $BaCoO_3$ is the cause of PBCC EIS degradation in 40% or higher water vapor concentration.

CHAPTER 6: RECOMMENDATIONS AND FUTURE WORK

Although the degradation of PBCC into BaCoO_3 on the PBCC surface was discovered, the exact mechanism that forms Barium Cobaltite is uncertain. Also, it is unknown if any Raman inactive phase formed. To uncover the exact mechanism, further understanding of the elemental composition and the electronic structure must be uncovered. In-situ X-ray Photoelectron Spectroscopy (XPS) and Extended X-ray Absorption Fine Structure (EXAFS) is recommended. From XPS and EXAFS, it would be possible to discover the intermediates phases that Barium reacts with before it forms BaCoO_3 , further validate if BaCoO_3 forms, and if Raman inactive phases form like BaO .

Another binder for adhesion of the cathode onto the electrolyte can also be investigated. From the ROCs under high steam and voltage/current showed that the current buffer layer solution formula is being corroded. A more resistant buffer layer to high steam would be greatly beneficial to SOEC operation under high steam and prevent delamination of the cathode and electrolyte.

Further investigations can be done on the water promoting effect seen in PBCC and PBSCF vs NBSCF. There may be some property in Praseodymium and not Neodymium that leads to an initial water promoting effect that reduces the cathode polarization resistance. By uncovering what that property is, new materials can be fabricated that would be more resistant in high humidity environments for SOFCs/SOECs. The water promoting effect is most likely due to some surface change on the material so in-situ Raman Spectroscopy would be used.

In-situ Raman could also be used to investigate the EIS degradation in NBSCF and PBSCF. There was no permanent structural change in NBSCF and PBSCF based on XRD

and Raman spectra after 500 hours of long-term operation in humidity, but the EIS data showed degradation. Therefore, if there is a structural or chemical change in high humidity, in-situ Raman could characterize it. If it is an electronic change, then XPS and EXAFS would determine if there is any change in electronic structure of double perovskite after electrochemical testing at high temperatures with moisture. The performance change could also be due to water adsorption onto the cathode surface or interaction with the material may affect oxygen reduction process on the cathode and electrochemical performance while retaining structural stability. Here, in-situ TGA can be used to see how moisture interacts with the double perovskite on cathode surface.

Some other tests that can be done would be to test PBCC in various contaminant environments such as CO₂, sulfur contaminants (SO_x), chromium, or etc. Infiltration or other techniques could be used to further enhance the cathodes performance and resistance to high humidity. PBCC performance as full cells in SOFCs/SOECs should also be tested.

APPENDIX A. SUPPLEMENTARY DATA

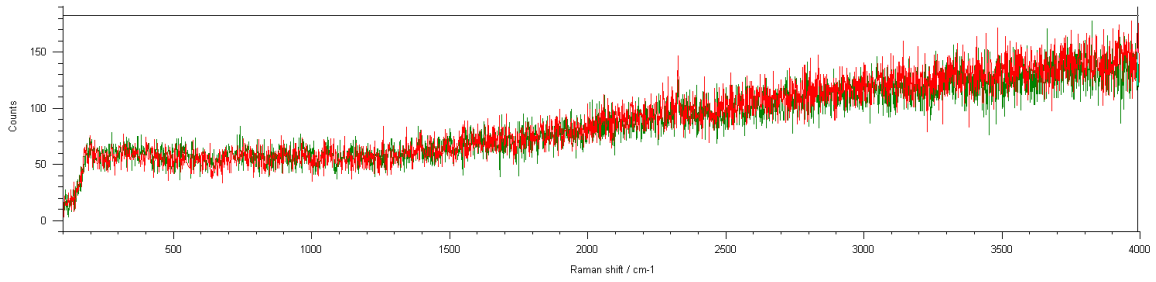


Figure 55. Raman scan of initial PBCC powder, 2 samples

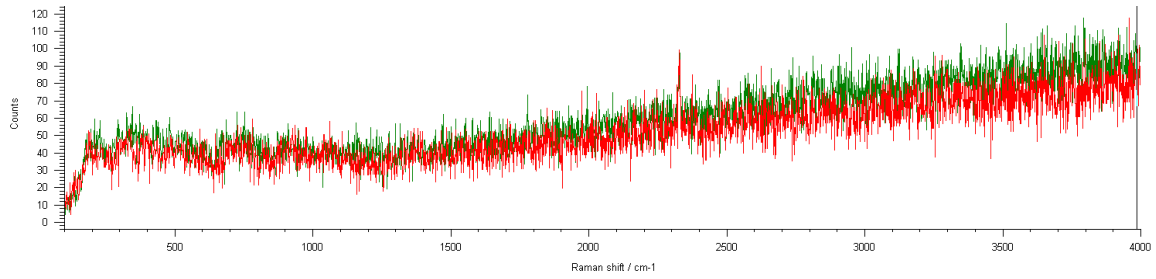


Figure 56. Raman scan of initial PBSCF powder, 2 samples.

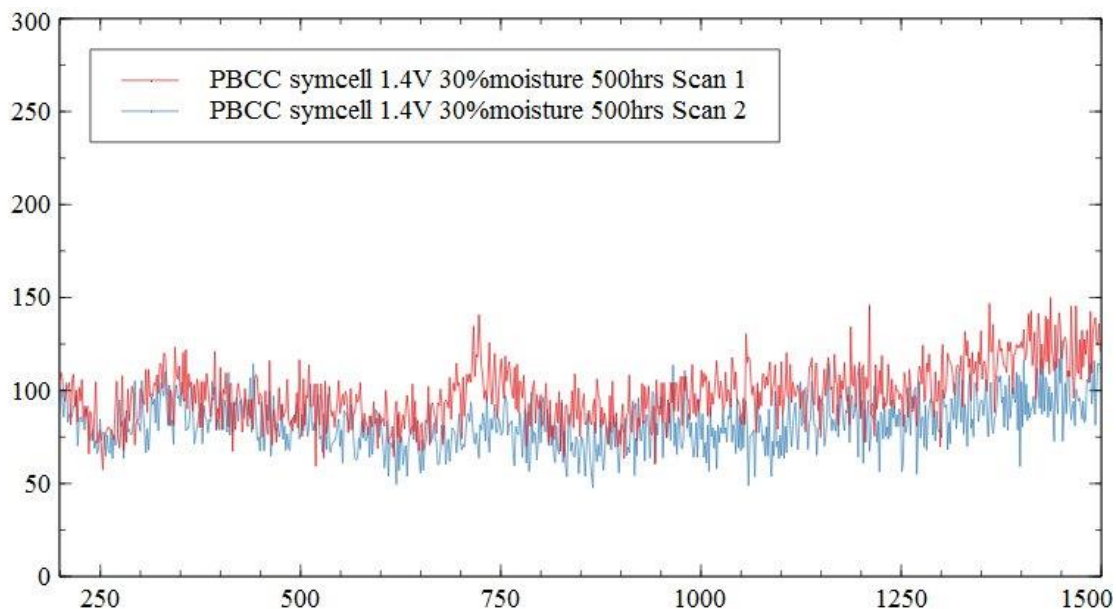


Figure 57. Raman scans from PBCC symmetric cell after testing from Figure 53

The PBCC symmetric cells tested under applied voltage in Figure 53 was tested using Raman to compare with the Raman data of PBCC in Figure 54. Figure 57 shows that there is no significant Raman peak, however there may be a peak between 700-750 cm^{-1} raman shift, but the signal-to-noise ratio makes it inconclusive. Therefore, the degradation of PBCC in 40% water vapor is due to some change on the PBCC surface. More information is needed since BaCoO_3 formed on the PBCC surface in 40% water vapor possesses good catalytic activity for ORR.

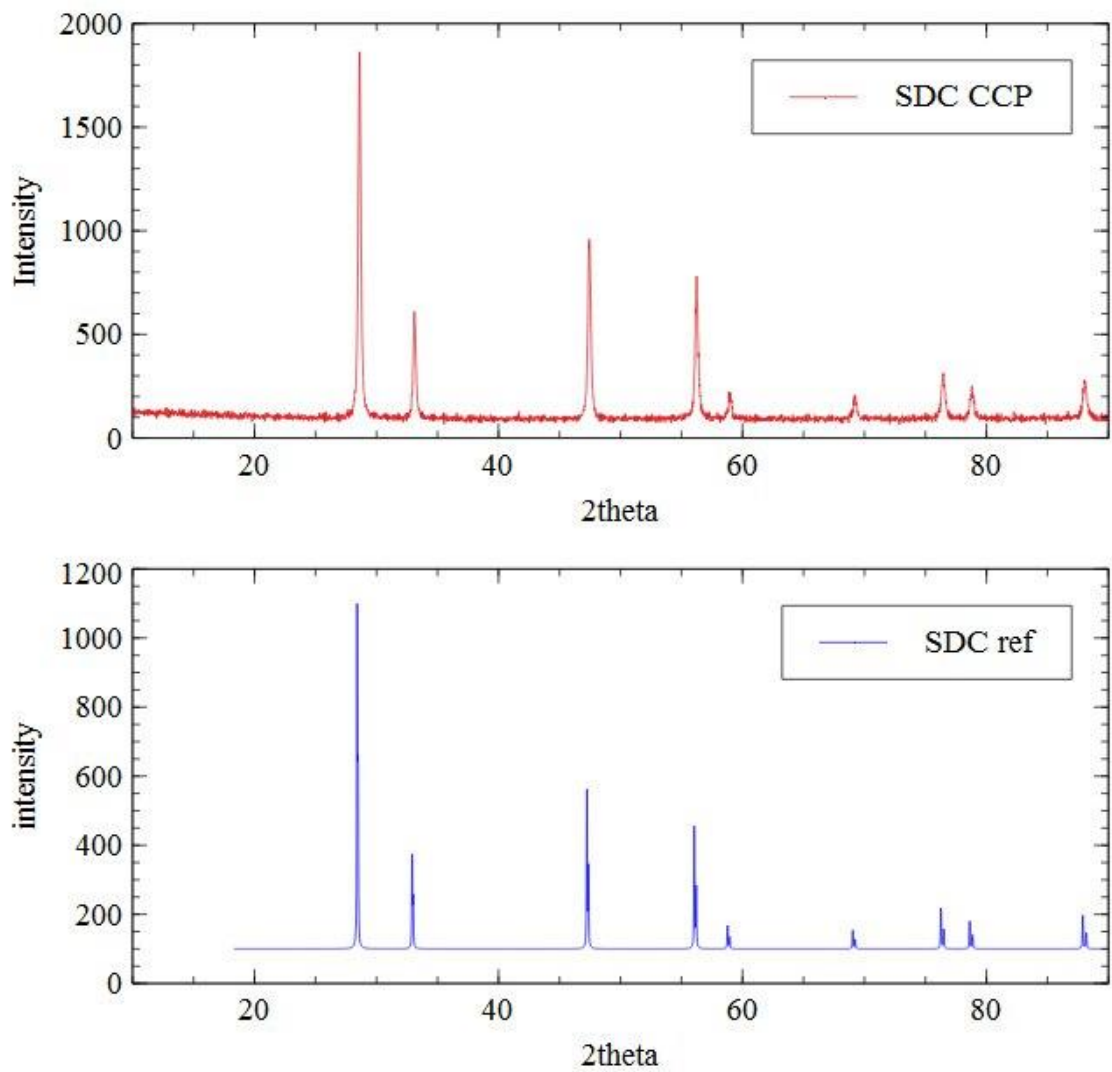


Figure 58. XRD of Carbon Co-precipitated SDC vs. SDC reference (01-080-5538) from PDF-4+ database.

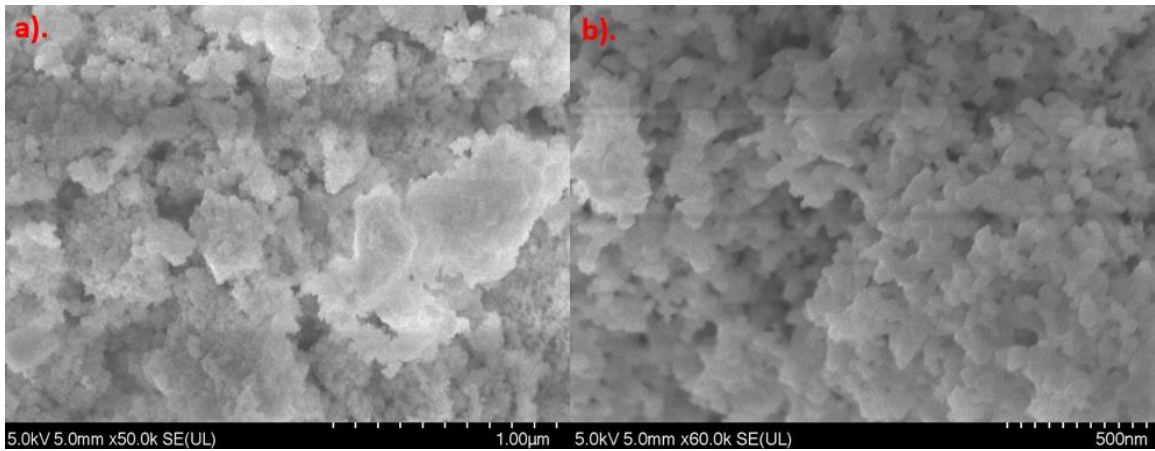


Figure 59. a) Midgrade SDC from Fuel Cell Materials b). Carbon Co-Precipitated SDC. CCP SDC has a finer grain size.

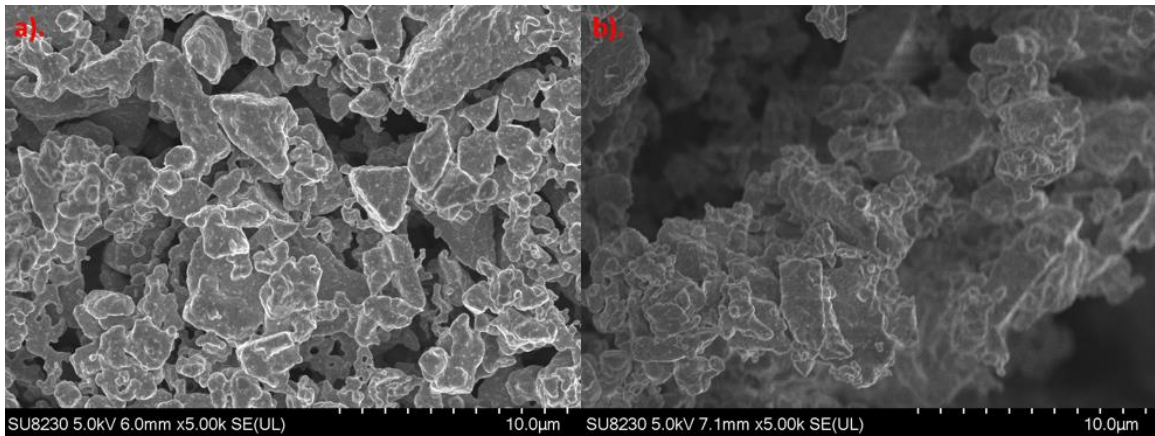


Figure 60. SEM image of PBSCF a) surface and b) cross-section before testing

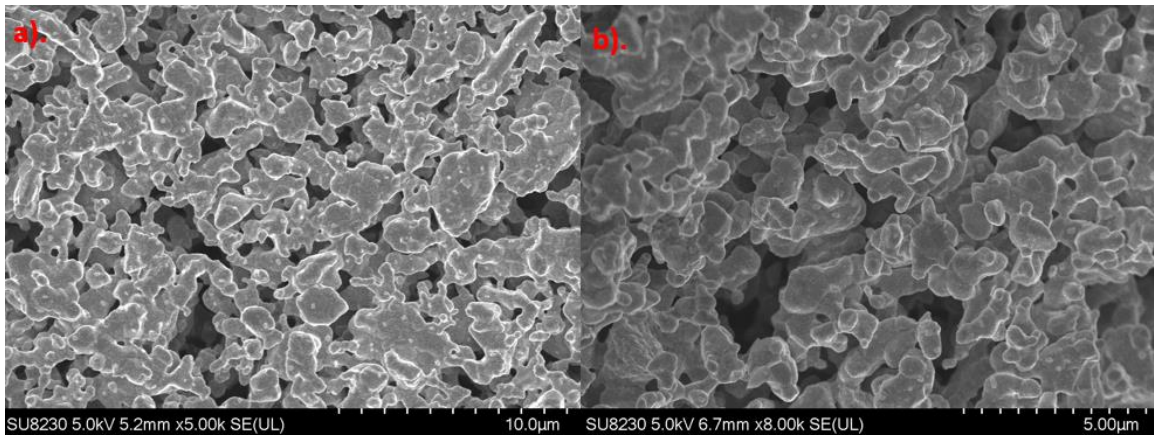


Figure 61. SEM image of NBSCF a) surface and b) cross-section before testing

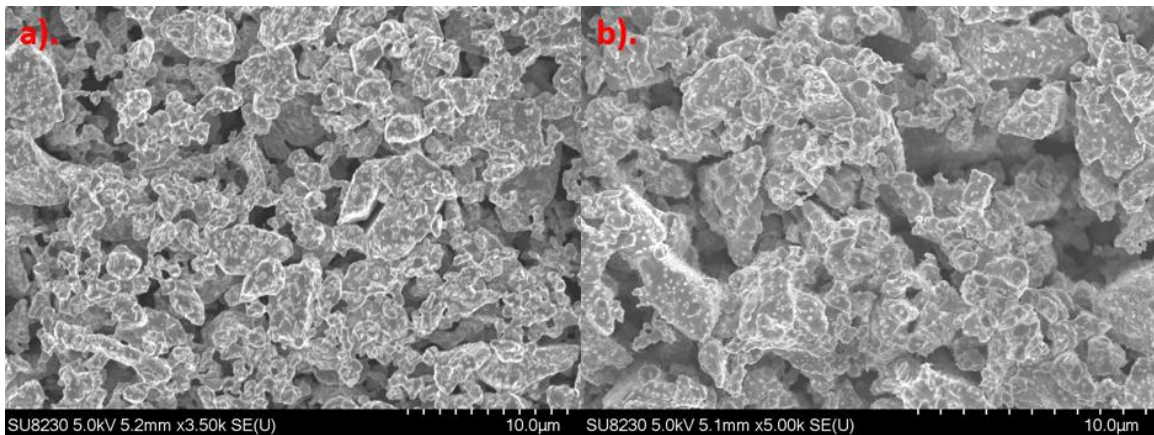


Figure 62. PBSCF symmetric cell a) surface and b) cross-section after testing (40% moisture, balance air) for 500hrs at 700 Celsius under OCV.

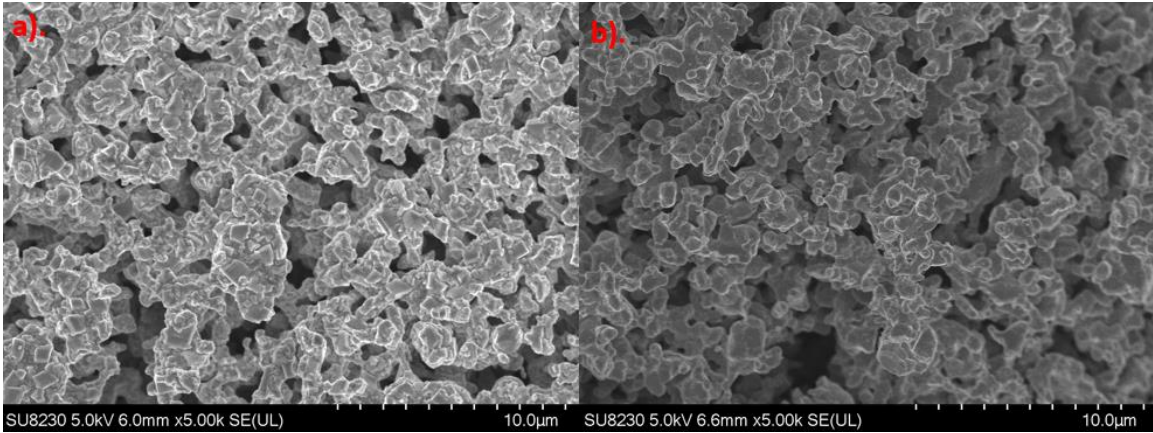


Figure 63. NBSCF symmetric cell a) surface and b) cross-section after testing (40% moisture, balance air) for 766hrs at 700 Celsius under OCV.

Figure 60 to Figure 63 show grain growth due to long-term heat exposure for the cathodes.

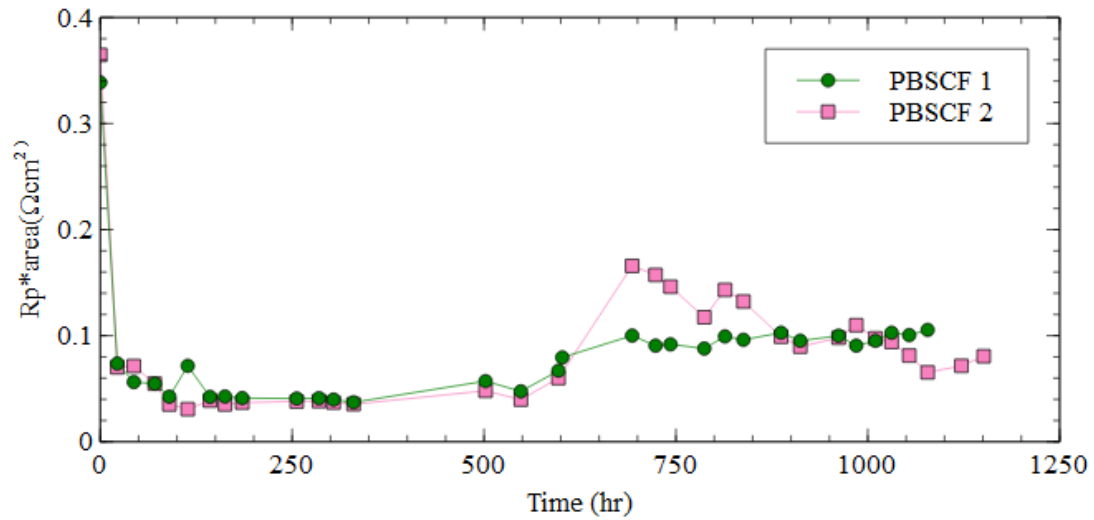
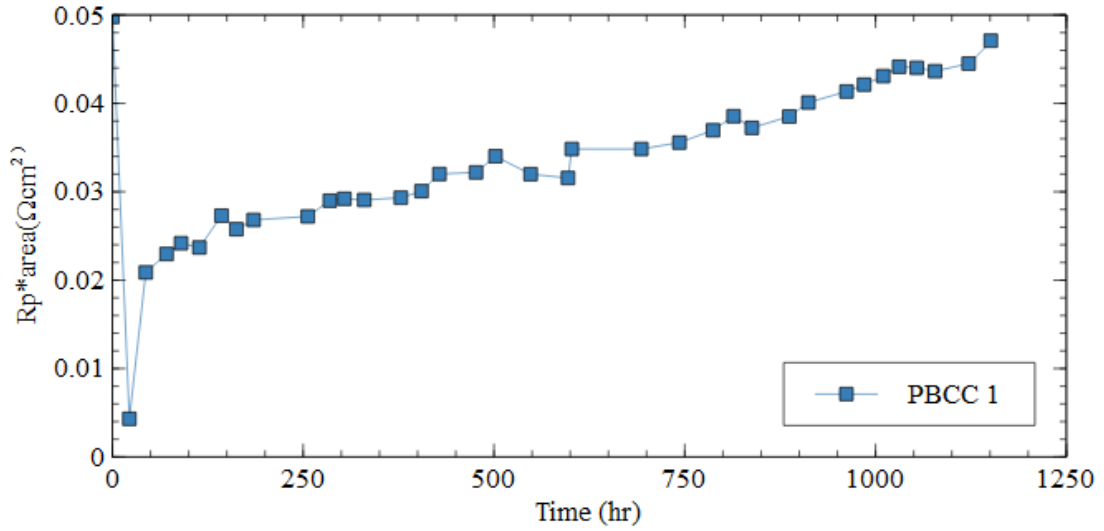


Figure 64. Long-term ASR for PBCC and PBSCF (both cells same) symmetric cells with SDC electrolyte in 40% moisture and balance air at 700 Celsius under OCV.

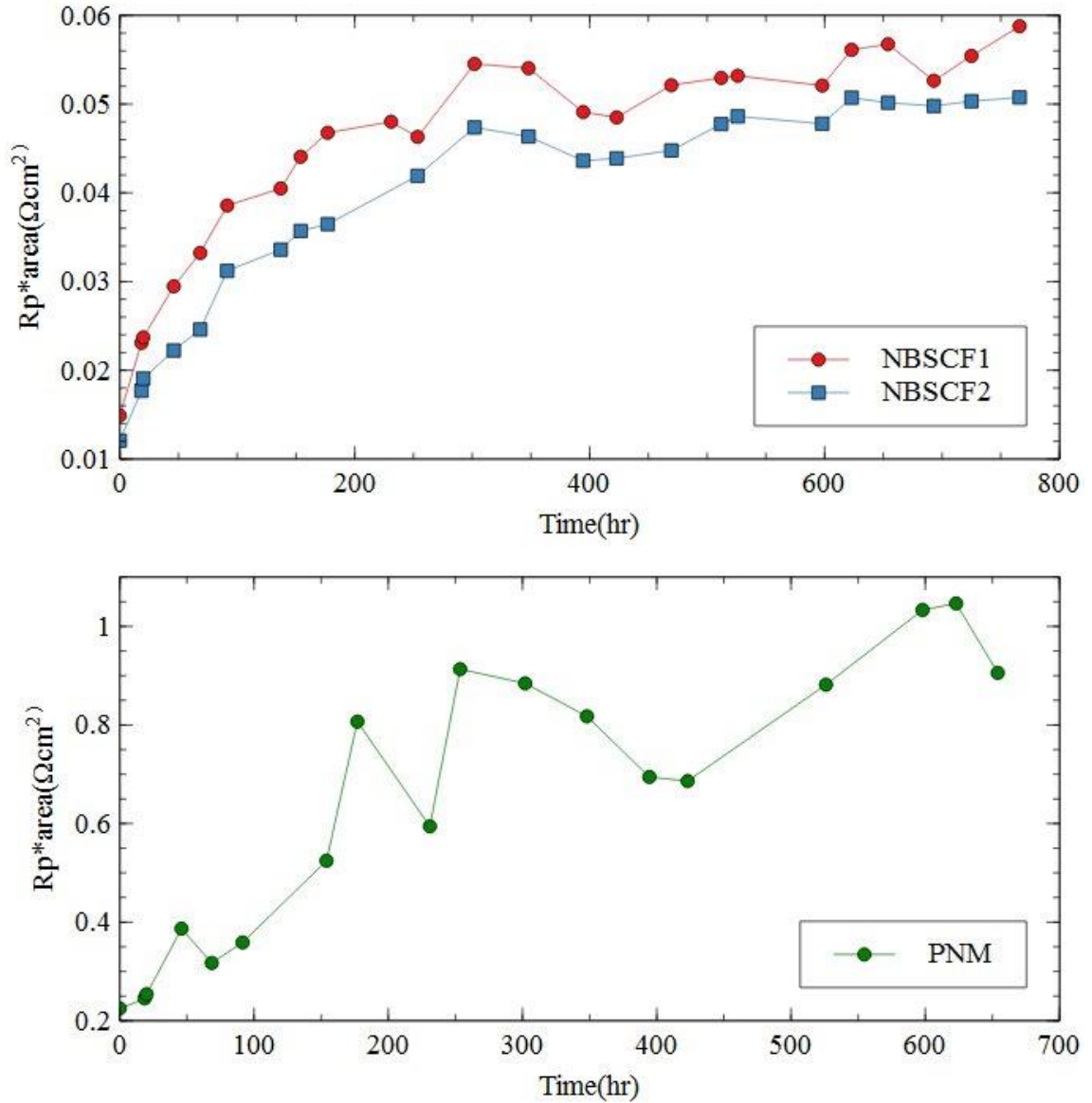


Figure 65. Long-term ASR NBSCF (both cells same) and PNM symmetric cells with SDC electrolyte in 40% moisture and balance air at 700 Celsius under OCV.

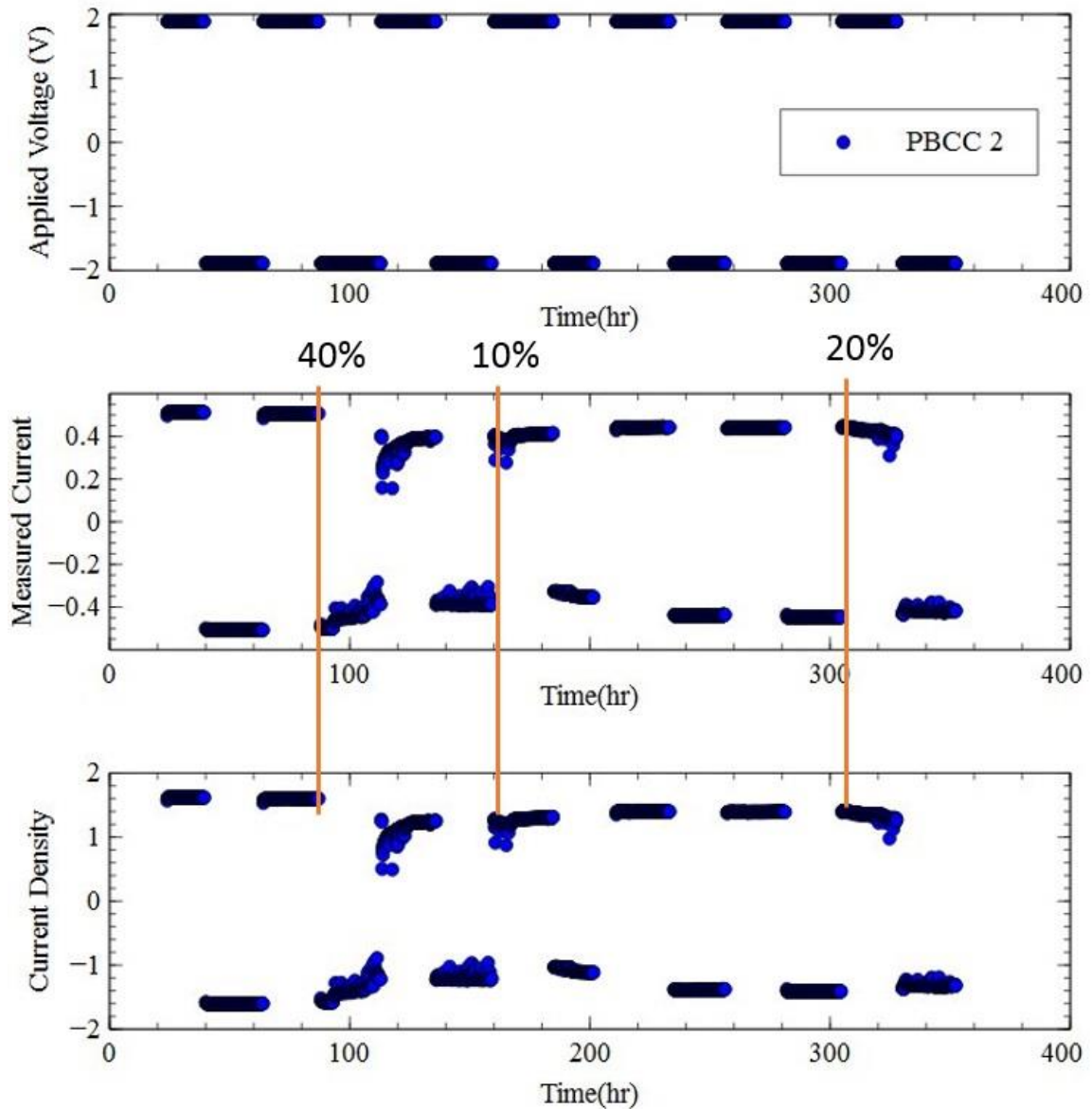


Figure 66: Data of a PBCC/SDC/PBCC with a constant alternating +/-1.8 Volts. It shows the voltage, current, and current density based on the time in hours. The orange line at 93hrs is when the air/moisture feed is switched to 40% moisture. 160hrs it is swapped to 10% moisture and 305hrs it is swapped to 20% moisture. The initial moisture is 0%. 700°C

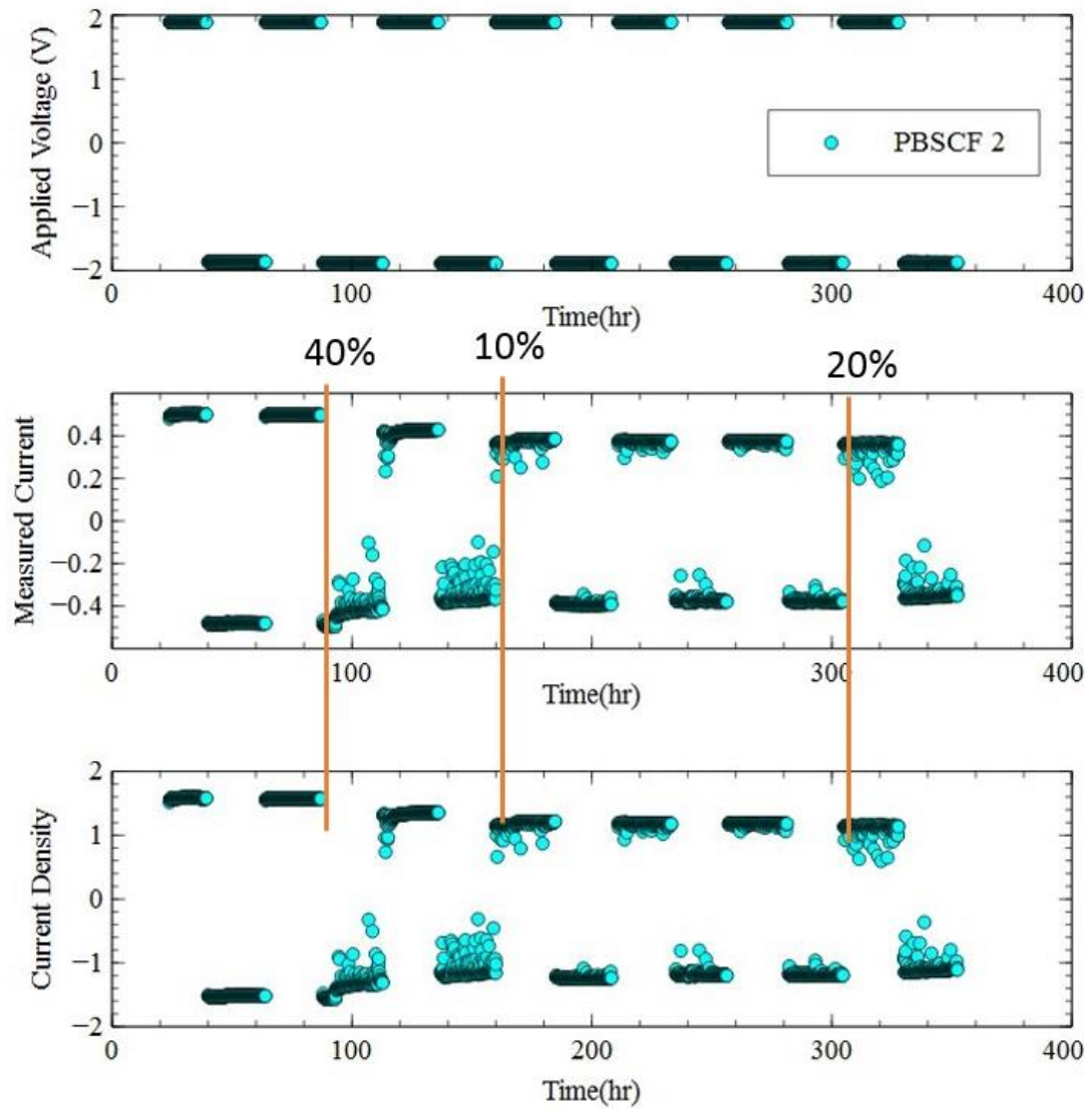


Figure 67: Data of a PBSCF/SDC/PBSCF with a constant alternating ± 1.8 Volts. It shows the voltage, current, and current density based on the time in hours. The orange line at 93hrs is when the air/moisture feed is switched to 40% moisture. 160hrs it is swapped to 10% moisture and 305hrs it is swapped to 20% moisture. The initial moisture is 0%. 700°C

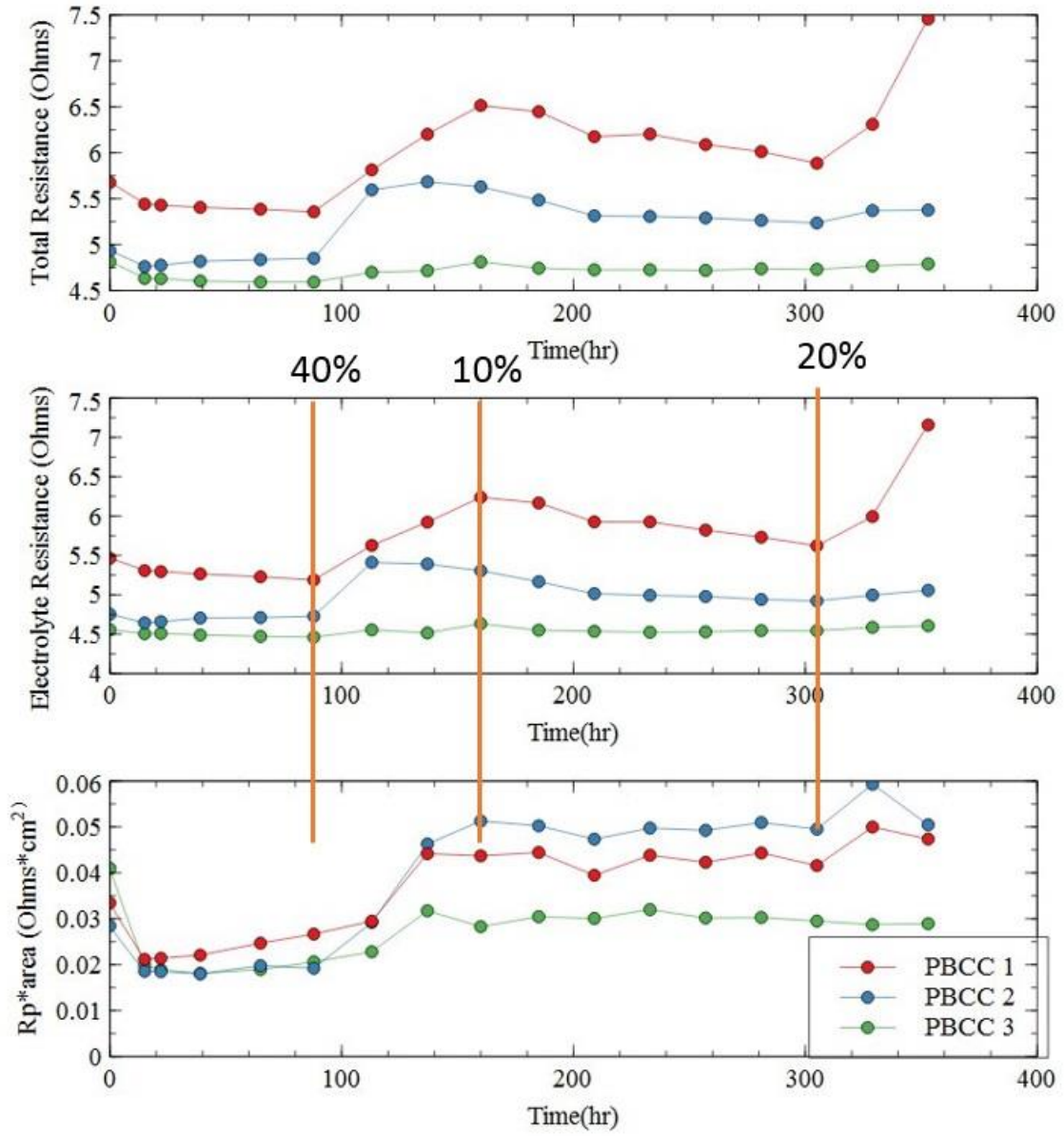


Figure 68: EIS results for PBCC/SDC/PBCC under constant +/-1.8 volts for cells 1 and 2. Cell 3 was not under voltage. The figure shows the total symmetric cell resistance, the electrolyte/ohmic resistance and Rp*area of one cathode vs time(hr). The orange lines are the same as Figure 67. 700°C

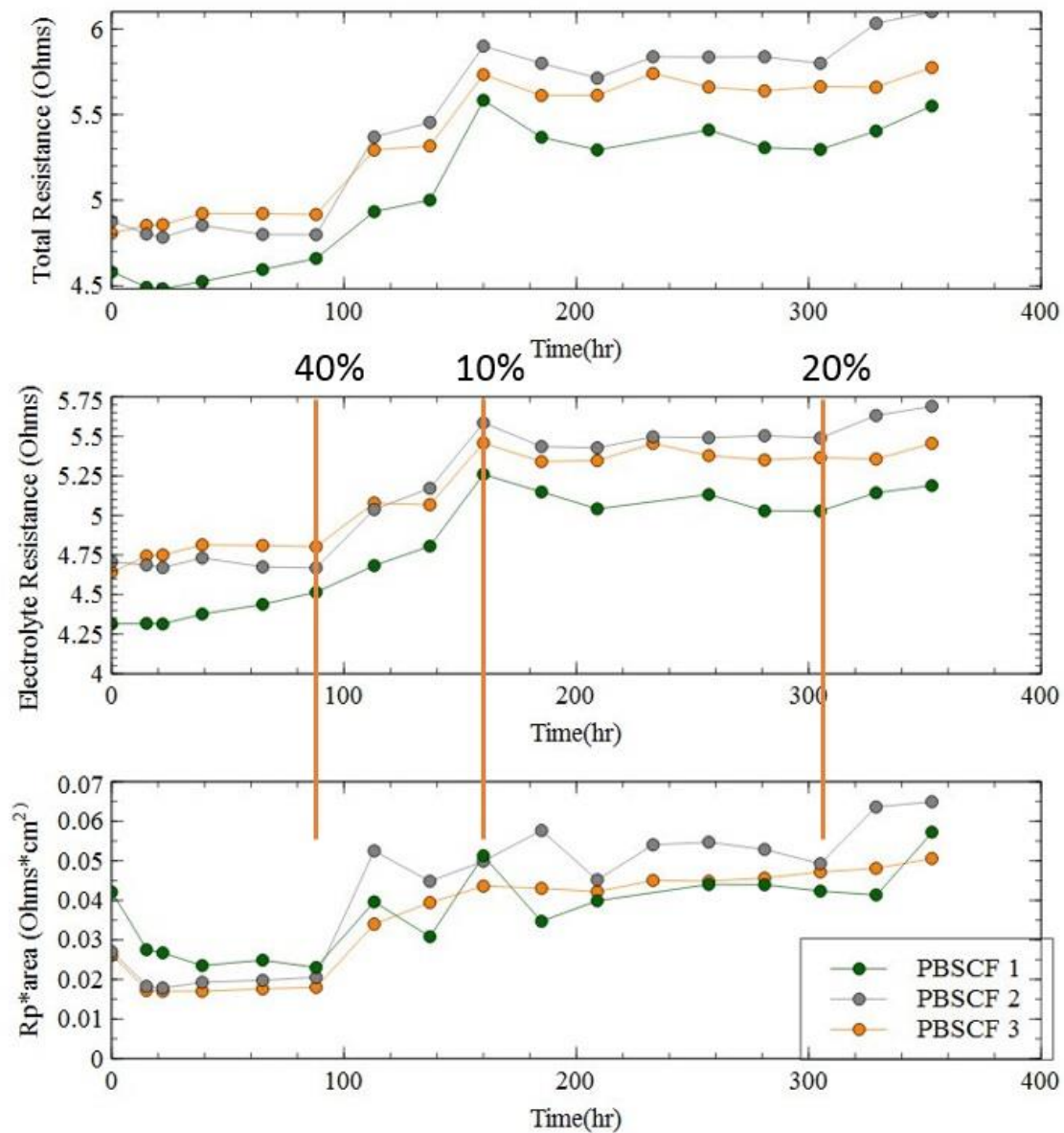


Figure 69: EIS results for PBSCF/SDC/PBSCF under constant +/-1.8 volts. The figure shows the total symmetric cell resistance, the electrolyte/ohmic resistance and $R_p \cdot \text{area}$ of one cathode vs time(hr). The orange lines are the same as Figure 67. 700°C

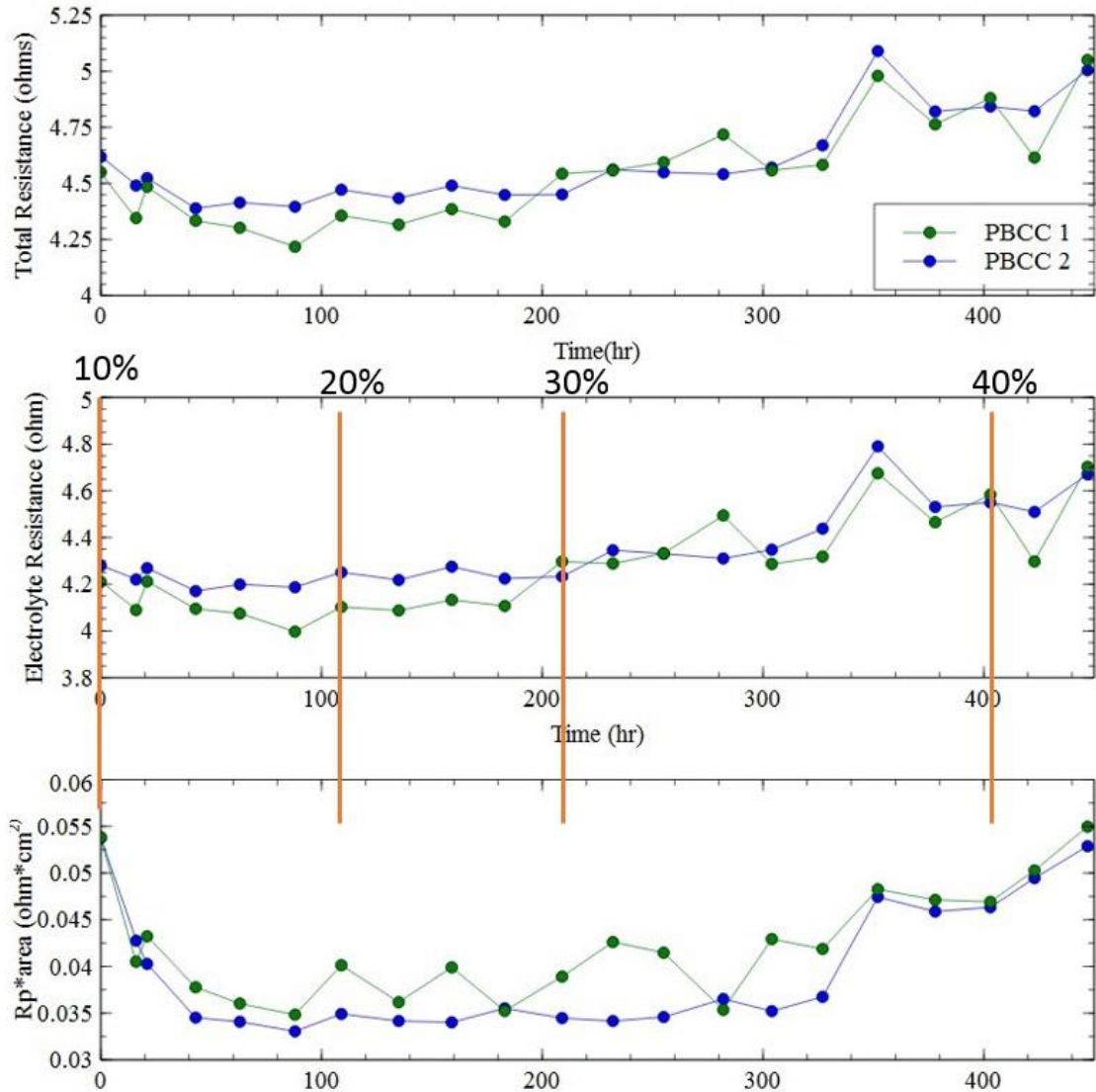


Figure 70. PBCC/SDC/PBCC EIS data under constant +/- 1.5 Volts at 43hr. Initial 10% moisture at 0hr, switch to 20% moisture at 109hr, 30% moisture at 209hr and 40% moisture at 403hr. Balance air at 700 °C. Current Density 1.3Amp/cm². Plots total resistance, ohmic resistance and ASR vs time.

Table 8. Overpotential (V) on electrode for applied voltage on PBCC symmetric cells under 1.3 Amp/cm².

	Time (hr)	Volt	Moisture	Amp/cm2	Current(A)	Rp	Vcathodes	Overpotential
PBCC 1	63	-	10%	1.33	0.4212	0.2275	0.0958	0.0479
PBCC 1	88	+	10%	1.32	0.4180	0.2200	0.0920	0.0460
PBCC 1	183	+	20%	1.29	0.4085	0.2225	0.0909	0.0454
PBCC 1	209	-	20%	1.23	0.3895	0.2458	0.0957	0.0479
PBCC 1	378	+	30%	1.15	0.3642	0.2976	0.1084	0.0542
PBCC 1	403	-	30%	1	0.3167	0.2963	0.0938	0.0469
PBCC 1	423	+	40%	1.14	0.3610	0.3175	0.1146	0.0573
PBCC 1	447	-	40%	1.04	0.3294	0.3471	0.1143	0.0572
PBCC 2	63	-	10%	1.3	0.4117	0.2152	0.0886	0.0443
PBCC 2	88	+	10%	1.3	0.4117	0.2087	0.0859	0.0430
PBCC 2	183	+	20%	1.27	0.4022	0.2243	0.0902	0.0451
PBCC 2	209	-	20%	1.26	0.3990	0.2177	0.0869	0.0434
PBCC 2	378	+	30%	1.13	0.3579	0.2897	0.1037	0.0518
PBCC 2	403	-	30%	1.111	0.3518	0.2926	0.1029	0.0515
PBCC 2	423	+	40%	1.14	0.3610	0.3123	0.1127	0.0564
PBCC 2	447	-	40%	1.08	0.3420	0.3339	0.1142	0.0571

About half of PBCC's change in overpotential is due to exposure in 40% moisture, which signifies that PBCC with applied voltage is not stable at 40% moisture.

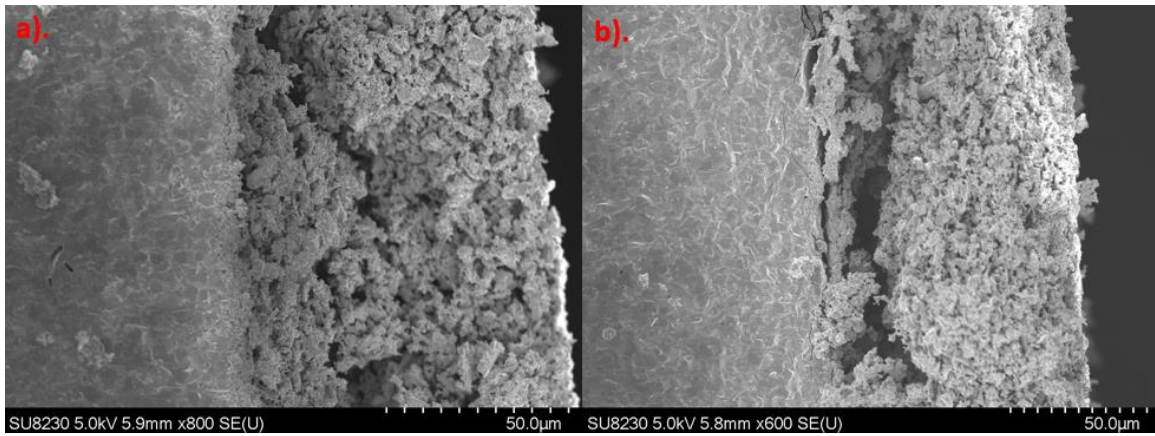


Figure 71. PBSCF symmetric cell after testing from Figure 67 and Figure 69. a). shows cathode still adhered to the electrolyte while b). some sections of the cathode are delaminating from the electrolyte.

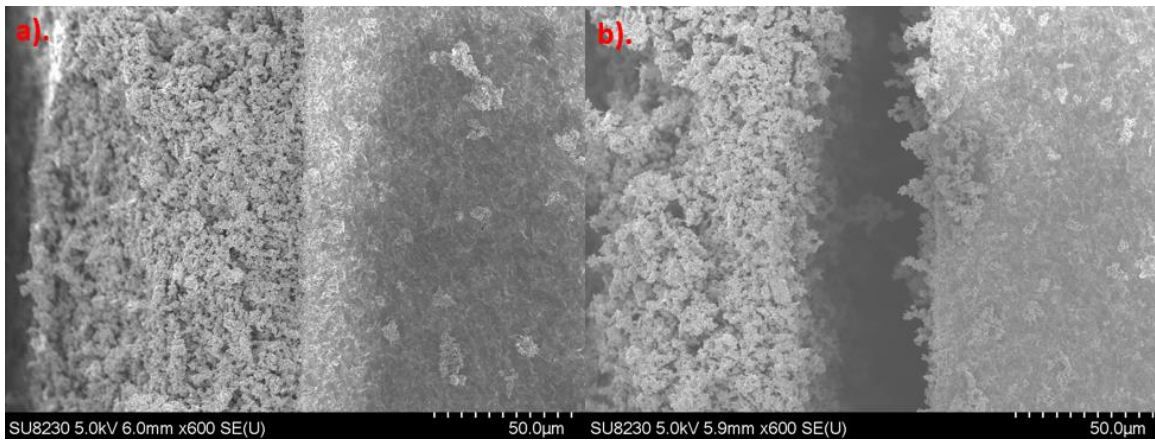


Figure 72. NBSCF symmetric cell after testing from Figure 48 to Figure 50 a). shows cathode still adhered to the electrolyte while b). some sections of the cathode are delaminating from the electrolyte.

REFERENCES

1. Kamat, P. V. "Energy Challenge and Nanotechnology." from <https://www3.nd.edu/~pkamat/pdf/energy.pdf>.
2. NASA (2019, March 6, 2019). "Global Temperature." from <https://climate.nasa.gov/vital-signs/global-temperature/>.
3. Barbante, C., et al. (2017). "Man's footprint on the Arctic environment as revealed by analysis of ice and snow." Earth-Science Reviews **168**: 218-231.
4. Dale, B. (2012). "Energy consumption, wealth, and biofuels: Helping human beings achieve their potential." Biofpr **6**(1): 1-3.
5. Sun, C., et al. (2009). "Cathode materials for solid oxide fuel cells: a review." Journal of Solid State Electrochemistry **14**(7): 1125-1144.
6. EIA (May 23, 2018). "Frequently Asked Questions." from <https://www.eia.gov/tools/faqs/faq.php?id=107&t=3>.
7. William, S., et al. (2017). Biofuels technology: A look forward, World Institute for Development Economic Research (UNU-WIDER).
8. Mahato, N., et al. (2015). "Progress in material selection for solid oxide fuel cell technology: A review." Progress in Materials Science **72**: 141-337.
9. Kim, J., et al. (2018). "Hybrid-solid oxide electrolysis cell: A new strategy for efficient hydrogen production." Nano Energy **44**: 121-126.
10. New York State Energy Research and Development Authority. (2014). "Hydrogen Production – Steam Methane Reforming (SMR)."
11. O'Hayre, R., Cha, Suk-Won, Colella, Whitney, and Prinz, Fritz B. (2016). Fuel Cell Fundamentals. Hoboken, New Jersey, John Wiley & Sons, Inc.
12. Jun, A., et al. (2016). "Perovskite as a Cathode Material: A Review of its Role in Solid-Oxide Fuel Cell Technology." ChemElectroChem **3**(4): 511-530.
13. Yang, Z., et al. (2017). "A short review of cathode poisoning and corrosion in solid oxide fuel cell." International Journal of Hydrogen Energy **42**(39): 24948-24959.

14. Zhang, X., et al. (2017). "Co-electrolysis of CO₂ and H₂O in high-temperature solid oxide electrolysis cells: Recent advance in cathodes." Journal of Energy Chemistry **26**(5): 839-853.
15. Chen, Y., et al. (2015). "Advances in Cathode Materials for Solid Oxide Fuel Cells: Complex Oxides without Alkaline Earth Metal Elements." Advanced Energy Materials **5**(18).
16. Hardy, J., et al. (2015). "Effects of Humidity on Solid Oxide Fuel Cell Cathodes." U.S. Department of Energy.
17. Li, Y., et al. (2017). "Controlling cation segregation in perovskite-based electrodes for high electro-catalytic activity and durability." Chem Soc Rev **46**(20): 6345-6378.
18. Huang, Y. L., et al. (2015). "Fundamental Impact of Humidity on SOFC Cathode Degradation." The Electrochemical Society **68**(1): 699-712.
19. Wang, H., et al. (2016). "Mechanisms of Performance Degradation of (La,Sr)(Co,Fe)O_{3-δ} Solid Oxide Fuel Cell Cathodes." Journal of The Electrochemical Society **163**(6): F581-F585.
20. Zhou, X. D., et al. (2012). "Electrochemical performance and stability of the cathode for solid oxide fuel cells: V. high performance and stable Pr₂NiO₄ as the cathode for solid oxide fuel cells." Electrochimica Acta **71**: 44-49.
21. Jiang, Z., et al. (2010). "Turning carbon dioxide into fuel." Philos Trans A Math Phys Eng Sci **368**(1923): 3343-3364.
22. Lim, R. J., et al. (2014). "A review on the electrochemical reduction of CO₂ in fuel cells, metal electrodes and molecular catalysts." Catalysis Today **233**: 169-180.
23. Zhang, Y., et al. (2016). "Evaluation of the CO₂ Poisoning Effect on a Highly Active Cathode SrSc_{0.175}Nb_{0.025}Co_{0.8}O_{3-δ} in the Oxygen Reduction Reaction." ACS Appl Mater Interfaces **8**(5): 3003-3011.
24. Xiong, Y., et al. (2009). "Sulfur poisoning of SOFC cathodes." Journal of the Electrochemical Society **156**(5): B588-B592.
25. Wang, F., et al. (2013). "Evaluation of Sulfur Dioxide Poisoning for LSCF Cathodes." Fuel Cells **13**(4): 520-525.
26. Bucher, E., et al. (2013). "Sulphur poisoning of the SOFC cathode material La_{0.6}Sr_{0.4}CoO_{3-δ}." Solid State Ionics **238**: 15-23

27. Wang, F., et al. (2012). "Effect of strontium concentration on sulfur poisoning of LSCF cathodes." Solid State Ionics **225**: 157-160.
28. Piccardo, P. and R. Amendola (2009). "SOFC's Interconnects Materials Development." European Community's Seventh Framework Programme.
29. Jiang, S. P. and X. Chen (2014). "Chromium deposition and poisoning of cathodes of solid oxide fuel cells – A review." International Journal of Hydrogen Energy **39**(1): 505-531.
30. Schrödl, N., et al. (2016). "Phase decomposition in the chromium- and silicon-poisoned IT-SOFC cathode materials La_{0.6}Sr_{0.4}CoO_{3-δ} and La₂NiO_{4+δ}." Solid State Ionics **288**: 14-21.
31. Schrödl, N., et al. (2015). "Long-term stability of the IT-SOFC cathode materials La_{0.6}Sr_{0.4}CoO_{3-δ} and La₂NiO_{4+δ} against combined chromium and silicon poisoning." Solid State Ionics **276**: 62-71.
32. Zhao, B., et al. (2017). "A tailored double perovskite nanofiber catalyst enables ultrafast oxygen evolution." Nature Communications **8**: 14586.
33. Johnsson, M. and P. Lemmens (2006). *Handbook of Magnetism and Advanced Magnetic Materials*. H. Kronmüller and S. Parkin (eds), Volume 4: Novel Materials, John Wiley & Sons Ltd, Chichester: UK, 2098-2106.
34. Park, S., et al. (2014). "A collaborative study of sintering and composite effects for a PrBa_{0.5}Sr_{0.5}Co_{1.5}Fe_{0.5}O_{5+δ}IT-SOFC cathode." RSC Adv. **4**(4): 1775-1781.
35. Kim, J., et al. (2014). "Triple-conducting layered perovskites as cathode materials for proton-conducting solid oxide fuel cells." ChemSusChem **7**(10): 2811-2815.
36. Chen, Y., et al. (2017). "A robust and active hybrid catalyst for facile oxygen reduction in solid oxide fuel cells." Energy & Environmental Science **10**(4): 964-971.
37. Chen, Y., et al. (2018). "A highly active, CO₂-tolerant electrode for the oxygen reduction reaction." Energy & Environmental Science **11**(9): 2458-2466.
38. Huber, A.-K., et al. (2012). "In situ study of electrochemical activation and surface segregation of the SOFC electrode material La_{0.75}Sr_{0.25}Cr_{0.5}Mn_{0.5}O_{3±δ}." Physical Chemistry Chemical Physics **14**(2): 751-758.
39. Dean, J. A. and N. A. Lange (1999). Lange's handbook of chemistry. New York, McGraw-Hill.

40. Chen, Y., et al. (2018). "An In Situ Formed, Dual-Phase Cathode with a Highly Active Catalyst Coating for Protonic Ceramic Fuel Cells." Advanced Functional Materials **28**(5).
41. Milt, V. G., et al. (2005). "NO_x trapping and soot combustion on BaCoO_{3-y} perovskite: LRS and FTIR characterization." Applied Catalysis B: Environmental **57**(1): 13-21.
42. Zhao, L., et al. (2014). "Insight into surface segregation and chromium deposition on La_{0.6}Sr_{0.4}Co_{0.2}Fe_{0.8}O_{3-δ} cathodes of solid oxide fuel cells." Journal of Materials Chemistry A **2**(29): 11114-11123.
43. Kim, J., et al. (2014). "Triple-Conducting Layered Perovskites as Cathode Materials for Proton-Conducting Solid Oxide Fuel Cells." ChemSusChem **7**(10): 2811-2815.
44. Chen, Y., et al. (2018). "A Highly Efficient Multi-phase Catalyst Dramatically Enhances the Rate of Oxygen Reduction." Joule **2**(5): 938-949.